TU Delft Delft University of Technology

THALES

Reduction of Mutual Coupling and Influencing the Antenna-Element Pattern in Array Environment

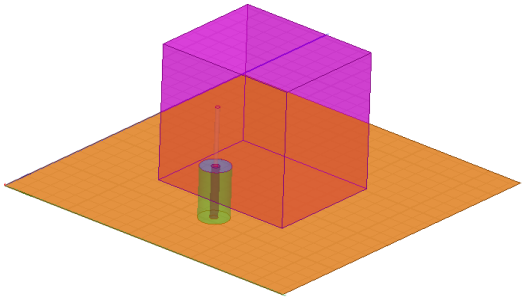

Master of Science Thesis

Hambalis Michael

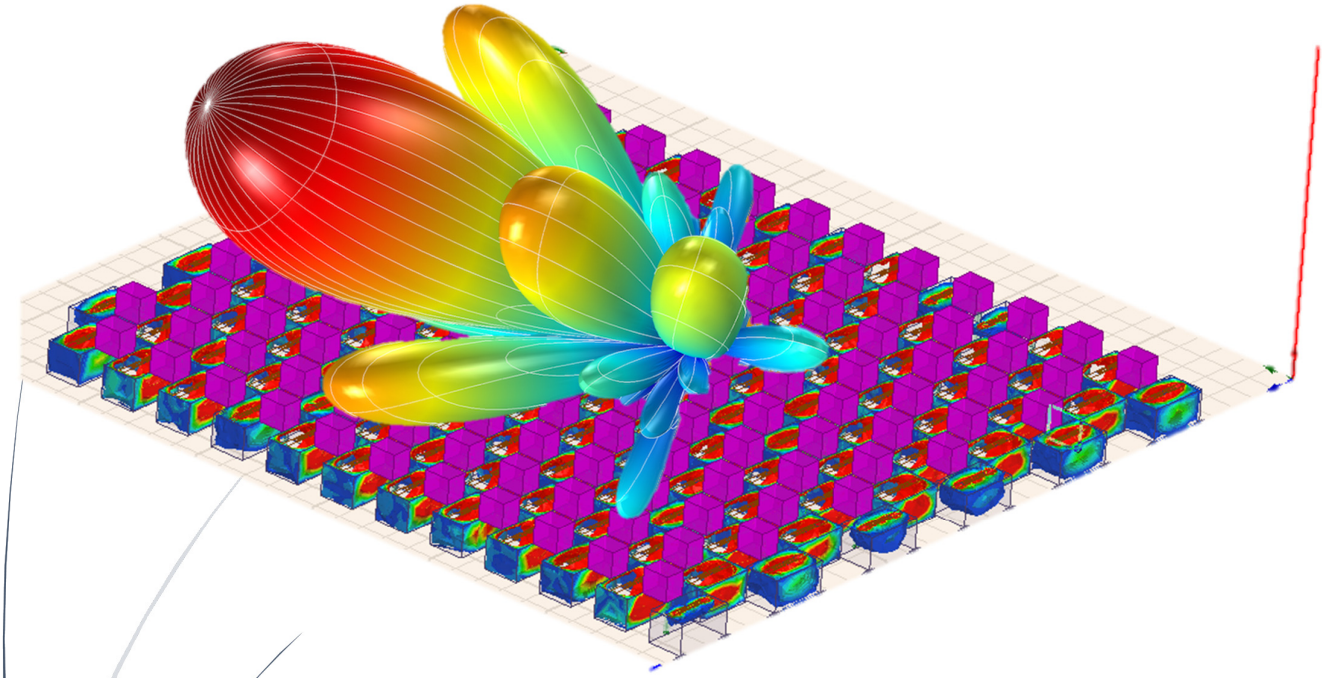

September 2016

Microwave Sensing, Signals and Systems Group
Faculty Electrical Engineering, Mathematics and Computer Science
Delft University of Technology
Delft, The Netherlands

Reduction of mutual coupling and influencing the antenna-element pattern in array environment

By

Hambalis Michael

THESIS
Submitted for the degree of
MASTER OF SCIENCE IN ELECTRICAL ENGINEERING

at the Delft University of Technology,

Supervisors:
Prof. Alexander Yarovoy
Dr. Michal Polewski

DELFT UNIVERSITY OF TECHNOLOGY
DEPARTMENT OF ELECTRICAL ENGINEERING

The undersigned hereby certify that they have read and recommend to the Faculty of Electrical Engineering and Computer Science for acceptance a thesis entitled "**Reduction of Mutual Coupling and Influencing the Antenna-Element Pattern in Array Environment**" by **Michael Hambalis** in partial fulfillment of the requirements for the degree of **Master of Science**.

Dated September 23, 2016

Supervisors: Prof. DSc. Alexander Yarovoy

Dr. Michal Polewski

Committee Members:

Prof. DSc. Alexander Yarovoy, TUDelft

Dr. Oleg A. Krasnov, TUDelft

Dr.ir. Rob Remis, TUDelft

Dr. Michal Polewski, Thales Nederland B.V.

Acknowledgements

This report has been written in September 2016 and is a result of a nine month master thesis internship at Thales Naval Nederland. It will serve as a proof for the partial fulfillment of my studies at the Technical University of Delft for pursuing a Master of Science in Electrical Engineering.

It would not have been possible to successfully complete this master thesis and communicate my work in this report without the help and support of the kind people around me. I am most grateful to my supervisors which I mention here with alphabetical order, Alexander Yarovoy (in TU Delft) and Michal Polewski (from Thales Nederland) for their support and help through these nine months. Their guidance helped me to surpass any difficulties throughout my exciting journey of investigating and creating.

I would also like to acknowledge Michal Polewski for his patience, support and guidance when he introduced me to basic software tools that were used to achieve the implemented studies in array antennas.

I thank my fellow Thales office-mates for their help in practical and theoretical aspects, as well as the time they spent with me in brainstorming to solve particular problems.

Last but not least, I would like to thank my family and my friends for their support and encouragement throughout the aforementioned period.

For any errors or inadequacies that may remain in this work, of course, the responsibility is entirely my own.

Hambalis Michael
Netherlands, September 2016

ABSTRACT

This thesis work provides insights in electromagnetic phenomena in order to improve the scan performance for phased arrays by RF structures. It is assumed that by reducing mutual (MC) coupling between the antenna elements, that constitute the array antenna, it can be possible to obtain a better matching stability for various scan angles.

In this layout, considering ease of fabrication, defected ground structures (DGS) are studied further than literature does. For this reason, the commercially available software ANSYS HFSS, based on the finite element method (FEM), is used to perform the numerically full-wave analysis of infinite and finite arrays.

Based on requirements on operational frequency bandwidth a suitable defected ground structure was synthesized for dielectric resonator antennas (DRA). The constraints on spacing between antenna elements (0.5 lambda) leaded to the modifications of dumbbell DGS that provided the flexibility in the structure geometry. In addition, electromagnetic analysis was performed taking into account radiation effects below the ground plane. Based on that it was concluded that the best RF performance from the MC reduction point of view is obtained when DGS elements are isolated.

Tuned DGS structure is further used in infinite arrays where the results illustrate stabilization in the scan performance and bandwidth enhancement. A large 11x11 novel antenna-DGS array in triangular configuration is analyzed further where the DGS location is able to benefit E, H and diagonal coupled elements. The embedded element analysis verified the bandwidth enhancement in parallel to lower coupling and improved quality for the embedded patterns. The active reflection coefficient showed similar trends with the infinite array reflection coefficient and improved active matching for all the array elements. In addition, by applying DGS between antenna elements the realized gain for the case of 11x11 array improved by 1.3dB.

It is concluded that MC reduction by applying DGS with cavity for DRA arrays with strong coupling between antenna elements, can be used as a method to stabilize the active impedance match for various scan angles.

Table of Contents

1 Introduction

Phased array antennas are well known for their ability of electronic beam steering and adaptation of the beam shape, through adaptation of digitally and analog controlled array elements excitations. These features provide significant advantages over other types of antenna, such as reflector systems, leading to a variety of applications of arrays including (weather) radar and mobile communication.

An array antenna comprises a collection of smaller antennas, referred to as radiating elements, which are located on a regular array grid while arrays with irregular element spacing are used as well. The radiation pattern of the full array is the result of the summation of the element patterns of the array. These element (embedded) patterns will be quite different to the pattern one would obtain by measuring a single element, so without the array environment (Figure 1.1).

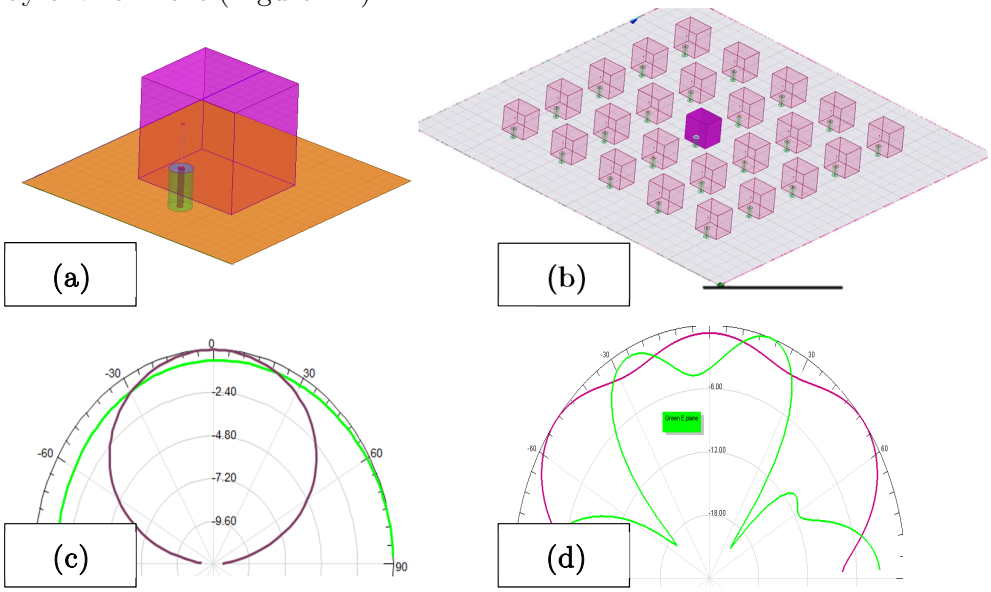

Figure 1.1: Dielectric resonator antenna: a) single radiating element antenna b) planar array antenna c) radiation pattern of (a) d) center element embedded patter of (b): Green E-plane and purple H-plane

The reason for this is that an array-element pattern (the pattern of an element in the array) is strongly influenced by other radiating elements, since the elements do not only radiate in free-space but also towards each other (Figure 1.2). The resulting mutual coupling (in this thesis defined as

"MC") between antenna elements is closely connected to the element spacing, the geometry and radiation mechanism of the individual radiators.

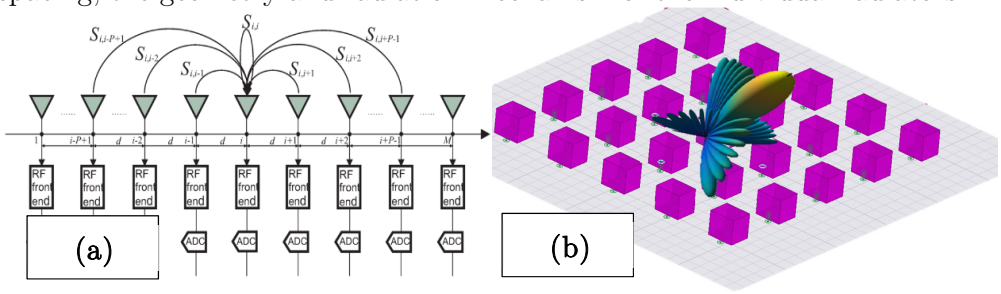

Figure 1.2: (a) MC in array antennas: a portion of power is not radiated in the far field but received by the nearby elements (b) phased array: beam steering

1.1 Mutual Coupling and element-array impact

In antenna RF designs MC is primarily taken into account from the feeding point of view (on the backside of the antenna), by considering the input reflection of an element in an array environment, for instance using the so-called periodic array approximation (in this thesis referred as infinite array suitable for a large arrays). This leads to the so-called active refection coefficient, which is the reflection of a chosen element while all the rest elements are also excited. This interpretation in reality corresponds to an antenna element centered in a large fully excited dense array. Thus, this does not represent the effects for the rest elements in a finite array.

From radiation point of view, the antenna element performance in an array environment is altered compared to the case of being isolated, referred as the embedded element behavior. The pattern that is radiated when a single element is excited consists of the contribution of the primarily excited element, and of the contribution of element patterns that are parasitically excited. The effective element pattern (embedded) is therefore the combined pattern from all elements that are radiation-coupled.

Overall, considering the feed point of view as well as the radiation point of view, MC affects in general the array performance. Specifically, variability of element impedance results in variability of return loss (from element to element) which influences the element excitation and the embedded pattern, affecting globally the array beam characteristics for phased array applications.

1.2 Thesis description

In radar systems 0.5λ spacing between the antenna elements (in this thesis it is defined as "d") is preferred. For larger element separations, the Bragg condition is validated with the consequence of grating lobes. Multiple maxima appear in the visible spectrum creating ambiguities for the main beam position. On the other hand, a denser element ($d \leq 0.5\,\lambda$) arrangement creates strong inter-element coupling, arising the fundamental tradeoff for lattice compactness and MC. Moreover, studies on the coupling mechanism show that antennas arranged in the plane of the electric field (E-coupled elements) are mutually coupled stronger than elements which are in the plane of the magnetic field.

Furthermore, for an array where MC is increased, the main beam gets broader and the side-lobe levels get higher. Moreover, scan performance experiments for strongly coupled antennas like DRAs in a $0.5\,\lambda$ grid show different matching stability for the principal planes. When the main beam is directed from broadside towards bore-side, the elements in the array start to detune. The impedance match characteristics are altered while shifts in resonant frequency occur for the different scan angles. Sharp resonance variations may occur for specific angles, making the element antennas to be excited weakly, creating blind angles for the radar system. Therefore, these phenomena restrict the effective scan operation to a limited angular range.

Overall, the radar lattice preferences ($d=0.5\lambda$) in combination with the scan and coupling phenomena motivate the proposed work to investigate how MC is limiting the scan performance. Specifically, the relation between the reduction of MC and improvement of impedance match stability which in consequence should result in improvement of the scan performance and improvement of element patterns is the scope of this work.

It is important to add that the main goad of this thesis is to observe the impact of mutual coupling reduction on antenna array performance and not to find a general solution for mutual coupling reduction. That means that proposed techniques and structures may not be applicable to all types of antennas but only to the restricted class of radiators.

1.2.1 Research questions

Although many dielectric resonator antennas (DRA) examples in the last decade were investigated (for various applications by the research community), limited examples are provided for DRA planar arrays. Information is more limited for the phased DRA arrays as well as the methods to reduce MC for those types of arrays. Therefore, considering the negative impact of MC on phased array antennas and the DRA design flexibility that allows to modify the antenna element geometry in three dimensions, this project investigates the possibility of using DRA elements for phased arrays and in parallel to improve their scan performance.

Specifically, this study is focused on the methods to reduce MC, for a wide frequency range, for DRA arrays based on the following assumptions:

❖ by reducing MC in a dense DRA array, it should be possible to:
- stabilize the antenna return loss for various scan angles
- improve the embedded element radiation patterns quality

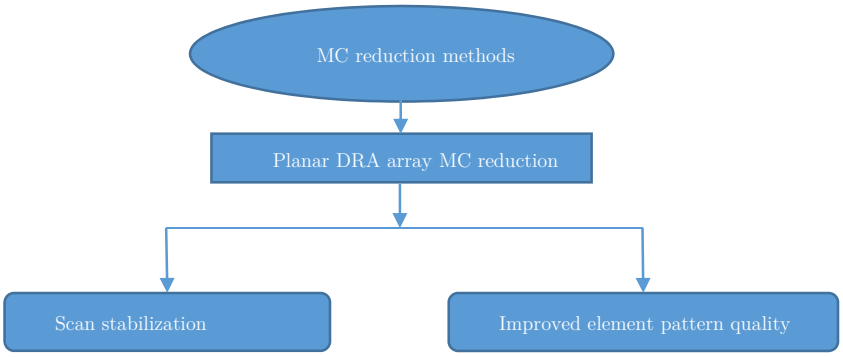

Figure 1.3: Research questions

1.2.2 Challenges

The major challenge in this project was to find an effective MC reduction method which would be applicable to planar DRA arrays. Sub-challenges to achieve this are mentioned below:

- Synthesis of a desired RF structure to meet the requirements concerning wide and stable isolation bandwidth response (see §4.3 for more information)
    - broadband decoupling ability which covers the operational bandwidth
    - minimum impact on the matching antennas
    - performance of MC reduction minimum dependent on variation of design parameters of antenna element
    - physical size adoptable in an array grid
- Applicability of MC reduction over a large sector of scanning angles
- Combination of various techniques used for micro-strip line filtering purposes for MC reduction in antenna arrays.
- Limited support by closed form expressions existed for the coupling phenomena. The complexity of the designs grew exponentially which made the need of a full wave simulator necessary.
    - This analysis requires time and computational resources for accurate results
    - Moreover, this method provides limited physical insights
- Design of large finite arrays which need significant computational resources and time for analysis

1.2.3 Approach

❖ The selection of a MC reduction method among various approaches that are found in literature was the first task of this research work. Therefore, a comparative study follows to indicate the MC reduction technique. The criterion that defines the selection is operational bandwidth and ease of fabrication.

❖ From the selected method, possible designs need to be defined according to certain requirements. Those requirements are satisfied when a proposed structure provides sufficient decoupling ability, minimum impact on the matched antennas, stable operation with antenna element geometries and a physical size adoptable in an array grid. Therefore,

various designs are studied between two E-coupled antenna elements which are evaluated with a commercially available full-wave solver.

- After establishing the designs, which satisfy the requirements, array considerations need to be investigated for the proposed designs. In order to avoid very time consuming simulations of the large arrays the verification of the properties of the structure for MC reduction was performed on the configuration of two antenna elements.
- Furthermore, to answer the first research question the optimized designs are used as test structures for infinite arrays. This is done in order to verify if by reducing MC the impedance match would stabilize for various scan angles.
- As a next step, the final design of DGS is applied to finite arrays (11x11). In this way, it is possible to validate the observations from the infinite array. The finite array configuration gives an overview on matching for all the 121 elements in the array. In addition, allows to observe the impact of the MC reduction structure on the physical coupling phenomena between the array elements. Moreover, the element patterns can be easily compared. Nevertheless, the effect of MC reduction can be studied for the total array pattern.

1.2.4 Novelty

- Novel DGS design applied to planar arrays consisting of DRAs characterized by:
  - stable and broadband frequency response by combination of modified dumbbell and cavity
  - reduced geometry that can fit in DRA arrays with $d=0.5\lambda$
- Study of impact of DGS when applied to planar DRA arrays (11x11)
  - stabilization of return loss
  - bandwidth enhancement
  - improvement of element pattern ripples and more equalized pattern levels (applicable for also small arrays: 5x5)
- Proposed novel design of a dielectric resonator antenna-DGS array, in a triangular configuration, for phased array applications. The location of

the proposed DGS can benefit both E and H plane coupled antenna elements.

- Electromagnetic field study that characterizes the interaction between multiple defected ground structures (in array antennas). It is concluded that the multiple DGS radiation, below the ground plane, is affecting the element DGS resonance response.

1.2.5 Thesis Outline

Chapter 2

This is an introductory chapter which reveals the motivation of this work based on literature studies and simulated examples. The effect of MC in the array scan performance is discussed.

Chapter 3

In this chapter, the state of the art on MC reduction methods offered in literature are presented and categorized in two representative directions. As a next step the reasoning that leads to a particular method and techniques follows. Among a broad set of candidate techniques, parasitic scatterers and defected ground structures are decided to be examined.

Chapter 4

Here, in order to provide a choice between the candidate techniques the requirements for the desired RF structure and the validation configuration are established. Thereafter, comparison between the selected RF techniques from chapter 3 by representative structures are demonstrated in order to make a selection. The final selection takes into account the fabrication complexity, the MC reduction effectiveness and the effects on the element antennas (from feed and radiation point of view).

Chapter 5

The chosen class from chapter 4, which are the defected ground structures (DGS), is further analyzed to provide a suitable structure which is in-line with the established requirements. Specifically, in order to provide a promising DGS RF structure for antenna arrays bandwidth constrains are

investigated first. The experiments on antennas on substrate showing design limitations indicate the necessity to switch to different antenna class, antennas on metal plate. For this class, the amount of design variables is reduced (lack of dielectric substrate) which simplifies the design process. DRAs with DGS were chosen for further studies. It will be shown that this configuration is satisfying bandwidth and stability constrains when a cavity is added below the ground plane.

Chapter 6

The selected RF DGS structure from chapter 5 is further examined for the design constrains for an array application. Therefore, this chapter, is focused on modifying the DGS to synthesize a design that is satisfying bandwidth constraints and in parallel can meet the geometrical requirements regarding the array lattice of 0.5λ. Furthermore, the multi element DGS interaction is studied by analyzing the DGS radiating nature and insights for the inter-DGS isolation are provided. The final proposed DGS array component is examined for different antenna elements. It is concluded that properties of mutual coupling reduction of the proposed DGS structure remain almost unchanged when applied to DRAs made of different material of having different radiators shape.

Chapter 7

This chapter evaluates the infinite array performance based on the array element characteristics. The arrays under study are based on the antenna-DGS element combination presented in chapter 6. Based on a single unit cell element, the assumption of identical infinite excited antenna elements is made. The evaluation of the array is based on how well the embedded element can be excited for various scan angles with and without the DGS.

Chapter 8

Large finite array (11x11 array) analysis examines the impact of MC reduction. This array configuration is analyzed using embedded and active element approach. The analysis is primary focused on the feed point of view (embedded reflection coefficient, coupling effects and active reflection coefficient) and then on the radiating point of view (embedded patterns quality and array beam patterns). Furthermore, the proposed DGS with a cavity provides the ability to characterize the coupling profile using near

field analysis. Finally, the summarized array parameters are provided to show the advantage of using the proposed synthesized method.

Chapter 9

The thesis results are summarized and discussed. Recommendations for future work are given as well.

2 Mutual coupling and array scan performance

The following introduction on the coupling preferences for E and H coupled antenna elements connects MC and the array scan performance. Literature studies are provided for elements coupled along the principal planes. The coupling observations are then compared with corresponding array scan stability tests, from the feed point of view, which show the motivation of this thesis work to reduce MC.

2.1 E and H coupled elements

Microstrip patch antennas are well known elements used for various fields such as satellites, military systems, aircrafts, naval systems and many more. Their metallic versatile shape based on a dielectric grounded substrate provides interesting features for designing them. Low profile, light weight and ease of fabrication made researchers to come up with extensive theoretical analysis and experimental verifications. Among them, studies on the coupling mechanism between E-coupled and H-coupled elements where done [1], [2]. For different electrical distances between patch antennas, in terms of wavelength (0.2λ -1.6λ), the coupling between E and H coupled elements was simulated and measured. In Figure 2.1(a) it is demonstrated that E-coupled element antennas are mutually coupled stronger than H-coupled elements. However, by altering the design properties E-coupled elements couple stronger for longer element separations (see Figure 2.1(b)-(c)).

Despite the design impact on MC that is observed in microstrip antennas, E-coupled elements for a certain element distance and on are coupled stronger than H-coupled elements. This is an important observation for array applications. For example in a rectangular planar array the element separation at 0.5λ, which defines the array lattice, is preferred to avoid multiple maxima in the visible spectrum [3]. Therefore, this spacing is large enough to consider that the elements which are placed along the E-plane are coupled stronger compared to H-plane elements.

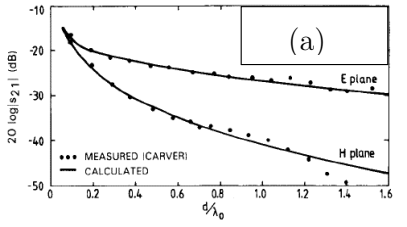

Fig. 2. E-plane ($d = -a$) and H-plane ($s = -b$) mutual coupling. (a) t = 1.59 mm and (b) t = 3.2 mm. a = 105.7 mm, b = 65.5 mm, x_0 = 17 mm, y_0 = 32.8 mm, ϵ_r = 2.5, f_0 = 1.405 GHz.

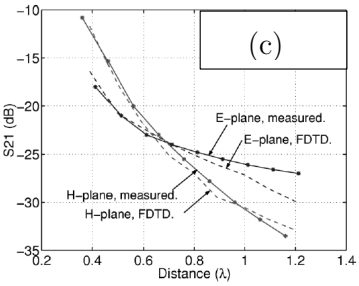

Fig. 7. Measured [20] and FDTD simulated mutual coupling results at 1.56 GHz for 5 cm (radiating edge) × 6 cm patches on a 0.305 cm thick substrate with a dielectric constant of 2.5.

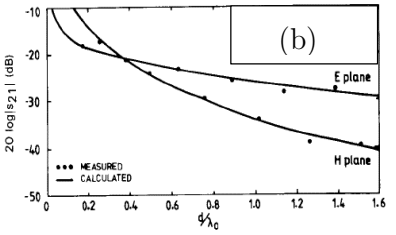

Fig. 3. E-plane ($d = -a$) and H-plane ($s = -b$) mutual coupling, a = 16 mm, b = 16.93 mm, x_0 = 5.5 mm, y_0 = 8 mm, t = 1.57 mm, ϵ_r = 2.55, f_0 = 5 GHz.

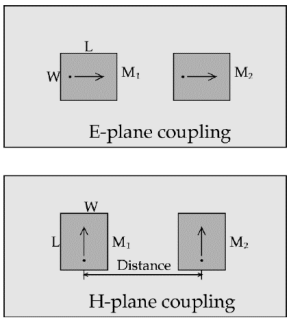

Figure 2.1: E and H coupled elements coupling for different element spacing's and designs: (a) and (b) adopted from one [1] and (c) from [2]

To demonstrate the array coupling preferences, E and H coupled cylindrical dielectric resonator antennas are examined for their scattering parameters. This element antenna is selected in order to avoid the MC dependence from the design properties that microstrip patch antennas encounter. Those design parameters which influence MC in patch antennas are the substrate thickness, the dielectric properties and the planar patch geometry. Therefore, the resonator antenna element example is chosen for the 3-D symmetrical geometry and its placement on a metal plate (see Figure 2.2).

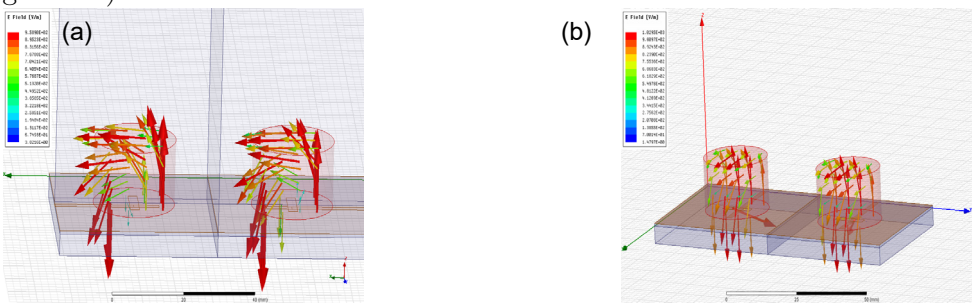

Figure 2.2: E and H coupled cylindrical dielectric resonators

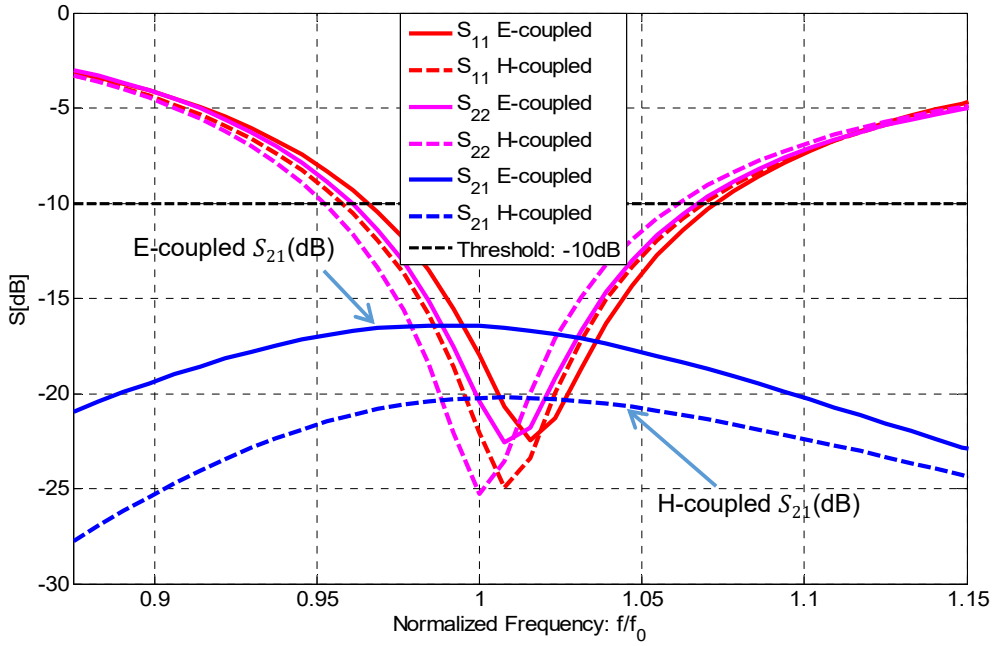

Figure 2.3: CDRAs in E and H coupled element orientation: MC (S21) comparison

As illustrated in Figure 2.3, at the E-coupled configuration the elements exhibit significant stronger coupling than the H-coupled elements.

2.2 E and H plane scan sensitivity

On phased DRA arrays, when the principal planes are examined, for various scan angles, H-plane presents to be more stable than E-plane. This stability, from the feed point of view, is realized by less frequency resonance shifts for different scan angles. Therefore, by combining the element coupling preferences, it is assumed that because of stronger coupling in E-plane this stability is not achieved as in H-plane.

To illustrate the aforementioned scan resonance sensitivity, the cylindrical dielectric resonator antenna, which has been examined for its coupling preferences, is now investigated for its scan performance. Assuming an infinite rectangular array with identical cylindrical dielectric resonator elements, in an equidistant lattice defined by 0.5λ (see Figure 2.3), scan from broadside towards boreside is evaluated.

In Figure 2.4 the element return loss for the scan angles from broadside to 60^{o} are demonstrated. From the scan frequency resonances, H-plane impedance match shows to be more stable than E-plane. For instance the

impedance match for wider angles than 15° (for E-plane), are considered radiation inefficient at 1.05fo. In contrary H-plane, for the examined frequency, can scan efficiently until 45°. Moreover, this sensitivity is not characterized only by frequency shifts. The return loss levels are detuned which indicate a more severe impedance mismatch from scan to scan.

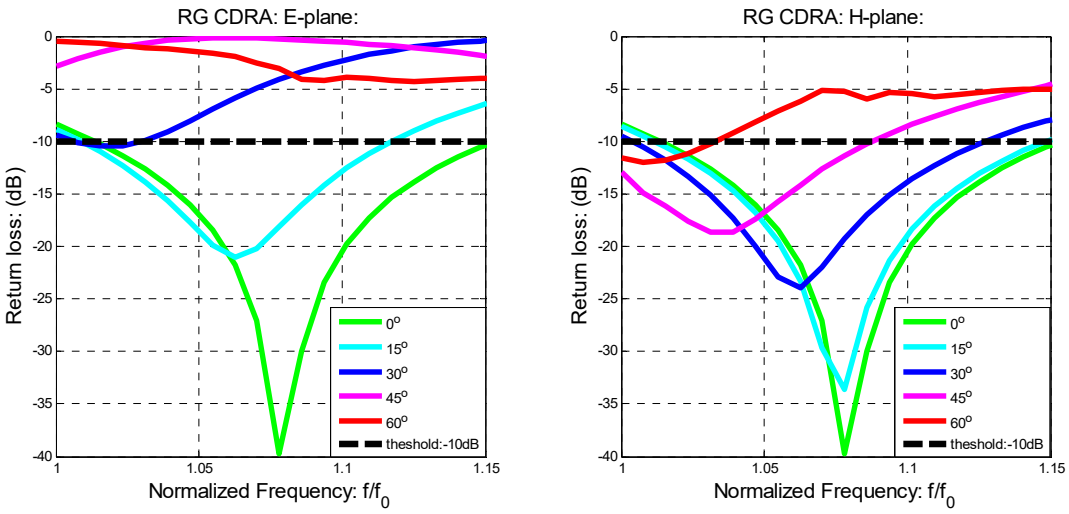

Figure 2.4: Scan performance of a CDRA element antenna in rectangular 0.5λ grid: Normalized at the stand alone CDRA frequency resonance (see Figure 2.3)

Knowing that MC is stronger in E-plane and that the resonator has a symmetrical shape (meaning equal conditions for E-coupled and H-coupled elements in the array), one can verify the impact of MC in the scan performance. MC in the array affects the element reflection coefficient which is parameterized in terms of the elevation and azimuth scan angles [4]. This is translated in performance variations from scan to scan which affect the impedance match, the embedded radiation patterns and moreover the total array pattern.

2.3 Discussion

The demonstrated impact of MC in the scan performance is therefore motivating the layout of this thesis work. It is aimed to investigate the DRA array MC reduction and the possible improvement in the scan performance. For this reason MC reduction methods follow in the next chapter. Possible methods from literature studies are provided and a suitable method is selected.

3 State of the art

3.1 MC reduction methods

The negative impact of mutual in the array performance has driven the research community to create sophisticated ways to minimize MC for the array antenna elements. Three different design directions can be identified, as shown in Figure 3.1.

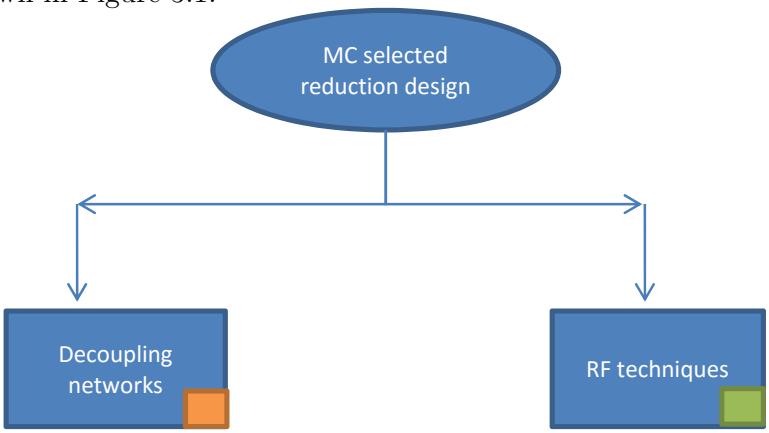

Figure 3.1: MC design directions

3.1.1 Decoupling networks

Decoupling networks with the use of compensation weights try to recover the element radiation characteristics [5]. This method is based on the concept of the active element pattern. The concept provides an effective way to make precise computations of the gain and array pattern of a finite array, by taking into account the MC effects [6]. In essence, it is aimed to allow the prediction of an array radiation pattern by pattern multiplication

$$G_A(\theta,\varphi) = G_e(\theta,\varphi)\text{x}AF(\theta,\varphi) \quad (1)$$

where G_A represents the array gain pattern, $G_e$the active element gain pattern and AF represents the normalized array factor. This is valid if the patterns are maintained the same in the array, which is the case of a simulated infinite array. In a finite array the embedded patterns vary from element to element. Therefore, if the active element patterns are recovered as in the isolated case the scan performance can be improved (avoiding deeps or scan blindness). In [7], [8] this was proposed by excitation voltages which are modified according to the active input impedance and the mutual impedances (see Figure 3.2). This led back to the isolated element patterns. However, in [9] it was strongly argued that the impedance mismatch that

is caused by the strong MC is maintained in the array, although the use of excitation weight compensation can restore the required beam patterns. In essence, the active element realized gain pattern does not benefit from this method.

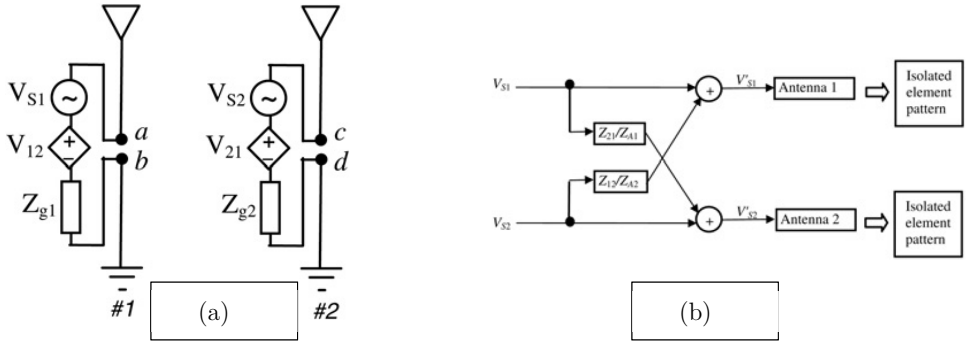

Figure 3.2: Voltage decoupling compensation by mutual impedances: a) Decoupling feeding networks of the array b)compensation feeding network for a two-element transmitting antenna array [8]

In order to overcome the mismatch limitation, wide angle impedance match sheet combined with the excitation voltages which required intensive iterative methods for an improved active reflection coefficient and good patterns. Therefore, this method did not followed as it is desired to tackle the impedance mismatch, by reducing MC, which it will result in enhanced pattern quality.

3.1.2 RF techniques

The next method, named as RF techniques describes periodically, non-periodically distributed elements as well as sophisticated substrate architectures in the array. These additions or the modification in the design architecture of the element antennas in an array exhibit band gap behavior or slow wave effects that aim to reduce MC. This category has been intensively studied and experimentally verified by various techniques. Therefore the RF method was selected to be investigated with the requirement of a technique which can be applied with ease of fabrication. Important techniques follow in the next paragraph and a comparative study follows at the end.

3.2 Selected RF techniques

3.2.1 Metal cavities

To reduce the surface waves that propagate in the substrate, microstrip patch antennas are installed in cavities. The cavities can be formed by metal walls in the substrate [10]–[12]. By adjusting properly the metal in dielectric areas around the antenna elements, MC reduction can be achieved in a specified band. Although this method is widely accepted, the necessity of the cavities in the substrate requires extra fabrication time and cost. Moreover, the cavity placement and its proximity to the antenna elements, creates reactive effects which affect the impedance match of the antenna elements. Therefore, optimization is required for correct tuning regarding different designs. Examples are illustrated in Figure 3.3(a-b) which address the design difference between a typical backed cavity patch antenna and a hybrid architecture. The hybrid architecture aims to reduce in parallel cross polarization levels in H-plane and MC.

To avoid the necessity of a large metal area per unit cell the substrate integrated waveguide technology is used which provides similar effects as the metallic base (see Figure 3.3(c)).

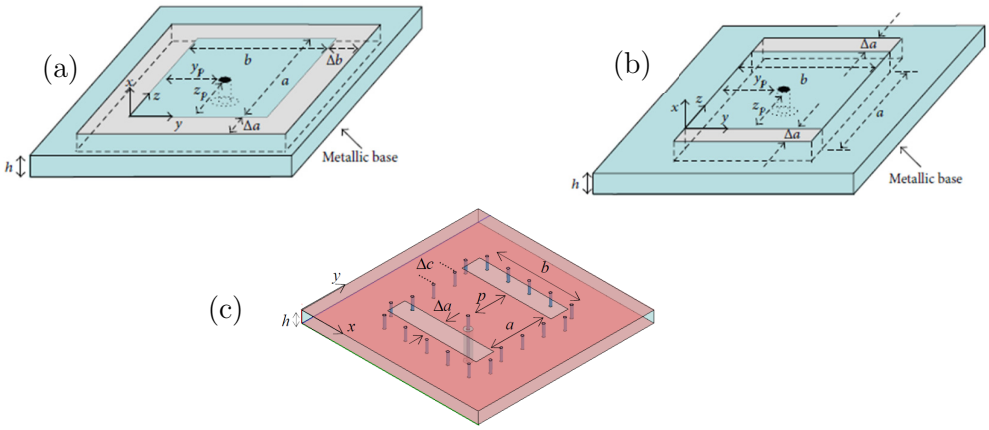

Figure 3.3: (a) Typical patch antenna centralized in a metal cavity (b) Hybrid cavity-backed probed fed microstrip antenna: adopted from [10] (c) substrate integrated waveguide (SIW) technology for a low cost, low weight microstrip antenna in an FR4 substrate: backing cavity implementation by shorting pins [11]

However, the metal walls replacement (that surround the rectangular patch antenna) by cylindrical shorting pins require fabrication complexity which can be vulnerable to design errors. Moreover, the number of pins and the distance from the antenna (compared to the substrate wavelength) are

affecting the efficiency of reduction in MC [13]. Therefore, a tradeoff holds between the MC reduction efficiency (plenty of shorting pins) and a low weight backed cavity (using less shorting pins).

3.2.2 Neutralization lines

This technique introduces an extra coupling path by a metal strip, which interconnects the antennas. The conductive line offers a medium for surface currents. which are mutual arranged in proper magnitude and phase (by the width and length of the metal strip), such that compensate for the existing coupling between the antennas [14]. As explained in [15], through the strip line the coupled power is redirected between the antennas but not through the feeding ports. Thus, although MC strongly exists, because of the extra coupling path, the antennas can in parallel radiate efficiently.

As a next step, for closely spaced PIFA antennas ($0.027\lambda_0$) folded lines were used in order to redirect the coupling currents. The proposed technique provided an alternative path (compared to the inter-element antenna direct path) which still made the currents not to be guided towards the feeding port of the non-fed antenna. The antennas where electromagnetically coupled by the grounded strips but, as before, isolated at their feeding ports. Figure 3.4, illustrates the mentioned design differences between the direct interconnected strip and the folded strips [16].

For diversity MIMO communication applications, the neutralization technique is considered suitable. The port-to-port isolation results in total efficiency enhancement for closely placed antennas, although they are coupled through a metal strip. The maintained strip line coupling is used to reduce the correlation between the antennas, which benefits the channel capacity [15](see Figure 3.5). This is a phenomenon that the scattering parameters are not able to describe, as they account for the amount of power that is transferred between the ports.

On the other hand, in a finite array this technique requires increased complexity for the feeding network. Considering an active large phased array, the necessity of interconnecting each of the elements by an ideal tuned metal strip makes the method not practical and costly in terms of fabrication. Furthermore, as it was shown from [15], the strip line can act as a delay line which provides phase shifts between the coupled antenna elements. Therefore further phase compensation should be consider for each antenna element in a phased array. Moreover the multiple added metal

strips in a dense array are expected to experience a reactive inter-element behavior, which will load the antennas. This load impact might further affect the array elements impedance match as well as the total array performance.

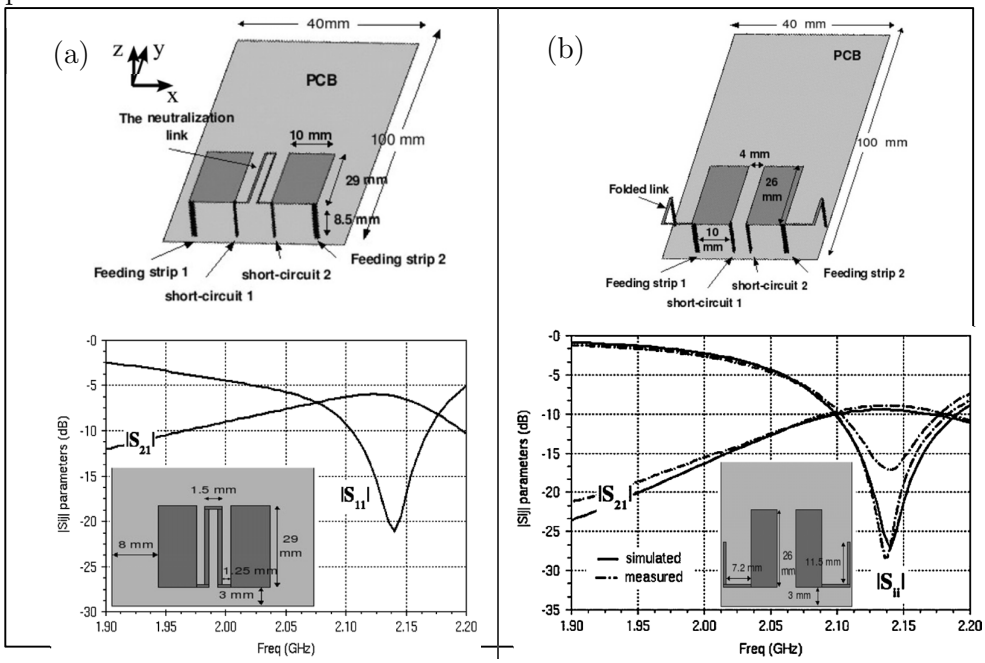

Figure 3.4: a) Conventional neutralization line, which interconnects closely spaced PIFA antennas b) Folded neutralization line, which is shorted on the ground plane: figures adopted from [16]

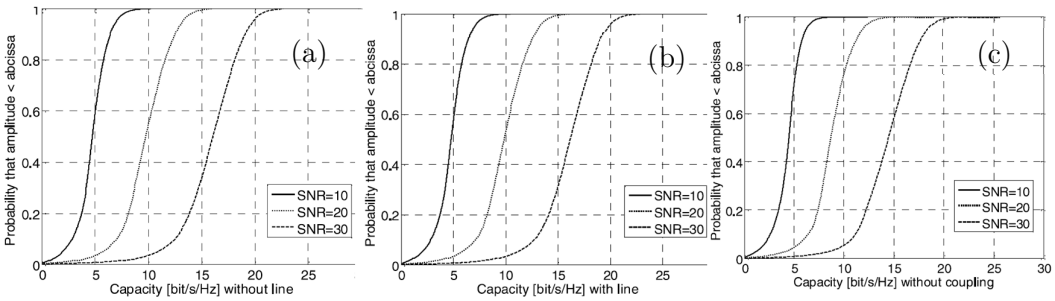

Figure 3.5: Median outage capacity for specific SNRs and channel capacity: With the neutralization line (see (b) SNR: 20) the capacity increased by 0.1bps/Hz. With and without the line (with coupling) the differences are negligible due to low transmission coefficient. Without coupling (c) compared to (a) and (b) 13% lower channel capacity is feasible. Figures and data from [15]

3.2.3 Electromagnetic band gap structures

EBG periodic structures consist of metal elements in a dielectric showing frequency band stop or pass characteristics. They find application in

antennas as MC absorbers by reducing surface waves. In [17] it was first defined the term EBG for RF geometries that maintain band gap characteristics in a tuned frequency band for all the incident and polarization waves. This method is a concept that originates from optics and solid state physics. Therefore, the term photonic band gap is frequently found in literature [18]. The main advantage of an EBG structure is that reflection happens only at specified frequency band gap, which makes it transparent for other frequencies. Therefore, in the forbidden frequency band there is no transmission though the structure.

3.2.3.1 3D substrate structures

In [2], [19] mushroom-like EBG structures are implemented in the design of micro-strip antenna arrays to reduce the strong MC caused by the thick and high permittivity substrate, without sacrificing the compact size or bandwidth of the antenna elements. These metallic elements consist of small square patches that are connected to the ground plane by vertical interconnected access (VIA) (see Figure 3.6a:4-1c) between E-coupled patch antennas. In [2], comparison with the normal patch antennas, substrate removal and cavity backed techniques indicated that the EBG structure provided superior performance.

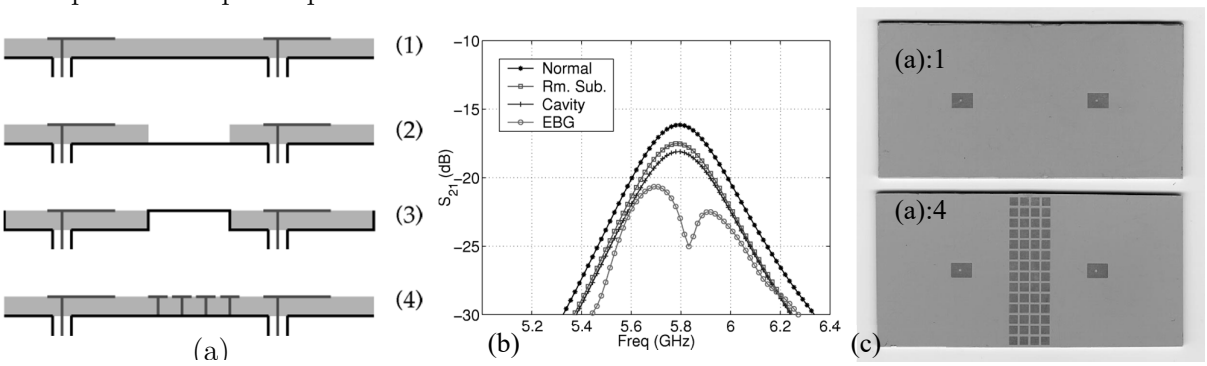

Figure 3.6: Comparison of E-plane MC using different microstrip antenna structures. (a) Four different patch antenna structures: (1) normal microstrip antennas, (2) substrate between antennas is removed, (3) cavity back microstrip antennas, and (4) microstrip antennas with the EBG structure in between. (b) MC results of four antenna structures. Patch antennas resonate at 5.8 GHz (c) Photo of microstrip antennas with and without the EBG structure. Figures and results adopted from [2]

Similarly, to the metal cavities, the necessity of shorting VIA increases the production time and the fabrication cost. Moreover as illustrated from Figure 3.6c, the EBG structure requires significant large area in H-plane, which questions the applicability of a tuned EBG in different array lattice arrangements. On the other hand, regarding the radiating point of view, no

reference (based on what is shown in literature) has been given for a negative radiation pattern impact which is considered as the advantage of this method.

3.2.3.2 Mushroom walls

Zhai, Chen and Qing suggested the isolation of 4 wave-guide slot antenna elements by the so called "mashrooms-walls". This concept faces MC reduction in an array in terms of the space wave coupling. As stated, walls were comprised from two layers of patches connected with VIA on the ground plane. Two such layers interconnected in the center, formed the mash-room walls. Although the slot elements in the array are spaced closer than 0.5lambda it is achieved high isolation. It is good to mention that the adjacent slot elements are placed in an orthogonal arrangement [20].

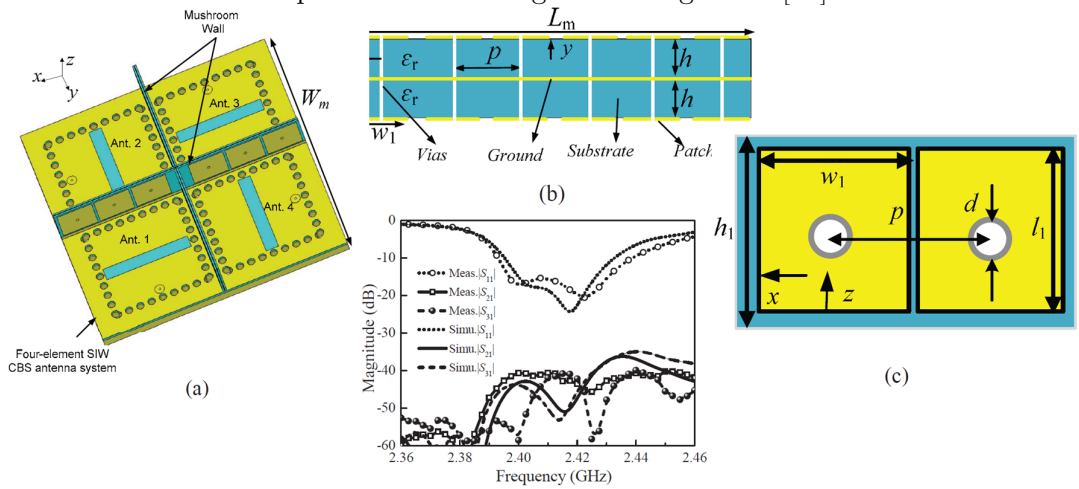

Figure 3.7: Configuration of the four-element SIW CBS antenna system with mushroom walls; (a) overall view, (b) cross-sectional view of the mushroom wall, and (c) top view of the mushroom wall and the scattering parameters of the design. Figures adopted from [20]

Despite the good isolation that is provided by the proposed method, no investigation has been carried out in terms of scanning which questions any scan operation for radar purposes, as the proposed walls exceed the antenna elements. The proposed illustrated design was intended for future MIMO applications, which neglects the effects that might occur when array scan operation is desired. It is expected that the extended walls will affect the array beam negatively, for wide scan angles. Scattering from the wall edges can induce reflections back to the element antennas, causing impedance mismatch and therefore lower efficiency. Moreover, the required VIA and the large wall elements, require extensive optimization algorithms for a

specified band gap behavior. Nevertheless, this concept makes the beam to squint, which causes considerable asymmetries in E-plane.

3.2.3.3 UniPlanar EBG structures

Planar EBG structures developed in order to provide less complexity for the fabrication process that the 3D EBGs required. This category is found in literature as "uni-planar compact EBGs", which are characterized by 2D shape and low manufacturing cost compared to the mushroom EBGs. The planar designs do not require the use of VIA, which makes them to integrate and fabricate relatively easy in microwave planar circuits. This is feasible by metallic patterns which are characterized with insets that make feasible band-gaps in lower frequencies (compared to the 3D mushroom EBGs) [21]. Those kind of structures are placed above or between dielectric substrates (if multiple dielectric layers are used). Therefore, combinations can be found in multiple or single layers. Some UC-EBG examples are shown in Figure 3.8.

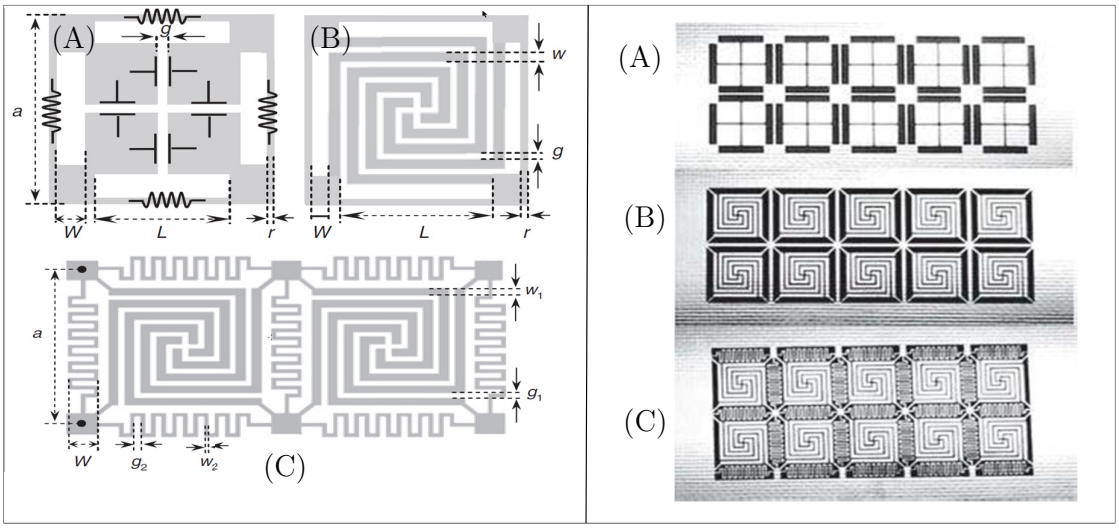

Figure 3.8: (A) Conventional UC-EBG, modified UC-EBG (B) and a proposed UC-EBG (C): figures - Left hand side infinite unit cell structures, Right hand side UCEBG for microstrip line: from: [21]

3.2.4 Parasitic scatteres

In a more simplified concept, parasitic scatteres are placed between the antenna elements in order to provide an alternative coupling path. Those elements can take 3D [22] or planar shape [23], [24] providing resonant characteristics with limited amount of elements. The frequency stop band

is achieved by destructive interference of surface currents. Those currents are parasitically excited on the planar surface by active components (e.g. transmission lines or antennas). A characteristic example is illustrated in Figure 3.9; a parasitic square patch was placed on top of a substrate between two excited antenna elements. As demonstrated, it is able to provide considerable isolation by reducing the surface waves for the excited backed cavity slot antennas.

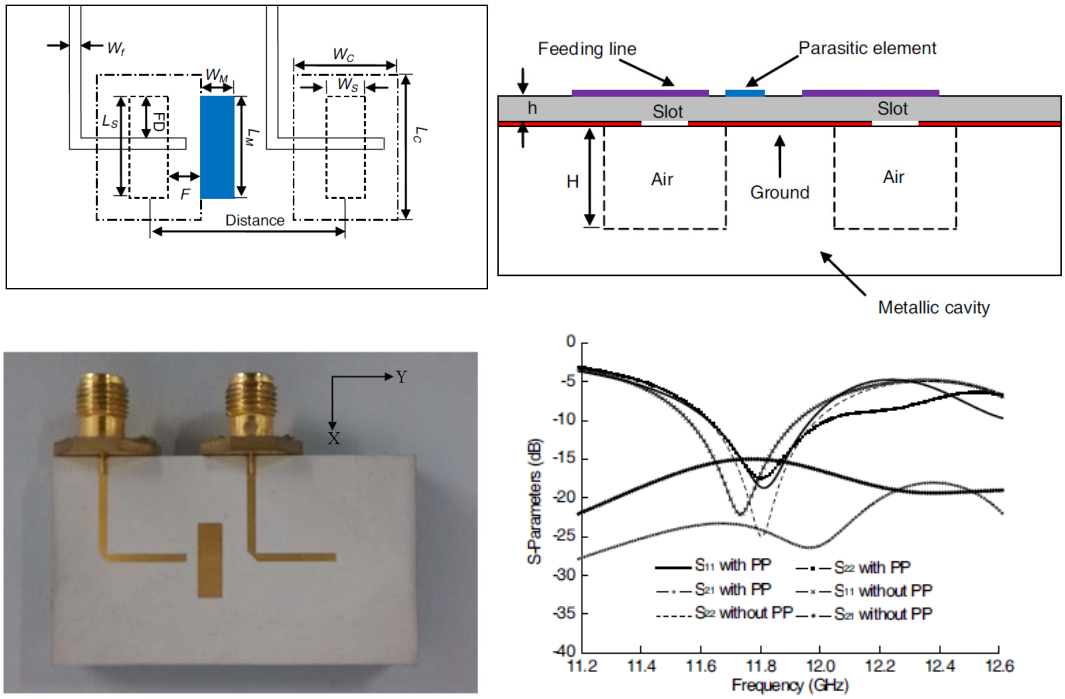

Figure 3.9: Structure of the dual-element slot antenna with parasitic element. (a) Top view. (b) Side view. (c) Photo: from [23]

3.2.5 Defected ground structures

A defected ground structure is a designed planar geometrical shape, on a ground plane, by etching out critical metalized areas. These areas are considered highly active by surface currents. Thus, the fabricated metallic discontinuities create certain inductance and capacitance which can result in filtering effects. Primary applications of the proposed technique are found below microstrip lines which provide higher impedance, band rejection or slow wave characteristics [25].

Compared to EBGs, similarly to parasitic elements, it does not necessary requires a periodic pattern lattice arrangement in order to create an

electromagnetic stop band response. This is because it maintains a resonant response without the need of a group effect. The first DGS layout was provided by [26] and from there and on many more followed. According to a geometrical shape different stop bands and quality factors can be obtained. Examples for some characteristic shapes are depicted in Figure 3.10.

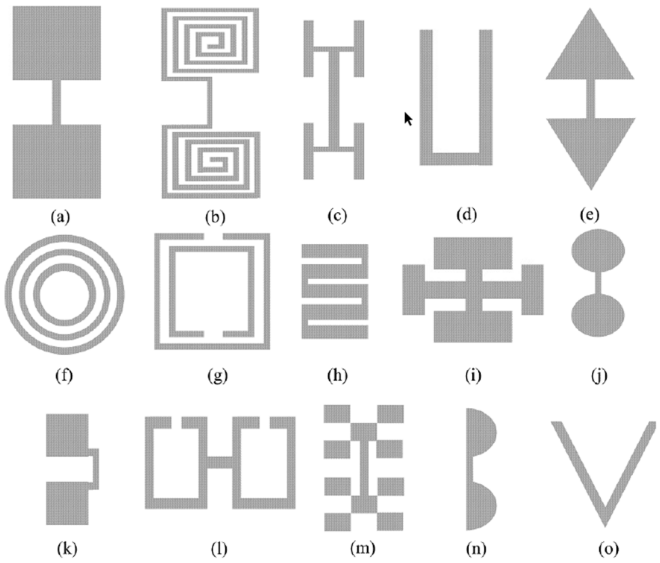

Figure 3.10:Different DGS geometries: (a) Dumbbell-shaped (b) Spiral-shaped (c) H-shaped (d) U-shaped (e) Arrow head dumbbell (f) Concentric ring shaped (g) Split-ring resonators (h) Meander line (i) Cross-shaped (j) Circular head dumbbell (k) Square heads connected with U slots (l) Open loop Dumbbell (m) Fractal (n) Half-Circle (o) V-shaped from: [27]

The first antenna-DGS application introduced in 2004. Studies up to date followed which provide various usages for microstrip patch antennas. Various examples are found for size miniaturization, harmonic reduction, cross polarization radiation suppression, MC reduction and scan blindness elimination (for infinite phased arrays). Usages for RFID tags and UWB applications are mentioned as well. In addition, examples show that it can improve the operational bandwidth (in a lower quality factor) and the impedance match of the antennas. The reader is suggested to follow the papers in [27], [28] which provide extensive overview on these advances. Figure 3.11, shows several examples where a proper DGS has been applied for several mentioned applications.

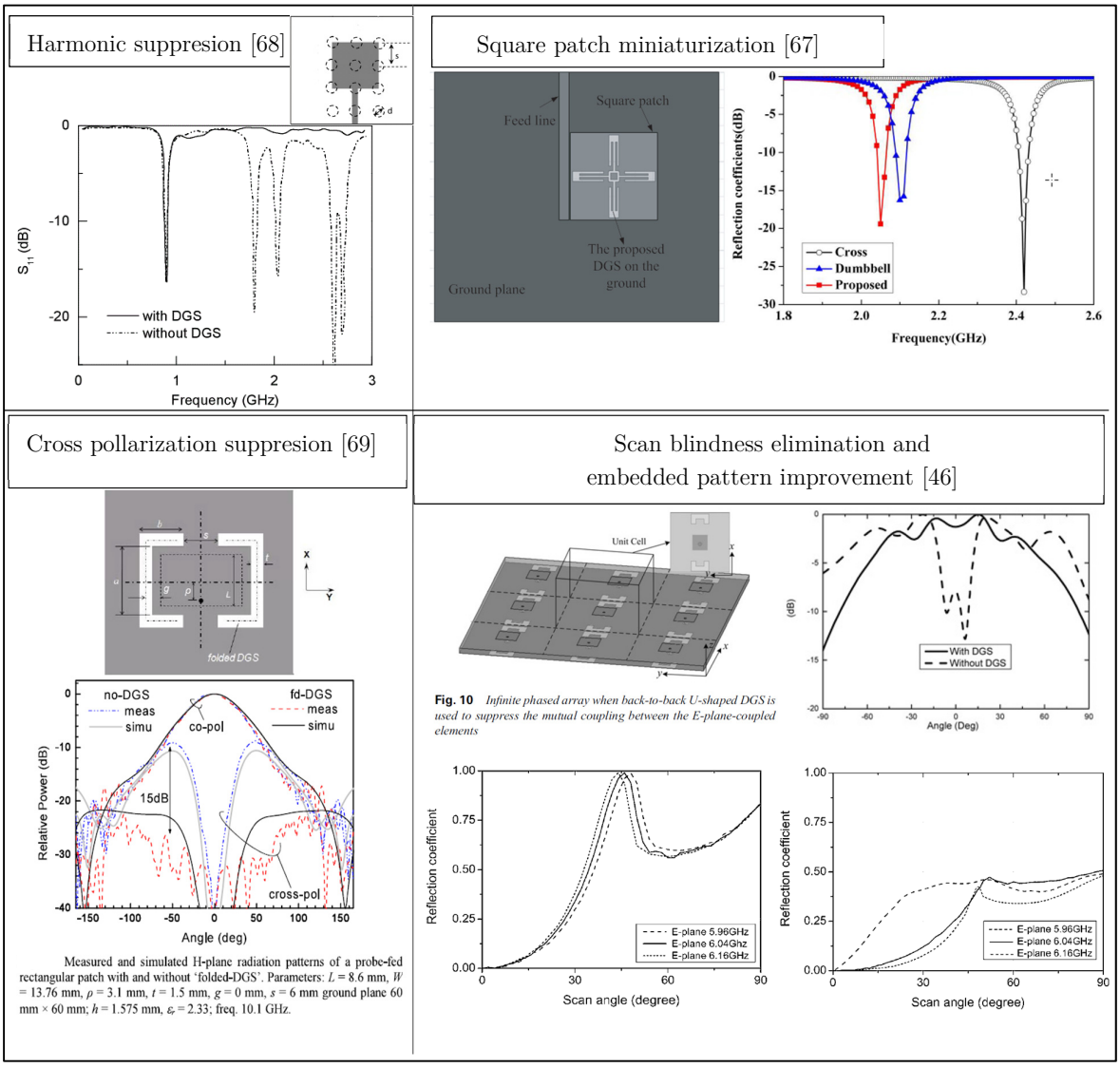

Measured and simulated H-plane radiation patterns of a probe-fed rectangular patch with and without 'folded-DGS'. Parameters: $L = 8.6$ mm, $W = 13.76$ mm, $\rho = 3.1$ mm, $t = 1.5$ mm, $g = 0$ mm, $s = 6$ mm ground plane 60 mm × 60 mm; $h = 1.575$ mm, $\varepsilon_r = 2.33$; freq. 10.1 GHz.

Fig. 10 *Infinite phased array when back-to-back U-shaped DGS is used to suppress the mutual coupling between the E-plane-coupled elements*

Figure 3.11: Different applications of a DGS for micro strip-patch antennas

Despite the multiple applications that a DGS can offer for antennas, here, focus is given on the band gap properties between antenna elements. Numerous examples in literature proved that a DGS can suppress surface waves effectively for E-coupled micro-strip patch antenna elements [29]–[31].

Although various examples for MC suppression for antennas exist, closed form expressions are not usually found in order to support the predesign DGS procedure. For that reason, a common method for validation is done

below a micro-strip line. Via iterative methods, a tuned structure is further studied between E-coupled antenna elements [29]–[32].

An exception is done for the dumbbell DGS that is shown in literature. A Quasi static model has been suggested which can provide a response about the centralized DGS excitation [33]. However, the model requires iterative methods because of the necessity to input data from the scattering parameters of a full wave simulator. Even though, for different antenna element configurations a DGS needs to be optimized in position and resonance [27]. This is because coupling from a micro-strip line to a centralized DGS is quite different from what is exhibited between antenna elements. These observations led the research community to implement genetic algorithms in order to tune and optimize a DGS effectively [34].

In terms of array antennas, examples are provided for linear arrays [35], [36] however limited information in terms of planar arrays [37] as well as phased antenna-DGS arrays is provided [38]. It is important to mention that a trade-off has been stated in [28] between surface wave reduction and back lobe radiation for a linear antenna-DGS array. As more DGS elements were used in the array, referring to 1 DGS element per E-coupled elements, the MC reduction efficiency decreased while the back lobe increased. Therefore, limited amount of DGS elements were used. In addition, for a planar array [38] although the embedded patterns improved the reduction in the realized gain observed. A possible explanation can be that although the coupling reduction made possible to improve the patterns, the added DGS elements loaded (capacitevely) the element antennas which altered the matching conditions. The aforementioned statements question the applicability of a DGS element in a large planar array where multiple DGS elements can be distributed.

Moreover, there are very few examples provided in the research area of antennas for arrays made of DRAs. However, it is observed that in the last decade the research interest on the DRA antennas increased significantly. Regarding the DGS applications most of the studied examples are limited to single or dual elements [32], [39], [40]. However, no examples for a dielectric resonator planar array constituted of antenna-DGS elements have been found in the literature up to now.

Overall, the literature declares that although the DGS requires ease of fabrication with no extra materials, predesign of DGS is a difficult procedure. Moreover, insights for the DGS behavior in a planar and active antenna array as well as on its effective design are still in need. Nevertheless, the DGS application in a planar array constituted of dielectric resonator antenna elements is not studied in literature up to now.

3.2.6 Dielectric substrate modifications

3.2.6.1 Multilayer substrate

This technique modifies the substrate design of microstrip patch antennas by placing the antennas on top of an inhomogeneous substrate structure. The different substrate stratifications aim to change the wavenumber along the lateral dimension (along the substrate), which results in less excited power for surface waves [41]. Therefore, MC compared to a homogeneous substrate, for coupled antennas, in an array is reduced. However, the multilayer substrate creates an effective relative permittivity for the patch antennas. Therefore, the pre-design procedure may depart from the initial design. This means different operational bandwidth, frequency and modal characteristics with respect to a homogeneous substrate, requiring the use of a full wave simulator for a proper tuning. Moreover, the substrate layers should maintain a specified dielectric permittivity contrast, where limitations arise by the available material properties. On the other hand, the fabrication complexity is considered moderate, if properly the multilayer substrate architecture is designed, compared to EBGs and metal cavities. This makes the assumption that the multilayer structure comes with a reasonable amount of layers (avoiding extreme fabrication time and cost). An effective application for this method is illustrated in Figure 3.12. The authors effectively reduce MC for a dual band antenna in an array and provide design considerations regarding the height of the multilayer substrate, the dielectric contrast architecture and the number of layers. Thickness recommendations are given as well for the suggested substrate architecture [42].

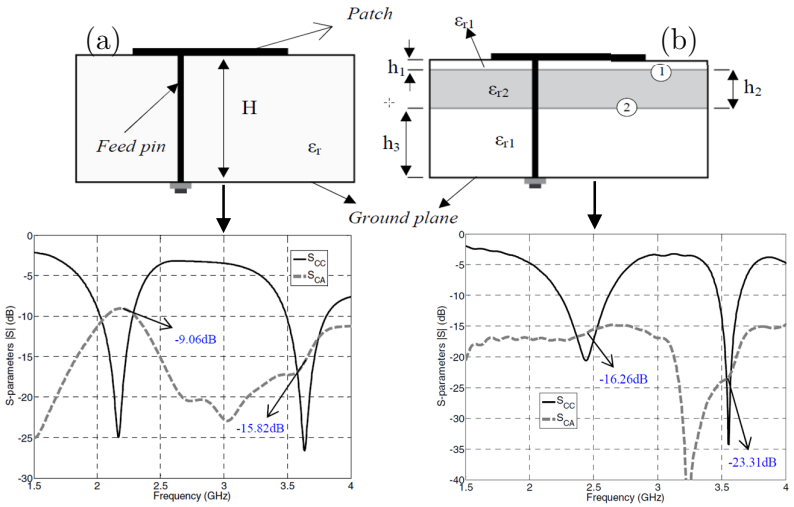

Figure 3.12: Homogeneous substrate (a) vs multilayer substrate (b) [42]

3.2.6.2 Superstrate-dielectric layer

In another concept, superstrate dielectrics can be on top of printed circuit antennas in order to enhance the gain, the radiation resistance and the efficiency of the antenna. The dielectric layer above the metallic antenna (see Figure 3.13b) acts as a coating cover which when properly designed becomes part of the antennas. A resonance condition is created by adjusting the dielectric thickness which ideally eliminates the surface wave excitation [43]. For this effect, the substrate thickness requires to be electrically thin. In an array, this can be considered as a method to reduce the substrate surface wave coupling.

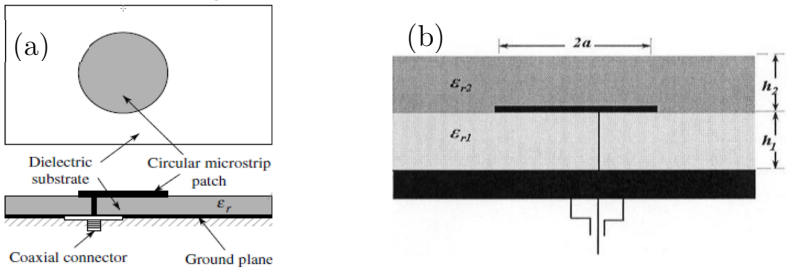

Figure 3.13: a) structure of a circular patch antenna b) microstrip antenna with superstrate geometry [44]

However, as demonstrated in [45] leaky wave modes couple the array elements (when a superstrate is used) which are deteriorating the embedded patterns directivity for close-by elements. Therefore, a trade off exists between the embedded directivity enhancement and a small antenna

element spacing. Last but not least, the antenna parameters are modified according to the properties of the super-layer dielectric [44].

3.3 Discussion

In the beginning of this chapter, two basic categories for MC reduction in antenna arrays have been addressed. The RF techniques have been preferred compared to decoupling networks. This was decided because they do tackle the impedance mismatch while various reduction techniques are provided in different architectures. Thus, the state of the art on RF mutual decoupling techniques followed.

Focused on design aspects for each technique the fabrication requirements were addressed. In parallel, the impact on the antenna elements tried to unfold, wherever was feasible from literature. Based on the examined decoupling techniques a selection is required in order to investigate the project assumption. The criterion for the desired selection is primarily ease of fabrication (regarding complexity and cost on current antenna arrays). It is worth to mention, that except the DGS case, rare information is provided on the array scan performance [38]. Therefore, it was not considered as a criterion for the final selection.

3.3.1 Comparative study

Cavities and neutralization lines were not selected, as they require fabrication complexity compared to parasitic elements and the defected ground structures. The metal cavities require substrate modification for the cylindrical vias while the feeding network for the neutralization lines becomes costly and complex. Moreover, the pattern characteristics for the neutralization lines can be affected by phase shifts from element to element, because of the metal interconnecting strips.

The 3D dimensional EBGs (considering also the mushroom walls) where not preferred as they are considered bulky and large along the H-plane which require extra fabrication cost and time. In the manufacturing procedure, technical pitfalls can lead in discrepancies from simulated data.

By comparing the planar parasitic elements (scatteres) compared to the UC-EBGs, the first technique which is investigated in this thesis is chosen. Parasitic scatteres based on a single RF element with a stop band behavior are advantageous than the planar EBGs because they are non-periodic, meaning less fabrication effort.

On the other hand we cannot neglect the multiple applications that a DGS offers. Compared to other methods, which have been referred in the previous paragraphs, it collects multiple properties which can be potentially applied in antennas arrays in parallel to MC reduction. Thus, considering the ease of fabrication and the requirement of no extra materials that a DGS offers, defected ground structures are also chosen as another technique that will be examined further (despite that the DGS design procedure is still not properly clarified in literature for array antennas). Moreover, as the concept of the antenna-DGS array design still remains quite open, this work aims to provide further insights where literature does not yet shows (e.g. planar array performance for active and passive antennas). Therefore, the effective DGS design for a planar array antenna is assigned as a research milestone. As mentioned for the parasitic elements, more detailed analysis for the DGS structures follows in the next chapter.

The dielectric substrate modifications (multilayer substrate or superstrate) although they avoid the external parasitic or resonating structures, require specialized substrate fabrication below the patch antennas (or above) which means increased cost and manufacture time. On the other hand, the aim of this work is to provide a decoupling method for current antenna arrays, which comes in conflict with the pre-design procedure of this technique. The multilayer structure can result in a designed array which departs from the characteristics of a current array performance. Therefore, the substrate dielectric contrast is left for future studies which it can be combined with compact parasitic elements or DGS. Moreover, this technique is more applicable for micro-strip patch antennas, which automatically limits further studies for dielectric resonator antennas.

3.4 Overview and selected techniques

The summarized RF techniques that they have been studied in this chapter are illustrated in Table 1. Overall, the planar fabrication and the non-periodic lattice requirement proved to be a common advantage for both parasitic scatteres and defected ground structures.

Although the selected methods (parasitic scatteres and DGS) are characterized by ease of fabrication the pre-design procedure is considered complex as closed form expressions are not provided. This forms another milestone for this project to provide insights on the design and the physical

phenomena of such planar decoupling structures in order to avoid the extensive use of optimization routines (and genetic algorithms).

Studies follow in the next chapter for these planar techniques by analyzing selected examples on parasitic scatteres and defected ground structures. Thereafter, a direction is given towards an effective RF structure which in combination with a desired antenna element (operating in a band of interest), makes possible to investigate the assumption of the project.

RF MC reduction Technique	Manufacturing complexity	Scan Impact
Metal cavities	3D layout Increased modular weight Vulnerable in fabrication errors (use of VIA)	N/A
Neutralization lines	Increased feeding complexity Metal strip acts as a delay line	N/A
Mushroom EBGs (3D) & Mushroom walls	Periodic 3D layout Increased modular weight Vulnerable in fabrication errors (use of VIA)	N/A
UCEBGs (planar)	2D periodic layout Requirement for multiple metalized elements Moderate modular weight	N/A
Parasitic scatteres (planar)	2D non periodic layout Low extra modular weight	N/A
Superstrate Dielectric	Extra coating dielectric Antenna redesign Questioned MC reduction applicability (Enhanced embedded directivity)	N/A
Multilayer substrate	Multi layer structure Antenna redesign Extensive substrate fabrication routines	N/A
DGS	2D non periodic layout No added materials	Limited Information [46]

Table 1: Overview on the RF decoupling techniques from experiments between two E-coupled antennas

4 Potential structures for MC reduction

4.1 Intro

In the previous chapter it was concluded that RF structures are preferred than decoupling networks for MC reduction. This orientation followed because the voltage compensation does not improve the impedance mismatch for the antenna elements [9]. Among a broad set of methods (§3.2) parasitic scatteres and defected ground structures, which require ease of fabrication, decided to examine further.

Micro-strip patch antennas are one of the widely fabricated elements in commercial designs. However, they exhibit high MC when used as array antenna elements. The strong inter-element transmission power can be attributed to near field, surface wave and space wave coupling. The near field coupling dominates when antennas are closely spaced. This field is particularly strong near the edges of the patch and decays fast ($1/r^3$). For a half-lambda distance, it is assumed that this coupling is less dominant than surface waves and space waves. However, this depends from the design of the element antennas that are used. Therefore, MC in micro-strip antennas, for radar systems, has two dominant coupling sources. Surfaces waves and space waves, (direct radiation and coupling between antenna elements through air, correspondingly) [47]. Depending on physical realization of array antennas (antennas on substrate or antennas on metal) the coupling through surface waves or through air-waves becomes more dominant.

Defected ground structures redirect and isolate surfaces waves, while the resonant metallic parasitic scatterers provide stop-band characteristics mainly for space waves. Therefore, selected examples presenting resonant and design properties for each class are given in order to make a selection. For this selection, the validation method which tests the structural properties is defined as well as the requirements for the desired structure are established in advance.

4.2 Validation method

In order to validate the decoupling efficiency of the chosen techniques, candidate structures were examined using a relative simple layout. The structure under study is placed between two E-coupled antenna elements,

meaning elements that they are coupled along the plane of the electric field. This layout makes possible to represent similar coupling effects as they are faced in the E-plane of planar arrays. This plane compared to H-plane couples stronger the antenna elements in 0.5λ array grid (see §2.1). Thus, it is chosen as the preferred coupling orientation for the antenna elements in the validation study.

Thereafter, it is able to examine a potential method or structure between the coupled elements for its effect on the antennas. This examination is based on parasitic excitation through the antennas MC. It is desired that according to structural properties redirection and isolation of the propagating waves between the antenna elements will happen.

From resource point of view, the full wave simulator in HFSS (that is used in this thesis) applies the numerically based finite element method, which when the design complexity is increased resources in memory and time are exponentially increased. By observing, those effects in a simple layout pitfalls are avoided for large planar arrays, saving time and memory storage.

Overall, the E-coupled antennas placed in 0.5λ distance are consider as an electromagnetic problem array simplification and a validation test for the structures under study.

4.3 Requirements on the structure for MC reduction

In literature, various shapes can be found as defected ground structures. This is because the resonators are useful in various RF applications (§3.2.5). However, the selected structure should satisfy some criteria. Thus, in order to select the appropriate structure the following requirements established:

- Broadband decoupling ability:
    - A structure being able to resonate for a broad range of frequencies. The two-element configuration defines a simple coupling mechanism. Maintaining a large bandwidth of isolation in this verification stage (which requires low computational resources) is important for further studies in array antennas. There the coupling phenomena are quite much more severe which are expected to degrade the decoupling performance

- Minimum impact on the coupled antennas:
    - The proposed structure should have the minimum possible impact on the impedance match of the already tuned elements. The chosen structure should make sure that the redirected fields dissipate in such a way that the antenna elements are not affected (impedance match-operational bandwidth, resonance frequency, degradation in pattern characteristics).
- Stable with the antenna element variations:
    - The RF element should be able to maintain its characteristic operation irrelevant to the nearby active elements. For instance, the element antennas impedance or resonance optimization should have minimum impact on the decoupling resonance of the structure
- Physical size adoptable in an array grid
    - It is critical that the geometry of the RF structure maintains a geometrical size that fits to the grid of an array. For this study, the maximum grid size is defined at 0.5λ. This means that the largest dimension of the proposed structure should not exceed 0.5λ of a desired resonance frequency

The established criteria define bounds that aim to make possible the application of the structure for further studies. For instance, in antenna arrays, where the elements are active, multiple interactions between the resonators degrade the performance of an embedded antenna element. In the same concept, a parasitically excited structure will get affected providing a less efficient performance when it is applied in a dense array.

4.4 RF class selection

Regarding the direction dilemma in RF structures between parasitic scatteres and defected ground structures, a study aimed to define a selection. Here two representative structures from each class are adopted from literature, in order to reveal their operation and impact on excited nearby antennas. The antennas used for each class are identical. Therefore, it is able to derive comparisons regarding the design, feed and radiation

point of view for the added structures as for the influence on the antenna elements.

4.4.1 DGS: Ring Resonator

A compact defected ground structure described by a ring layout proposed by [29] to reduce MC between E-coupled patch antennas. The relative small dimensions of the combined slotted rings compared to the antenna layout made this RF structure more attractive than others (e.g. U shape, Spiral Head, Arrowhead-slot). The proposed design provided good isolation for the first and the second harmonic, as each of the rings formed the required resonance stop bands in the primary and the secondary antenna radiating frequencies.

In the examples, which will be presented in this document the patch antenna design and material properties in [29] remain the same. The example in literature simulated, verified and modified for a favorable operation. The double ring resonator converted to a single ring resonator creating isolation in a particular resonance of interest. In Figure 4.2, S11 and material properties of the stand-alone antenna are presented.

The ring resonance response is feasible because of the difference between the inner and the outer ring radius, which define the stop band frequency. When the radius difference is modified, the periphery of the ring is adjusted proportionally by the displacement between the two radiuses. Therefore, currents in the ground plane (which follow the contour of the ring), will either resonate in higher or in lower frequencies accordingly. Thus, properly choosing the position and the correct difference in radius results in a desired stop band.

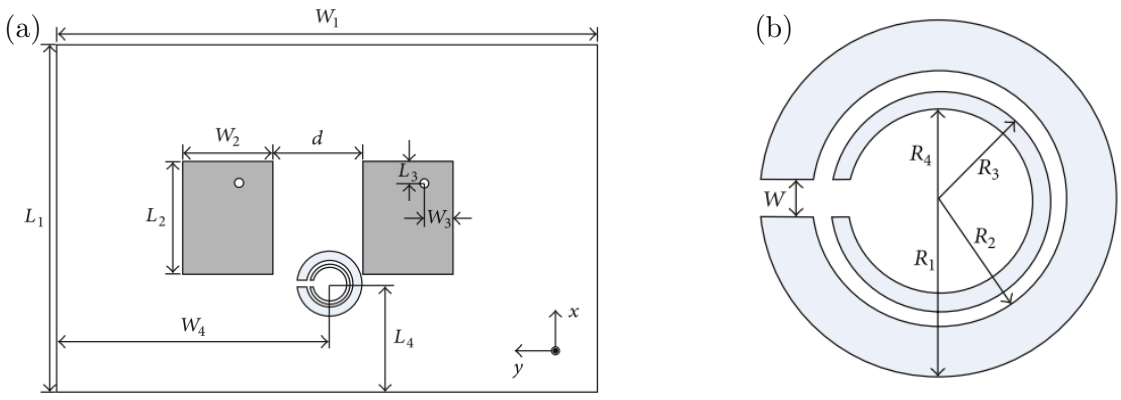

Figure 4.1: MC reduction by a double ring resonator DGS: (a) geometry of the patch array (b) geometry of the proposed defected ground structure [29]

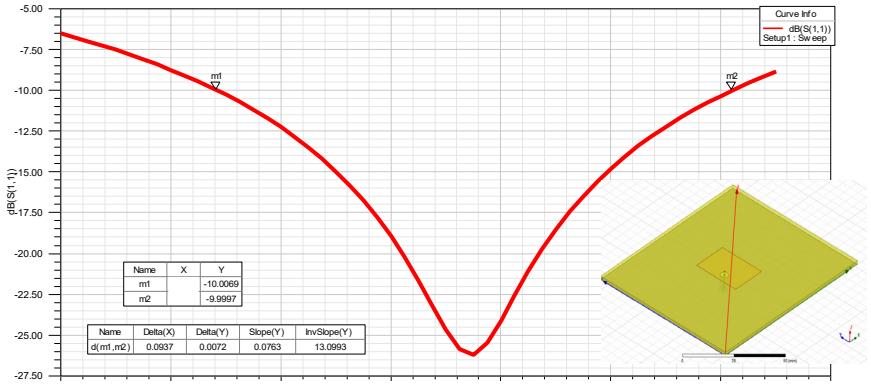

Figure 4.2: Single mictrostrip patch antenna used by [29]: Substrate EpoxyFR4 er=4.4 and tand=0.02, BW=0.0937GHz

Correct positioning is critical as it defines the efficient coupling reduction. The small shape, which characterizes the magnetic resonator, allows it to get in proximity to one of the patch antennas. This helps to maintain similar properties as it would have been excited below a microstrip line. Specifically, the ring is located below one of the patch slot corners, close by the nearby antenna element. Therefore, the high intensity fringing fields excite the DGS which forms an alternative decoupling path for the patch antennas. The surface currents are trapped around the DGS periphery instead of travelling along the ground plane. These currents are created, primarily, by the excited surface waves in the substrate. As the currents and the fields are coupled, the traveling surface waves convert to standing waves on the slots of the Ring DGS. Thus, MC is reduced between the element antennas (deeper reasoning how a DGS dissipates the excited energy is provided in

§6.4). To confirm this reasoning, for a desired stop-band resonance the S parameters of the E-coupled elements with and without the tuned ring are illustrated in Figure 4.3.

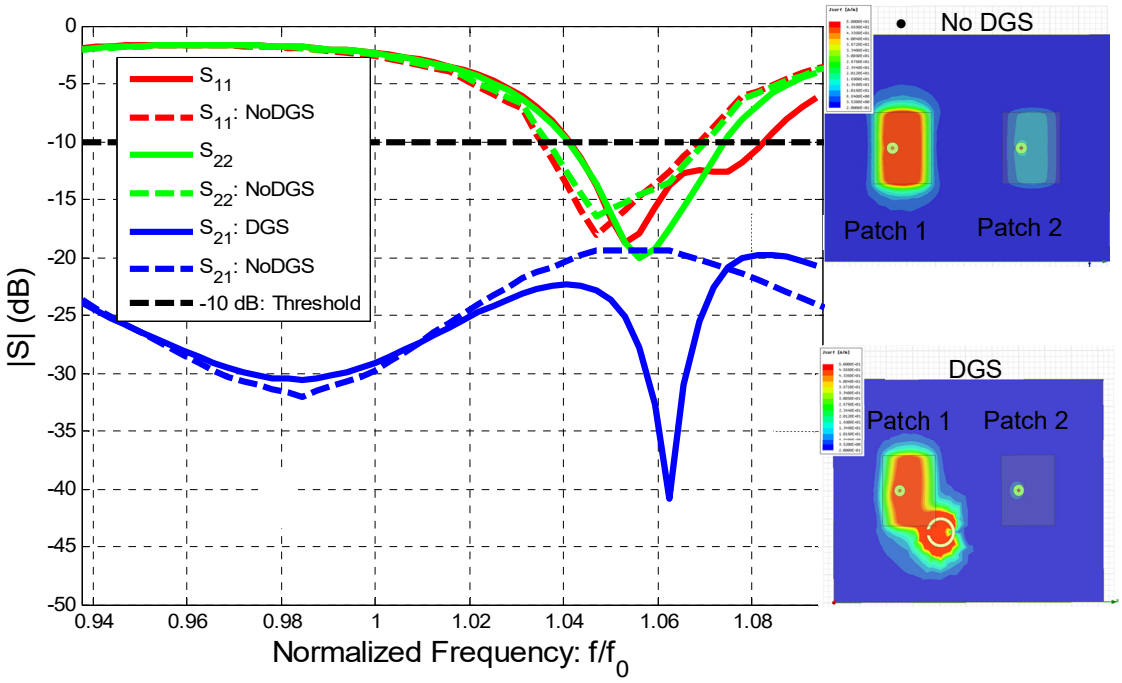

Figure 4.3: S-parameters of a two element patch array with and without the ring DGS and inlet layout pictures. The colors in the inlet pictures present the magnitude of the surface currents on the ground plane without (LHS) and with a DGS (RHS). In both cases the maximum value is the same (red color). The DGS causes reduced MC-by trapping the surface currents along its periphery (more info see § 6.4)

	DGS	No-DGS	BW DGS/ No-DGS
S11	BW: 0.1319 GHz	BW:0.1075 GHz	1.226: 22.6% BW increased
S22	BW: 0.1078 GHz	BW: 0.1075 GHz	1.002 0.2% BW increased
MC			Reduction
S21 (at 1.06 f0)	-40.9243 dB	-19.5 dB	21.42 dB

Table 2: Ring Resonator between E-coupled micro strip patch antennas: Return loss, antenna BW and MC with and without the DGS

The patch antennas are asymmetric with respect to the location of DGS after effectively placing it and tuning it. Therefore, the return loss from the

antennas is not coinciding. The cause of the asymmetry is due to the excited ring, which is producing capacitive effects to the adjacent to it antenna. However, this is not consider as a disadvantage as the operational bandwidth remains the same for Patch2 while enhanced BW occurred for the patch in the DGS proximity (22.6% increased compared without DGS). The measured coupling coefficient regarding the frequency where the DGS is resonating has been reduced by -21dB. Detailed results are presented in Table 2.

4.4.2 I-section parasitic scatterer

Parasitic scatteres, which are placed on top of a substrate, are efficient when the space wave coupling is strong. This effect takes place when the antennas are printed on a dielectric substrate which its thickness is small compared to the wavelength [48]. A characteristic example demonstrated in [49] where E-shape microstrip patch antennas were decoupled by a parasitic single metal resonator referred as I-section (PIR) (Figure 4.4). Here a similar PIR layout is designed for the coaxial feed rectangular patch antennas, which were used for the single slot ring resonator (§4.4.1).

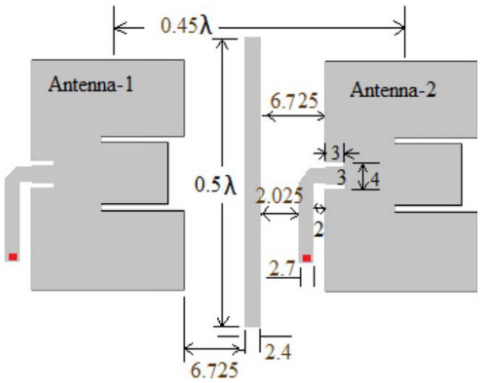

Figure 4.4: E-shaped microstrip patch antennas and an I-section parasitic scatterer [49]

For the effective MC reduction by the PIR, two adjacent I-sections were placed asymmetrically on the substrate between the coaxial feed patch antennas (Figure 4.5b). This combination created an indirect coupling path which when the design was optimized in resonance and position, two signals in comparable amplitude interfered destructively. Specifically, the H plane length of the resonator is close to half-wavelength in free space and $3\lambda/2$ wavelength in the substrate after tuning.

The structure is characterized by a simple shape and achieves (at resonance) reduction of -12 dB in MC, as shown in Figure 4.6. However, the optimization procedure concluded that this structure exhibits extreme sensitive tuning performance. Any variations in the design (antennas variation, displacement or impedance match) were detuning extremely the scatteres. Regarding the demonstrated example, the operational BW remained the same while it follows an asymmetrical trend at the reduction resonance for both antennas. The asymmetry is caused by capacitive interaction which occurred from the discontinuities in the metal-dielectric parts that separate the antennas with the PIR.

MC	PIR	No-PIR	Reduction
S21 (at 1.043 f0)	-30 dB	-18 dB	12dB

Table 3: I-Shape parasitic scatterer coupling reduction

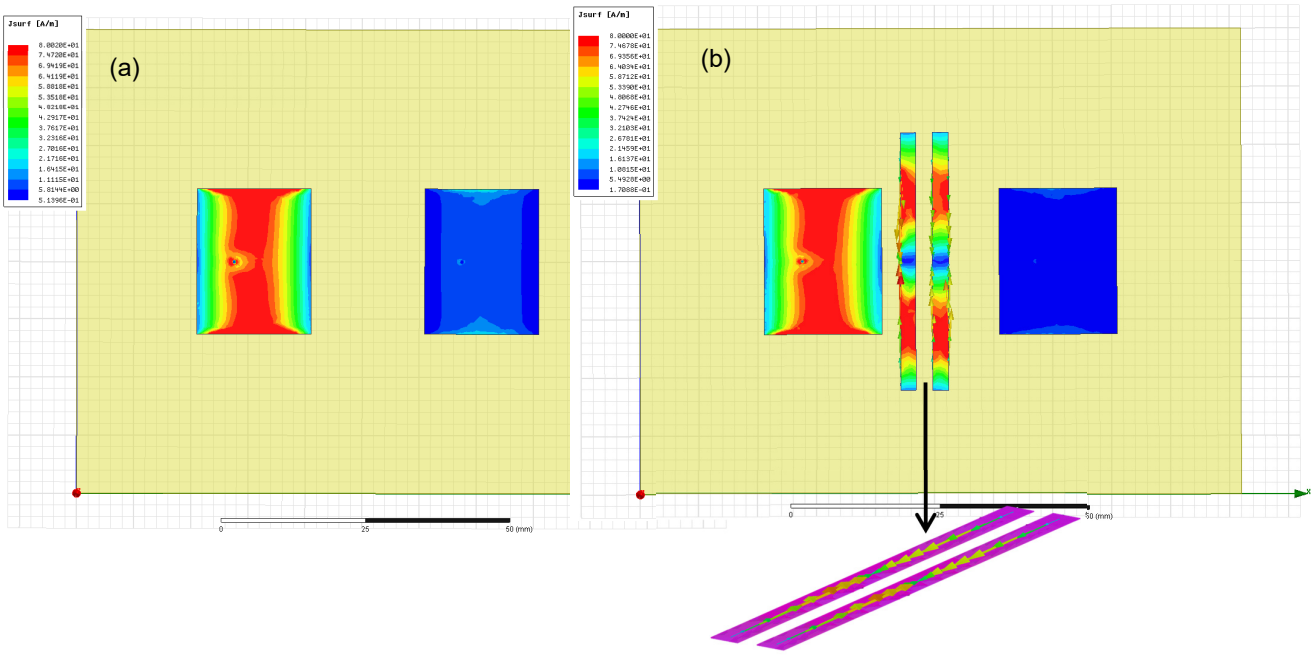

Figure 4.5: Parasitic I section resonator (PIR) and array Patch surface current: magnitude and vector representation: a) without PIR b) with (PIR). The arrows in (b) denote the high surface currents intensity on the PIR. Those PIR surface currents are excited on it which are destructively canceled.

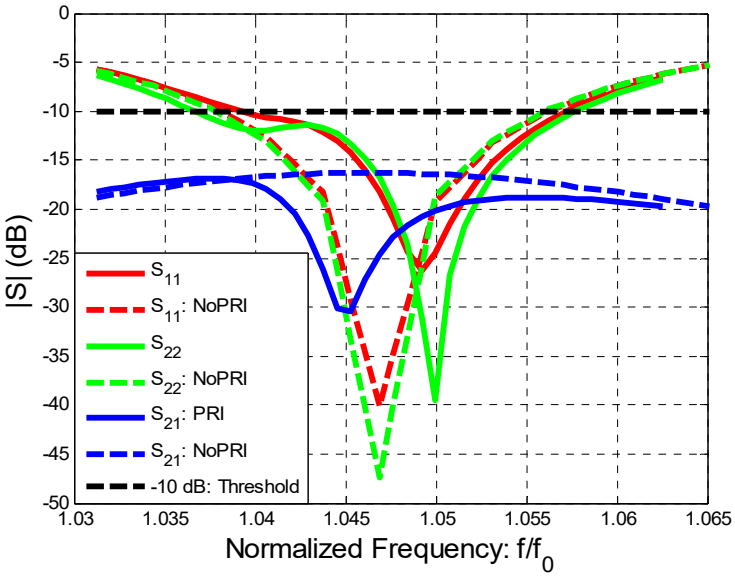

Figure 4.6: I shaped parasitic resonators between E-coupled patch antennas:

4.4.3 Radiation aspects ring DGS vs. PIR

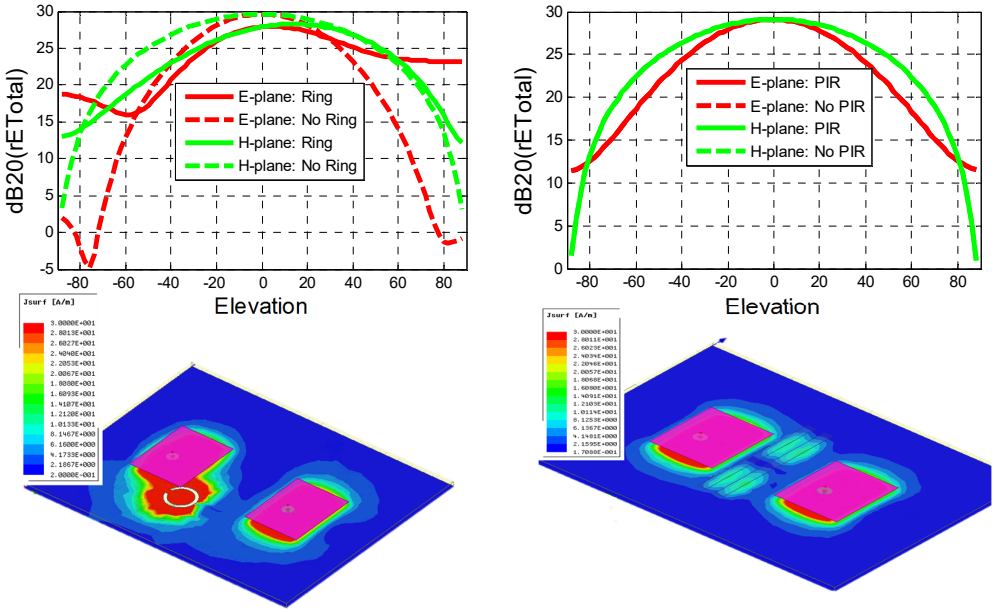

Figure 4.7: Array radiation pattern comparison between the defected ground structure (a) and parasitic I section (b): Solid lines represent patterns with resonators. For both illustrations red represents E-plane and brown H-plane. Below the patterns the corresponding designs are illustrated which are focused on the ground plane surface currents when the Ring and the PIR resonate. For the two cases, both antennas are excited and the maximum complex magnitude (red) is the same.

The simulated radiation patterns for the two element patch array at the effective resonance for the DGS ring resonator and the I-section parasitic scatterer are plotted in Figure 4.7. The difference in the pattern without a decoupling method is attributed to the non-identical resonant frequencies between the DGS and the PIR. This is because the PIR was extremely sensitive to be tuned exactly on the same resonance as the DGS.

Regarding the DGS case, the radiation pattern of the patch array (pattern obtained by exciting both elements) with the DGS is influenced for both planes. For wide angles in E plane (red), the radiation levels are enhanced and broader for the configuration with a DGS. However, the magnitude level decrease at broadside, which can be given to increased back lobe radiation and to the non-equal effects for the patch antennas. Patch 1 is loaded with the ring resonator while Patch 2 is less affected, as it is further away from it. Therefore, some asymmetries are shown in the pattern. Similar effects are seen in H-plane for the DGS ring resonator. These asymmetries are expected to be equalized for a planar array, as all the antenna elements will be equally loaded by DGS.

On the other hand, the radiation pattern is not affected by the resonant PIR. The currents that excite the PIR are flowing in opposite direction. Therefore, this causes cancellation of any PIR radiation.

4.5 Discussion

Overall, both methods are able to reduce MC. However, the parasitic scattering technique is not preferred because of the sensitive resonance shift behavior with the design variations §11.1. As experienced, displacing the antenna elements or impedance match tuning affect the resonance of the scatterer. Moreover, it is characterized by extreme narrowband resonance frequency and in a dense array the resonant characteristics can be detuned and become inefficient. Furthermore, the capacitive effects that reform the operational bandwidth did not provide any BW enhancement as in the DGS case. It is important to add that for PIR the length of the optimized resonator is greater than half lambda in free space, which is significantly larger than the DGS and exceeds the requirements of 0.5 lambda. On the other hand, the DGS in a compact layout affects in a positive way the operational bandwidth, promises to benefit the pattern for wide angles with a slight reduction in radiation levels (the last effect will be tackled later on).

Overall, the class of defected ground structure is further analyzed in the next chapter in order to provide an effective structure, which is in-line with the requirements in §4.3.

5 Verification of DGS properties for MC reduction

5.1 Intro

The DGS validation analysis demonstrated that not only it can be a decoupling method for antenna elements but it can also provide bandwidth enhancement, if is in proximity to the element antennas. Furthermore, a structure needed to be defined satisfying bandwidth and design constrains. The examined Ring resonator is characterized by a narrowband resonance. Therefore, ways to provide a desired broad resonant DGS structure followed.

5.2 Antennas on substrate:

5.2.1 Two ring resonators below edge slots

In this section steps towards the enhancement of the reduction of MC between antenna elements in wider frequency band were made. In order to provide broader frequency isolation the additional ring of slightly different dimensions was applied. The secondary ring was modified such that it provided a slightly lower resonance close to the primary tuned ring. Therefore, by merging both resonances enhancement for the isolation bandwidth was expected.

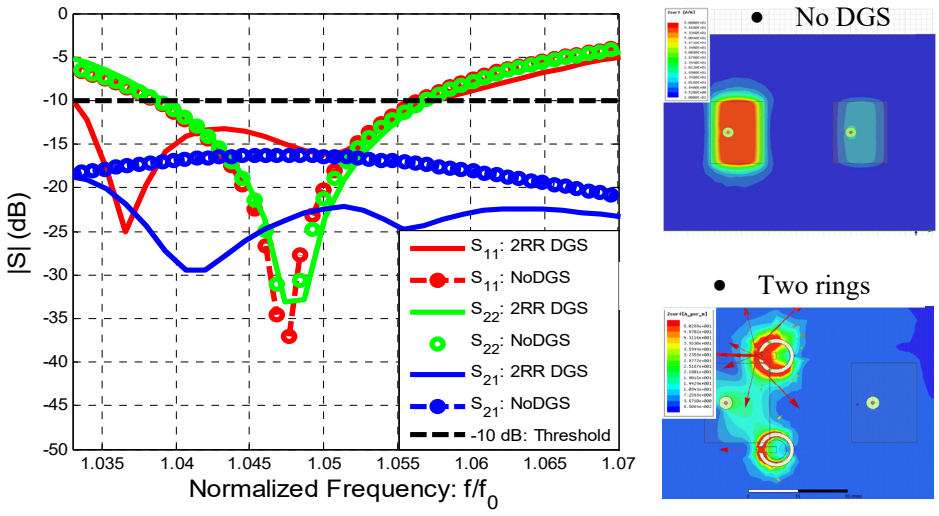

Figure 5.1: Two ring resonators in adjacent resonances

Figure 5.1, illustrates the tested configuration and the simulated S parameters. Indeed, in transmission two resonances are shown. However, the previous ring performance has been altered as the two rings interact (the secondary ring was excited dominantly). BW enhancement is shown for the patch antenna that is near the rings while the BW of the other patch remains unaffected. It is important to note that the achieved BW enhancement is not sufficient to fulfill the requirements given in section 4.3. Based on that further experiments were conducted.

5.2.2 Extended arms-dumbbell (etched dielectric):

The narrowband properties of the ring resonator emerge the need for an alternative structure. Moreover, MC in microstrip patch antennas depends on the substrate design with respect to the operational frequency ($\lambda_g = \frac{\lambda_0}{\sqrt{\varepsilon_r}}$). The substrate thickness and the chosen dielectric properties define the operational BW as well as the portion of power, which is given in surface waves, airwaves and near fields. Studies on the substrate antennas show that for a strong surface wave excitation the substrate thickness should be larger than $\frac{0.3\lambda_0}{2\pi\sqrt{\varepsilon_r}}$ [50]. In the examined case of the ring resonator, the substrate thickness was not verifying this condition. Therefore, the air-wave caused stronger coupling than the surface waves.

The above considerations inspired this study to face globally the coupling mechanisms by developing a compact and centered DGS (Figure 5.2). The dumbbell layout characterized by extended arms, was tuned to the patch antennas resonance and used instead of the ring resonator between the element antennas. In addition, the substrate area above the defection was etched out. Thus, the DGS was excited by surface and airwaves (Figure 5.2).

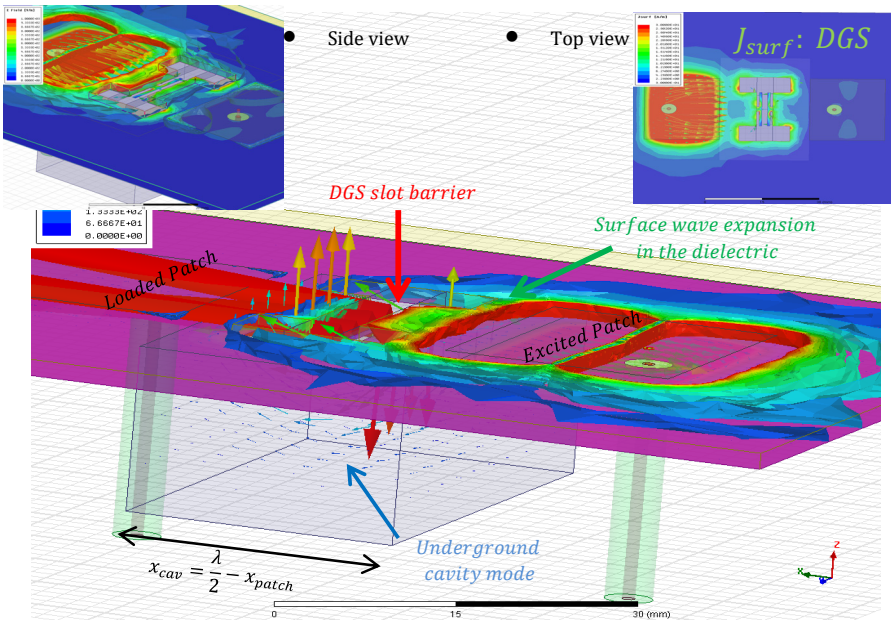

Figure 5.2: Dielectric substrate surface wave expansion and evolving resonant mode in the underground cavity: Electric field magnitude inside the dielectric substrate

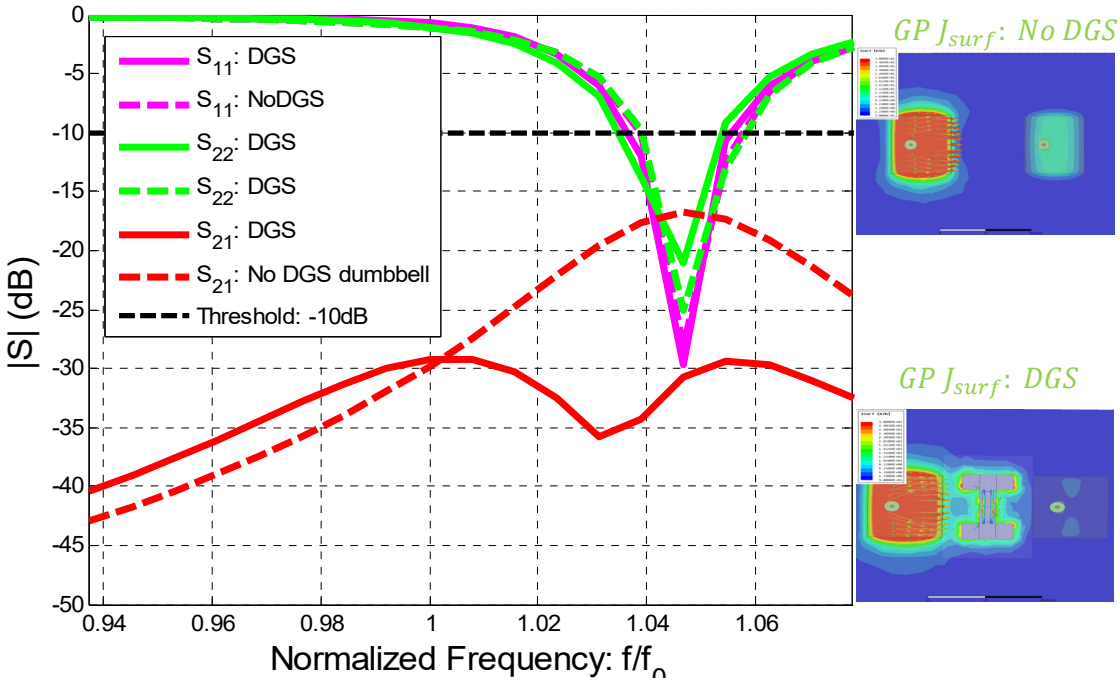

Figure 5.3: Dumbbell DGS with extended arms between E-coupled microstrip patch antennas: S parameters with and without DGS

The simulated S-parameters are shown in Figure 5.3. The centered DGS position equalizes the capacitive effects thus the resonance frequency for both antennas is maintained without any shifts. However, the difference in the return loss levels occurred because of the not-equal pin distance, in each patch, with respect to the DGS. In terms of MC, the reduction compared to the ring cases is improved and maintained for a broad range of frequencies. Summarized data is given in Table 4.

	DGS	No-DGS	BW-DGS/ No-DGS
S11	BW: 0.0624GHz	BW: 0.0621GHz	1.0048 0.48% increased BW
S22	BW: 0.0624 GHz	BW: 0.0621GHz	1.0048 0.48% increased BW
MC			Reduction
S21 (at 1.043f0)	-32.2355	-16.7836	15.452dB

Table 4: Modified dumbbell between E-coupled microstrip patch antennas: Reflection coefficients, operational BW and MC with and without the DGS

The results above are considered satisfactory as the reduction in MC is not only in a narrowband spectrum. In contrary to the ring resonator, by removing the dielectric area above the DGS the structure was able to redirect also the air-wave coupling which led to a broader isolation bandwidth. Although this technique can be considered as feasible, it demonstrates that the microstrip patch coupling drives limitations in the decoupling performance of a DGS.

5.3 Antennas on metal plate:

In the previous paragraph, it has been demonstrated that the effectiveness of a defected ground structure can vary with respect to the strength of the coupling source. Regarding the coupling source in substrate antennas, the dielectric properties and the stratification thickness define the strength of the excited surface waves. It was realized that continuing the research this direction can provide solutions only for a certain configuration between patch antenna and its substrate.

In order to make further study independent on the substrate properties it was decided to continue the research towards the antennas located on the metal plate. As a test antenna rectangular dielectric resonator (RDRA) with probe feeding was used as shown in Figure 5.4a. That way it was decided to make closer look on the MC reduction via near field air waves.

The RDRA design aimed to provide broader operational bandwidth than the micro strip patch antennas. This was able by the 3D geometrical rectangular shape in combination with a not high relative permittivity material. Moreover, the design still considered lattice constrains of 0.5λ array grid. Therefore, the multi-parameter antenna design flexibility makes possible of a broadband antenna able to fit in 0.5λ grid (Figure 5.4c).

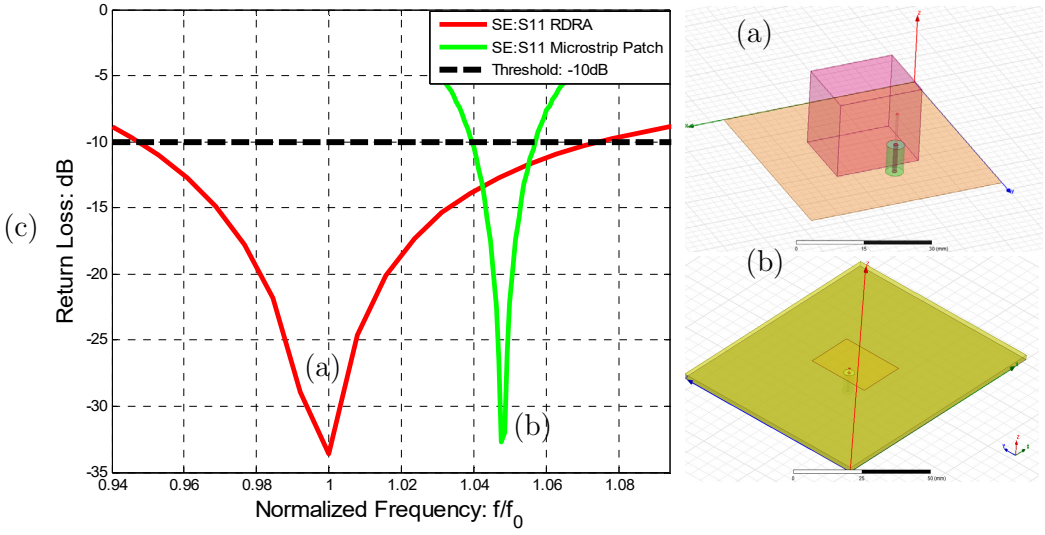

Figure 5.4: Broadband rectangular dielectric resonator antenna compared to the micro-strip patch

5.3.1 Slot DGS between RDRAs

A simple and accurate model for a slotted ground plane (SGP) is demonstrated by [51]. This model aim to connect the inductive and capacitive effects to the coupling mechanism between a micro strip line and periodic slots in the ground plane. Furthermore, the slow wave and the filtering properties are explained by the supporting coupled modes. These modes when coupled effectively (if the slot is centered below the microstrip line) excite standing waves on the slot (see Figure 5.5).

$$f_m = m\frac{c_0}{2d\sqrt{(e_{eff}^{slot})}}$$

m=1,2,3,4..

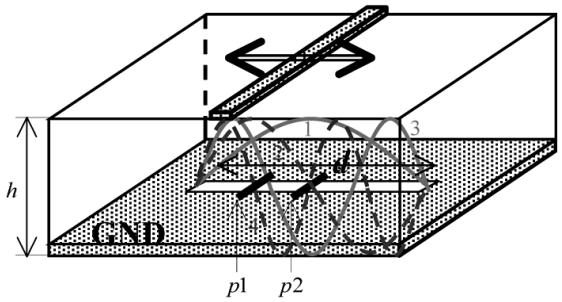

Figure 5.5: Supporting resonant modes by a ground plane slot coupled by a microstrip line [51]

As it is referred, when the microstrip line is excited at one of resonant frequencies (f_m) coupling to slot is achieved. From their experiments, it was concluded that when a slot is centered below the microstrip line only odd modes can be excited. This is because even modes have a null at the slot center, thus coupling to the slot is not accepted.

Considering the slotted ground plane concept, the resonator antennas can similarly act as coupling sources to a slot which is placed in a center location between them. To demonstrate this, two E-coupled RDRAs in S-band have been desirably tuned and located at half-lambda distance away. Between the RDRAs, in a center position a slot is designed on the fundamental mode (f_1, equation in Figure 5.5). The S-parameters are plotted in Figure 5.6 with and without the slot.

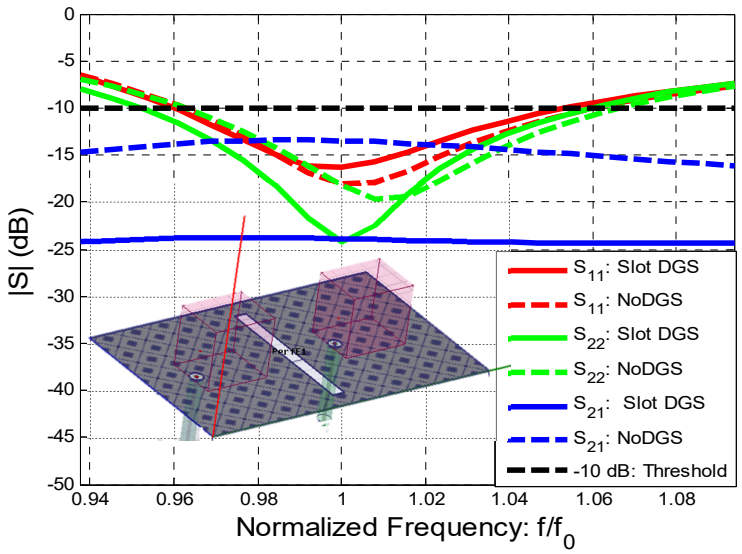

Figure 5.6: E-coupled RDRAs with and without a slot DGS

By applying the slot between antenna elements MC has been reduced by 10dB. It is important to mention the slot size in H-plane. The transverse slot (with respect to the RDRAs E-plane), physically equals exactly to half lambda compared to the RDRAs resonance frequency.

5.3.2 Slot between RDRAs backed by a large cavity

One can say that the broadband MC reduction achieved with the slot DGS resonator is acceptable (Figure 5.6). However, the flatness of the coupling reduction indicates that further improvement can be achieved. This can be extracted by comparing the ring resonator transmission (S21) response which it was characterized by a resonance pole.

As it is demonstrated by [52], [53], a secondary metal ground plane can enhance the DGS stop band. In details, by [12] the use of defected annular concentric rings below a microstrip-line (as well as between circular patch antennas) were used to provide an electromagnetic band gap response.

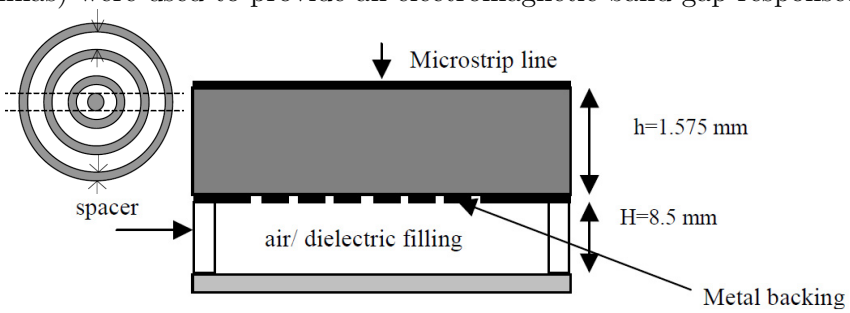

Figure 5.7: Defected ground plane backed by metal plate [52]

Among their studies, the use of another backing metal plate was examined for different dielectric fillings and spacing (Figure 5.7). The measured transmission coefficients with the backed metal plate resulted in enhanced stop band response.

In a similar concept, a large cavity was formed below the single slot-DGS which was placed between the E-coupled RDRAs. The S-parameters plotted in Figure 5.8, show enhanced MC reduction and a resonant pole. Specifically, at the lower and highest frequencies (where the antennas exceed the radiation threshold) -14dB and -22dB reduction in coupling has been achieved while at the resonant pole -30dB of reduction is observed. Design aspects about the cavity will be discussed in the next chapter.

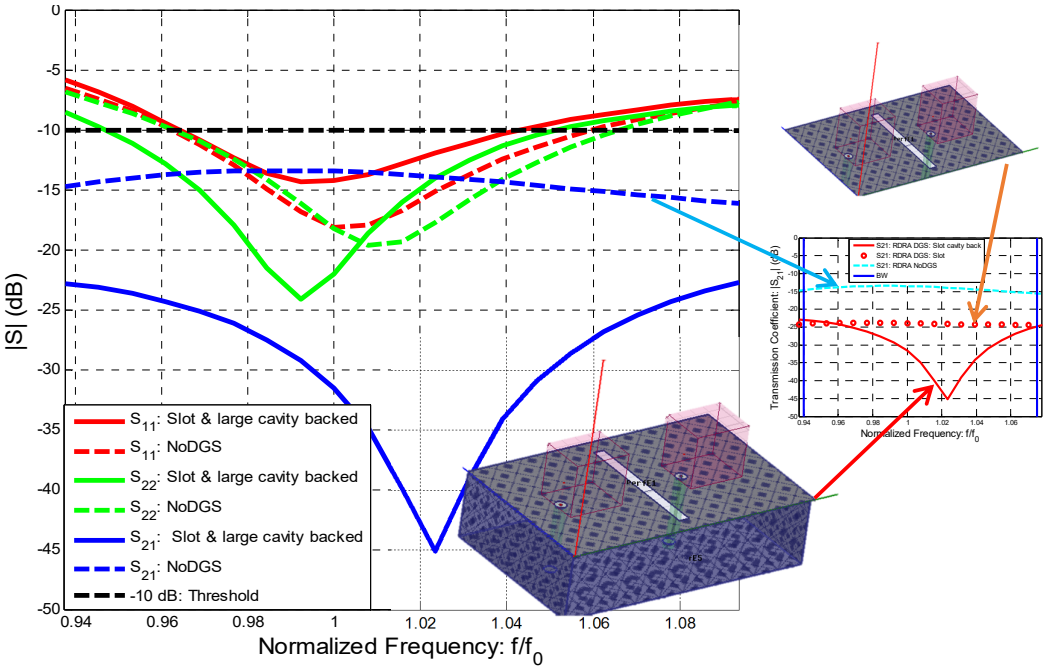

Figure 5.8: E-coupled RDRAs with and without a backed cavity slot DGS

5.3.3 Backed cavity slot DGS sensitivity test

The broadband isolation that the slot DGS provided for the coupled RDRAs satisfied the first constrain of the requirements given in section 4.3. In addition, Figure 5.8 illustrates the impedance match for the two resonators with and without the DGS. The slot DGS, by reducing MC, decreased the capacitive effect that it was build-up between the resonator antennas. Therefore, the two resonances shift slightly in lower frequencies. Moreover, the difference in the return loss levels is because of the non-equidistant position of the probes with respect to the DGS. Nevertheless, compared to the experiments on microstrip-patch antennas, the operational bandwidth for both radiators remains in a symmetric form. Based on that, the DGS slot impact on the antennas is considered negligible. This satisfies the secondary DGS constrain regarding the minimum impact on the coupled antennas.

The next constrain requires to test how sensitive is the DGS by the dimensions of element radiators. In this concept the RDRAs geometrical dimensions, in E and H plane (the height remain the same), where linearly varied in order to shift the resonance frequency of the radiating elements.

This aimed to observe how the DGS would react to those shifts. Figure 16 illustrates this experiment by comparing the return loss levels of the two radiators and the corresponding transmission coefficients. Specifically, Figure 16c shows that although the resonance frequency of the radiating elements was tuned from 0.975fo to 1.022fo the DGS provided stable mutual coupling reduction, with a transmission pole close to 1.02fo. The demonstrated stop band stability of the cavity backed slot DGS is superior compared to the DGS single Ring resonator and the PRI resonant structures, which were used for the micro strip patch antennas (see appendix §11.1). In addition, the reduction in MC presented slight small level variations which still remain below -20dB in the whole band. Based on that it can be stated that, the frequency stability requirement of the DGS is also satisfied.

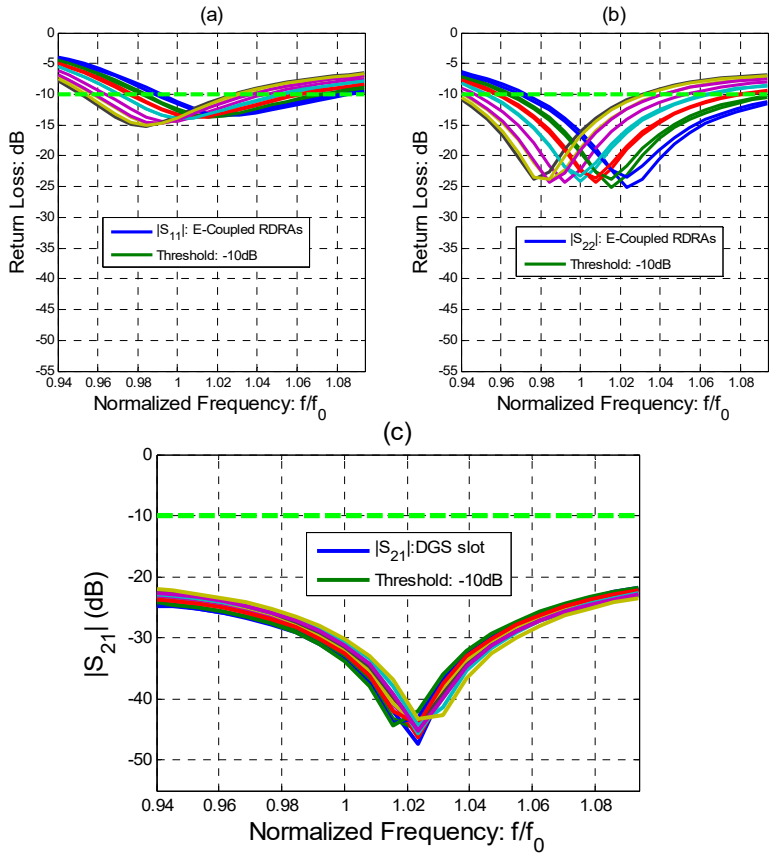

Figure 5.9: Resonance sensitivity of the backed cavity slot DGS by geometrical variations on the antennas: a) RDRA1 impedance match b) RDRA2 impedance match c) coupling coefficient between the RDRAs

5.4 Discussion

Having determined that a DGS is suitable for further studies, the definition of a structure with a relative large bandwidth was the purpose of the chapter. By performing various numerical experiments it was revealed that the BW requirement couldn't be satisfied just by the candidate DGS structures. The coupling mechanism between the antenna elements is affecting the efficiency of a DGS. This was revealed by experiments on substrate antennas. Therefore, in order to make further study independent on the substrate properties it was decided to continue the research towards the antennas located on the metal plate. From both studies the summarized conclusions are given here.

The examples on micro strip substrate antennas indicated that:

a) A DGS structure characterized by narrowband response, in a DGS array composed by elements similar to its self -replicated and modified for adjacent resonances - can provide merging of adjacent frequencies thus enhancing the electromagnetic band gap response (see §5.2.1).

b) For MC reduction by a DGS, the dominant coupling mechanism needs to be taken into account. The DGS is primary excited by surface currents between coupled antennas. These currents are created by surface waves that are guided between the substrate and the ground plane. Therefore if the air-wave coupling is dominant cross talk will still exists even if the DGS is able to redirect any surface waves. A DGS combination with parasitic scatterers can be suggested for these cases (see §5.2.2).

c) Modifications in the substrate design which aim to guide all the coupling sources towards the DGS can be a way towards sophisticated efficient decoupled designs (see §5.2.2).

The examples on a metal plate indicated that:

a) coupling between dielectric resonator antennas is a similar excitation source for a DGS as it would have been placed below a microstrip line

b) the slot DGS in electrical length of half-lambda, at a desired resonance, can decouple efficiently dielectric resonator antennas placed above a metal plate
c) the backed-metal plate reformed into a large cavity can enhance the performance of a DGS

Overall, Figure 5.10 summarizes all the demonstrated coupling reductions that were achieved for the configuration of two E-coupled antennas (from the trials in this chapter and the previous). The back-cavity-slot DGS between the RDRA elements (red solid curve) is having the broader and the deeper coupling reduction. Furthermore, the broadband operation of the chosen RDRA elements in combination with the broad DGS MC reduction properties makes this antenna-DGS element combination the most suitable.

In addition, this antenna-DGS element combination satisfies the needed constrains that were established at the beginning of this chapter regarding the definition of a broadband RF structure. Therefore, the slot DGS is selected for further studies to satisfy the array grid limitations, which will follow in the next chapter.

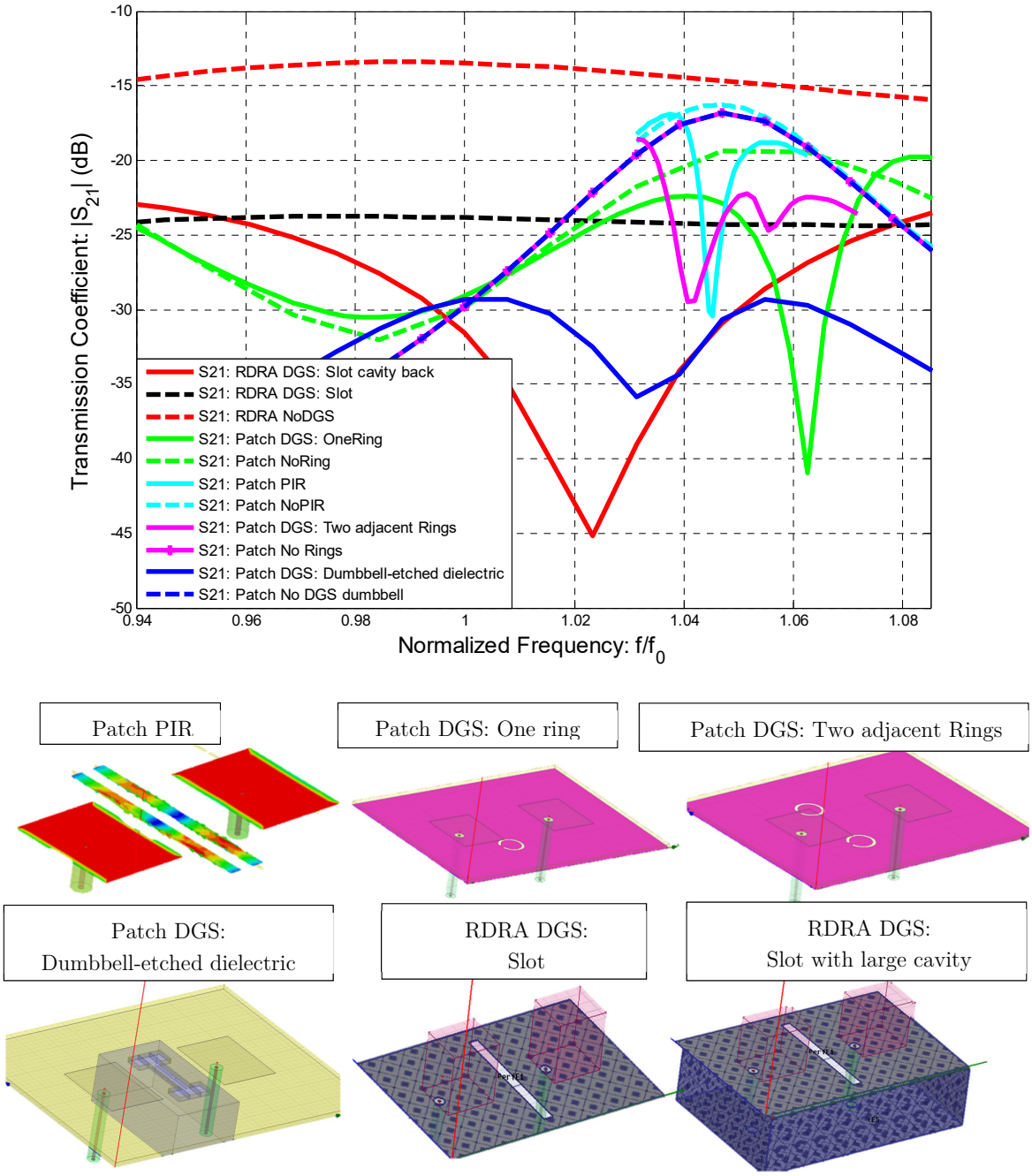

Figure 5.10: Transmission coefficient for all the trials with and without a resonator and the corresponding design configurations

6 DGS array element synthesis

6.1 Intro

The bandwidth and sensitivity constrains, which were established in the previous chapter, defined the DGS-antenna design of a magnetic slot resonator combined with a rectangular DRA element as acceptable. However, the tuned H-plane DGS length is restricting its application for an array defined by a 0.5λ element separation. Therefore this chapter, is focused on modifying the slot DGS to synthesize a design that is satisfying bandwidth constraints and in parallel allowing for frequency tuning possibilities, regarding an array lattice of 0.5λ. Furthermore, the multi element inter-DGS interaction is studied by analyzing the DGS radiating nature and as well as a supporting underground structure is provided.

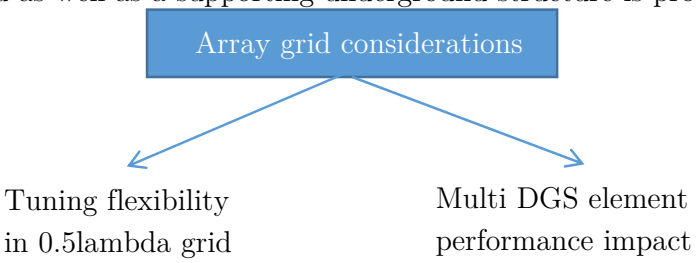

Figure 6.1: Array constrains

Overall, the final proposed RF structure makes use of a modified dumbbell DGS, backed by a compact cavity with the scope to provide the necessary isolation as well as frequency tuning operation.

6.2 From a slot DGS to a Dumbbell DGS

Considering a dense array, multiple defected structures can be distributed periodically. A rectangular grid defined with a lattice of 0.5λ, limits the spacing between two adjacent defections. An acceptable resonator should be well confined in the antenna element separation. Therefore it is required that its larger dimension should be smaller than 0.5λ. This limitation is obvious in H-plane where the slot DGS for the dominant magnetic mode is exactly 0.5λ (see Figure 5.8).

In order to obtain the DGS structure that fits comfortably in 0.5 lambda grid and in parallel has stop-band transmission characteristics at lower frequencies additional modifications are necessary. Therefore, the need for

physical modification for the same electrical length led to another similar structure referred in literature as dumbbell [33].
The transition from the slot to the dumbbell resonator can be explained by the concept of meander lines. These lines with their versatile shapes aim to create an alternative design solution by re-arranging the structure of a design, maintaining similar electrical properties. While the physical shape is altered the electrical length remains unaffected [54]–[56]. Likewise, the dumbbell defected ground structure is advantageous compared to the slot DGS as it provides 4 (a, b, c, g) parameters of design freedom instead of 2 (a, b) (see Figure 6.2). Applying it between E-coupled rectangular dielectric resonator antennas maintained similar wide stop-band as the slot case (see Figure 6.3d: (b)).

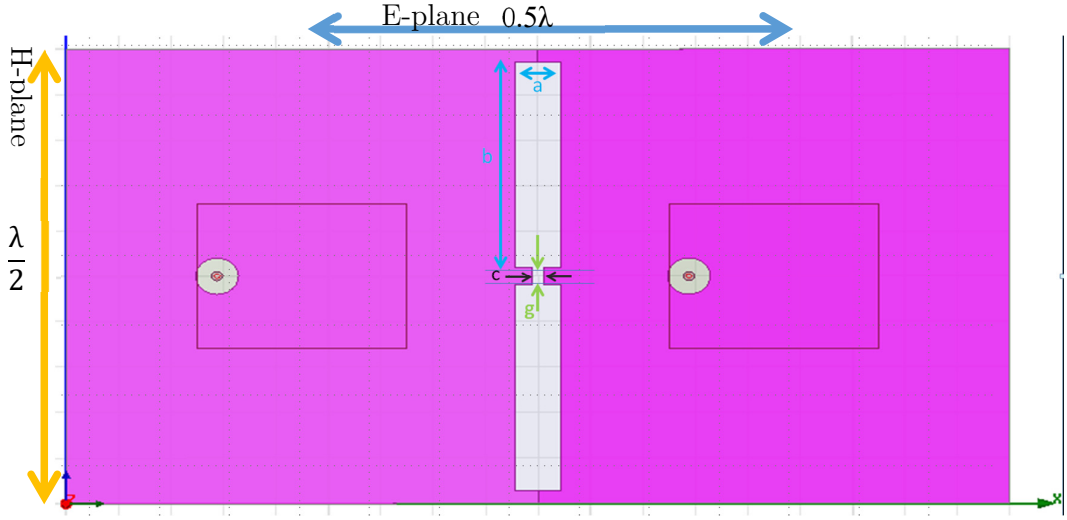

Figure 6.2: Comparison between the array grid lattice and general dumbbell DGS (dimensions of S-band)

The general dumbbell acts as a magnetic dipole resonator. This means that the most critical dimension is the resonance length in H-plane. This conclusion comes from the design process that it was used for the general dumbbell; it's synthesized by reforming a half wavelength slot. However, still the overall length in H-plane was barely able to fit (~0.95λ) in a half lambda array grid. Parameters c and g (see Figure 6.2) allowed to resonate at ~0.95λ/2 instead of λ/2. Consequently, small variations are allowed for tuning by parameter b if resonance at lower frequencies is desired. Figure 6.3c illustrates this concern as the general dumbbell has already reached the limits of the array grid.

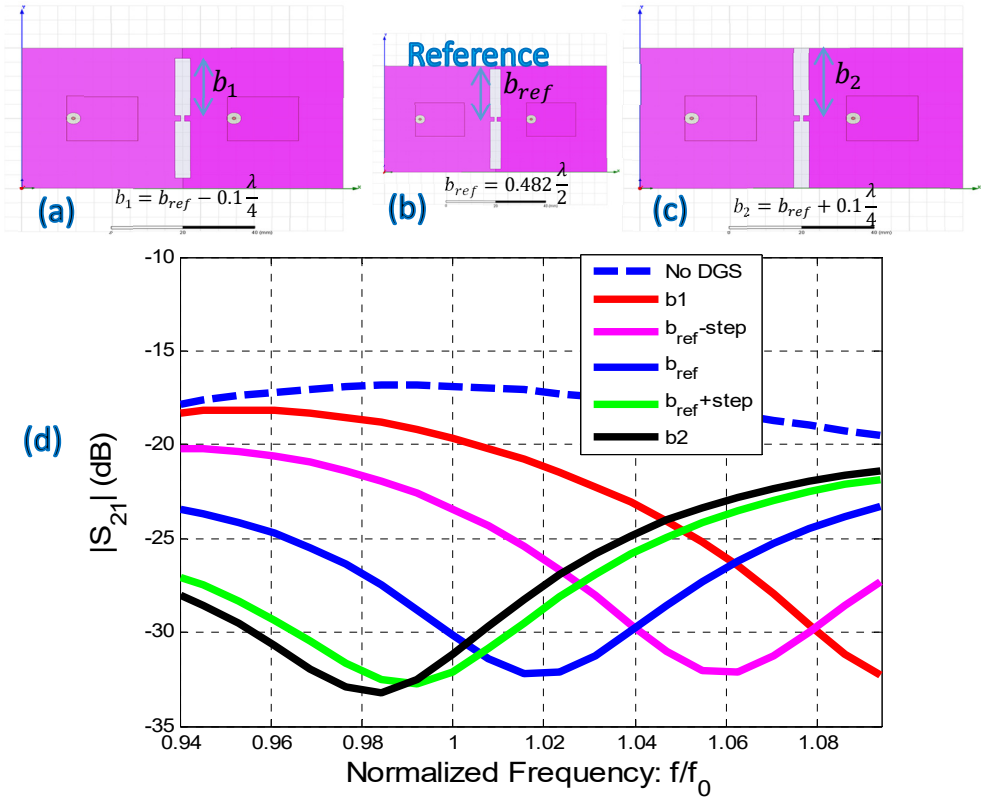

Figure 6.3: General dumbbell tuning abilities by parameter b: a) $b_1 = b_{ref} - 0.1\frac{\lambda}{4}$, b) $b_{ref} = 0.482\frac{\lambda}{2}$ c) $b_2 = b_{ref} + 0.1\frac{\lambda}{4}$ d) E-coupled RDRAs transmition coefficient for linear b variations from reference compared to no-DGS

6.3 Modified Dumbbell

As it is shown on the presented examples (Figure 6.3) basic tuning parameters where not enough to reduce the size of DGS, therefore further modifications where needed.

In a similar concept, for micro-strip line filter purposes, [57] altered the general shape of a dumbbell DGS by lengthening the etched gap areas to provide a compact shape, thus operating in lower frequencies (Figure 6.4). This reasoning can be explained referring to similar modifications, which are done on antennas. Structural irregularities (slots) on resonators or in the ground plane provide the ability to create a compact design [58] or operation in lower frequencies [59]. Coming back to the modified dumbbell, the additional discontinuity gaps to the etched headed areas increase the equivalent parallel capacitance, which makes possible to shift the resonance in lower frequencies.

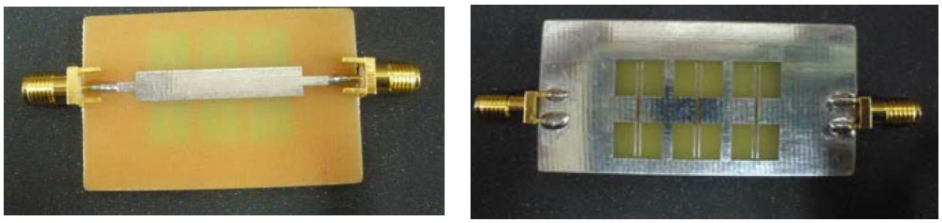

Figure 6.4: Microstrip line low pass filter by three modified dumbbell DGS by [57]: measured and verified

For this project, the challenge was to apply the discussed electrical lengthening in the general dumbbell which was used between the RDRAs (see tuning parameters: c, a, b, g in Figure 6.5). In order to further reduce the physical DGS dimensions, additional elements described by parameters L and W were added as shown in Figure 6.5b. Furthermore, to validate the modified dumbbell functionality, a linear variation of the inner length was studied (in terms of wavelengths) which is presented in Figure 6.6.

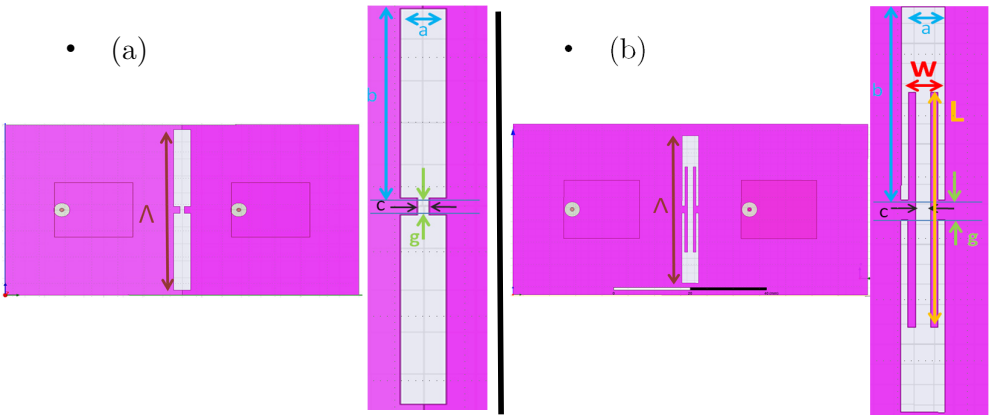

Figure 6.5: E-coupled RDRAs-DGS combinations in a half-lambda grid for similar resonance frequency: (a) general dumbbell DGS (c, g, a, b): external contour Λ=0.95 $\lambda/2$ vs (b) modified dumbbell DGS (c, g, a, b, L, w): external contour Λ=0.82 $\lambda/2$.

When the inner length is added (see Figure 6.5, parameter L and W), it creates an extra path in the ground plane for the currents to follow. Electrically the structure becomes larger which causes the response we observe in Figure 6.6d. The resonant pole is shifted linearly to lower frequencies (by increasing parameter L) maintaining similar bandwidth.

In order to address the importance of this modification comparisons follow between the general dumbbell:

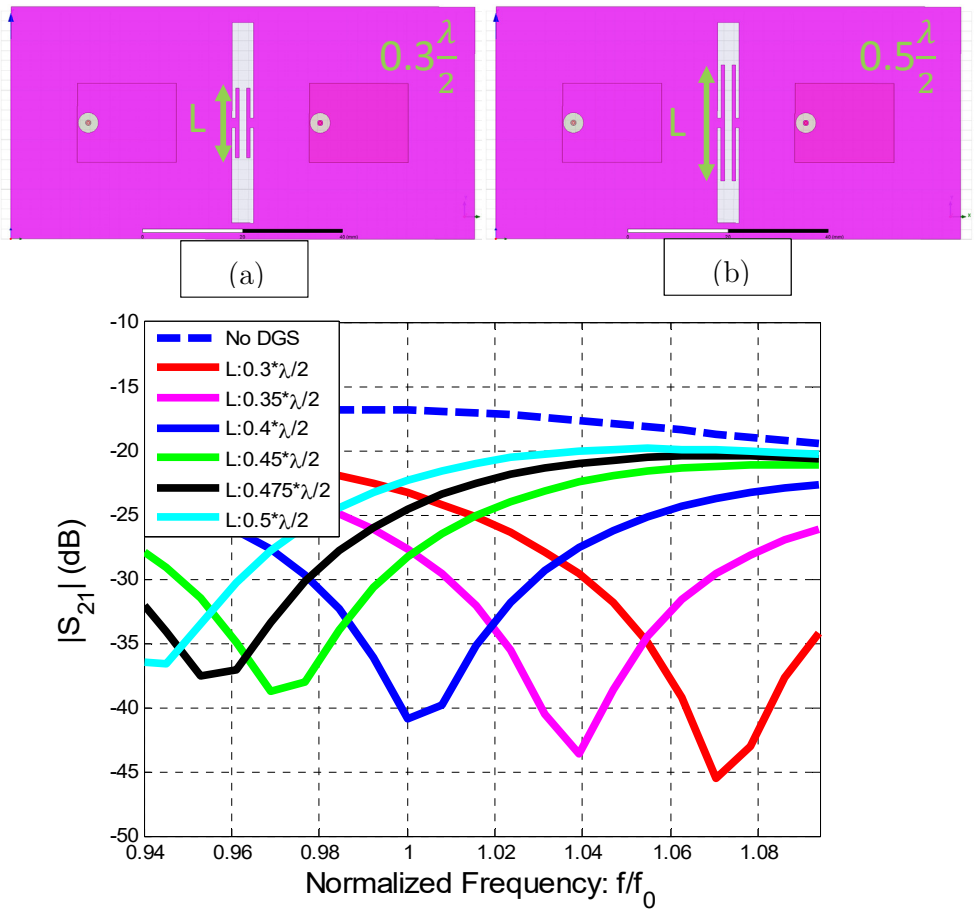

Figure 6.6: Modified dumbbell place between two E-coupled RDRAs inner length linear variation (delta L: $0.05\frac{\lambda}{2}$): (a) Reference inner length at $0.3\frac{\lambda}{2}$ (b) Final inner length at $0.5\frac{\lambda}{2}$ (c) coupling between the RDRAs for all the steps

- Regarding Figure 6.6d likewise Figure 6.3d, by comparing the case where no defected structure was applied, all the design steps provide significant coupling reduction in the required band.
- Comparing the designs in Figure 6.5, which are tuned for close by resonances, one can observe the compactness of the modified dumbbell. The frequency BW remained almost unaltered although the overall length in H-plane modified to 0.82 λ/2, instead of 0.95λ/2 that the general dumbbell was requiring (see Figure 6.3d:b and Figure 6.6c:0.4λ/2). This was achieved by reducing the external contour shape and in parallel compensating the electrical variation by increasing the inner length.

- Furthermore, the modified dumbbell while maintaining the same external contour shape is able to resonate towards lower frequencies by increasing the inner length (compare the design layouts in Figure 6.6: (a) vs (b)). Therefore, the new dumbbell configuration does not need to exceed the half lambda grid as in the case of the general dumbbell (Figure 6.3d:c vs Figure 6.6b).

6.4 DGS radiating nature

This paragraph aims to provide insights into the radiation effects below the ground plane by a DGS parasitically excited from adjacent antenna elements. The DGS radiation behavior is a concept that is not widely studied towards applications in phased array antennas.

6.4.1 Physical operation

The theory and application of defected ground structures was initiated to provide microstrip line filtering applications. A slow-wave effect is induced by the defected ground plane which disturbs the direct current path; low, high or passband responses can be achieved because of the PEC discontinuity points on the GP; this perturbation creates certain inductance and capacitance giving similar characteristics to one pole Butterworth filter [28].

For those applications, radiation effects are not taken into account. For simulation performed in [60], the boundary conditions are defined as absorbing (no reflections). This excludes the reflections in enclosed microwave systems by surrounding structures. The simplification can be valid for microstrip lines when the measurement setup makes sure that there is enough space below the ground plane. Similarly to microstrip lines, simulated antenna results with corresponding fabricated design measurements were evaluated free from obstacles below the ground plane [29], [34]. That approach would be difficult to implement in array antennas where the one common ground plane is often used. This made it an open point if a DGS can be considered as MC reduction method between array antenna elements.

Moreover, limited information is given by applying multiple DGS in proximity. The lack of examples questions the functionality of those structures in a dense array. On top of that, examples discarding DGS as a MC reduction method are mentioned in literature. For DGS applied in complex designs the desired filtering characteristics were detuned [[9]:p51].

From an electromagnetic point of view the slots in the ground, when adjusted properly, resonate and behave like slot antennas. The difference from typical antennas is that they are excited parasitically by near-field waves. In details, the pronounced surface waves near the antennas, which are considered as a loss of radiated power, propagate along the GP and if a direct path between the element antennas exists induce considerable interaction to them. Placing a defection between the antenna elements, for instance in E-plane, disturbs the described unwanted MC. The near field E-plane faces a slot barrier. There, the surface electric currents (J_{surf}=-$\hat{n}$×H) follow the DGS perifery and as concequence they come in resonance.

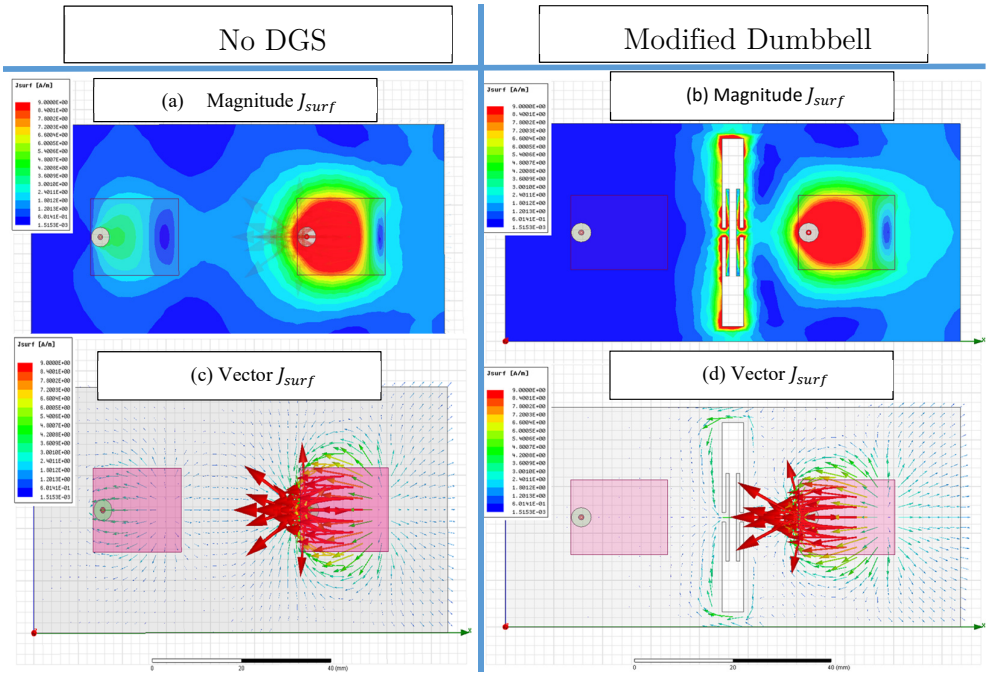

Figure 6.7: Surface currents with and without the modified DGS between E-coupled RDRAs-One excited RDRA

An example is shown in Figure 6.7 (all sub figures maintain equal magnitude). Figure 6.7a vs Figure 6.7b underlines the significant MC

reduction when the defected modified dumbbell was placed between the RDRAs. More interesting is the comparison between Figure 6.7c and Figure 6.7d where surface currents are completely altered after importing the DGS and redirected around the slot resonator. Neglecting possible reflections back to the antennas, the resonating currents are exciting the defection in the ground plane similarly as a slot antenna does.

6.4.2 Verification

An excited slot antenna radiates which arises concerns in terms of radiation direction; it can be above the ground plane so behaving as another source contributing to the far field or below the ground plane. The second statement is dominant as in most applied cases the increase in back lobe radiation is observed [29], [32], [46], [60].

To clarify this, several experiments followed both for the patch and dielectric resonator antennas in order to represent radiation from a parasitically excited DGS. Here we focus on patch antennas as they were the initial literature examples examined for this phenomenon.
Two E-coupled microstrip patch antennas are placed on top of a dielectric substrate (FR4) with relative permittivity 4.4 (Figure 4.2). Under the patches, on E-plane right-hand side, two DGS ring resonators are placed optimally to reduce MC as shown in Figure 6.8a (top view).

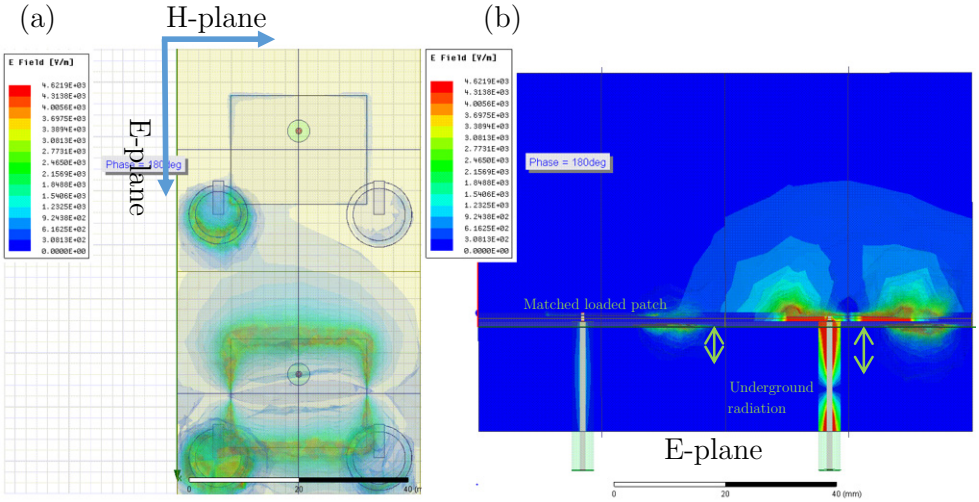

Figure 6.8: DGS radiating nature: E-coupled microstrip patch antennas one excited a) top view b) E-plane side view

In Figure 6.8b the electric field magnitude is shown for a certain phase instance. The sequence of instances in a phase period give the opportunity to study how radiation is periodically evolving (more instances see §11.2). In short, the electric field is propagating through the underground coaxial feeding probes, which are connected to the microstrip antennas with pins above the ground plane. The excited antennas radiate to the far field from the two edge slots on the sides.
At the same time, it is interesting to observe the coupling mechanism, which excites the DGS rings. Figure 6.8b shows the trend of the electric field which the excited antenna causes. The tangential components of the propagating electric field create electric current sources on the dielectric and as consequence to the ground plane in between the antennas. The electric currents created in the ground plane, on receive and transmit, excite the defected ring resonators. Therefore, the dgs elements near the patch edges create slot barriers which when excited create weaker coupling between the antennas. In this way, most of the unwanted coupling radiation (caused partly by the surface wave in the substrate and mainly by the air-wave above the dielectric because of a relative low permittivity) is absorbed by the defected rings and not directed to the feeding ports.

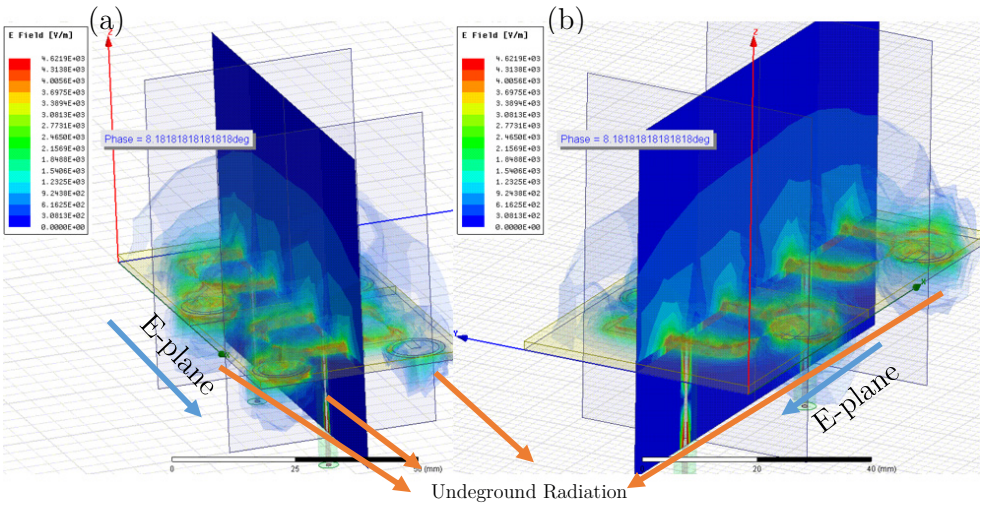

Figure 6.9: DGS radiating nature: E-coupled microstrip patch antennas both excited a) left-hand side 3D view b) right-hand side 3D view

Furthermore, it is critical to address where the absorbed energy is dissipated. The excited rings by the ground plane currents act as secondary slot antennas radiating dominantly underground. This is demonstrated in Figure 6.8b where significant radiation below the ground plane is

recognized. The phenomenon is more obvious when both patch antennas are excited (Figure 6.9 a-b). Looking on the 3-d view of the antennas significant electric field leakages below the ground plane is observed.

6.5 DGS cavity backed for frequency stable stop band

6.5.1 Multiple unshielded DGS

Knowing the radiating nature of a DGS, its application for integrated systems was immediately disputed. For radar applications, using high power in transmit, this back radiation could become an issue causing degaradion in efficiency.

In general, when DGS elements are not isolated below the ground plane they would behave as secondary radiation sources arising EMC issues by the back lobe electromagnetic radiation. Moreover, it arises health (SAR levels) and signal interference considerations.

From the DGS performance point of view, considering a dense array for phased array applications, multiple elements would be placed periodically between the antennas. If the radiation effect is not considered, a DGS coupling effect will take place below the ground plane. Specifically, underground radiation will mutually couple the DGS elements, meaning unstable performance. For instance, the underground reflections can shift the resonance frequency of an element.

To illustrate the aforementioned effect two different scenarios have been simulated, shown in Figure 6.10. Design (a) considers 3 simple slots, in small different physical lengths. They are placed between two E coupled RDRAs. In (b), the three slots are shielded by four PEC walls which form an underground waveguide effect for the coupled by the slots near-field airwaves.

When the three slots were unshielded (Figure 6.10a), although coupling compared to the stand alone E-coupled RDRAs was reduced only one resonance was observed. It is expected that by having three slots of different length (different geometrical dimensions) three discrete resonances should have been occurred. In case when PEC shielding is used between slots (see Figure 6.10b) three resonances are observed. This confirms that cross talk

is creating strong interaction between the DGS slots, thus altering the performance of the expected MC reduction.
In general, when DGS elements are not shielded they become as one global RF resonator (similar to EBG). Therefore, the performance of the element DGS in the array will diverge from the evaluated performance that it can be obtained for a single DGS, between two E-coupled antennas.

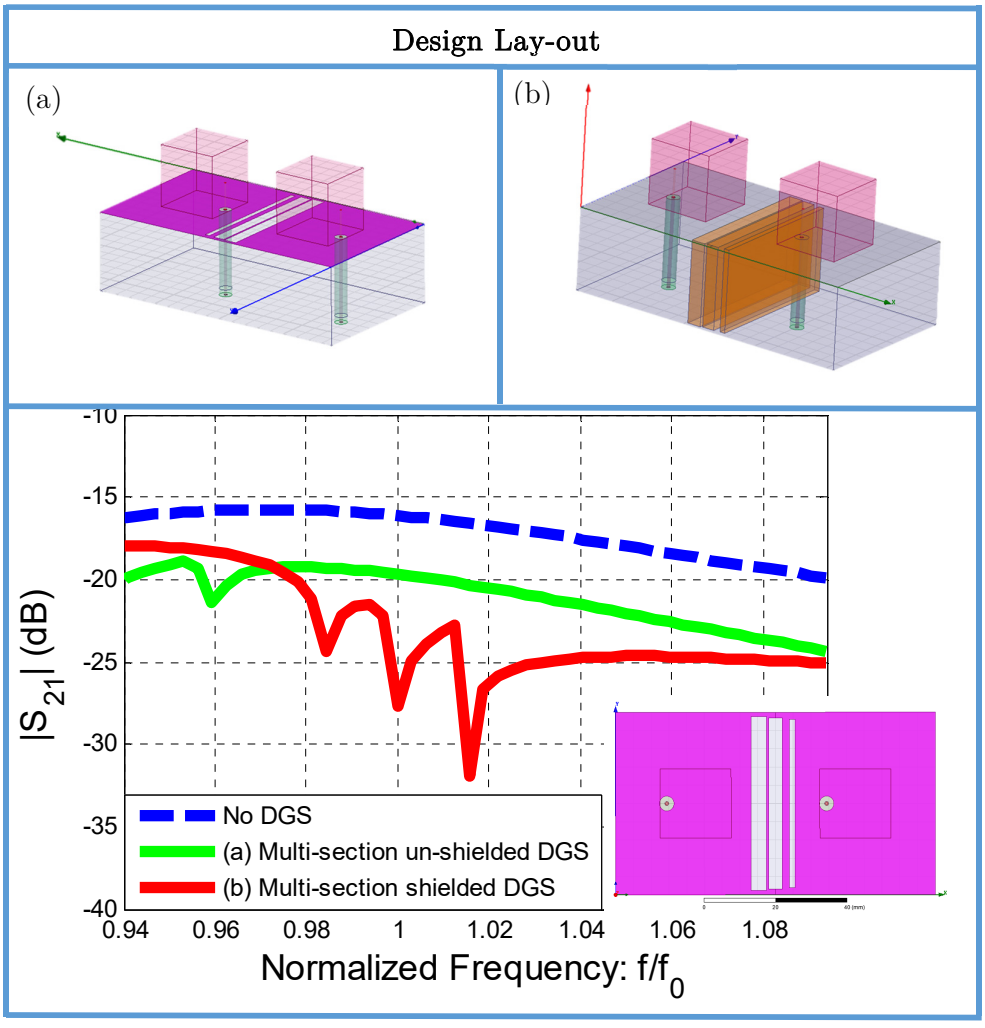

Figure 6.10: Multi section DGS response with and without shielding-three slight different physical lengths: a) un-shielded DGS b) shielded

Overall, with the perspective of radar application and in order to obtain the required DGS performance, underground isolation for each DGS is considered necessary.

6.5.2 Synthesis of the cavity backed DGS

The underground DGS radiation can cause degradation in DGS performance and as consequence in-efficiency between multiple elements, requiring individual isolation for each one of them. For example, this isolation can be done as demonstrated in Figure 6.10b by waveguide ports. The method is considered promising for future investigations (surface wave guidance and termination). However, from a practical point of view requires a complex underground decoupling network.

On the other hand, individual cavities can be created in order to support the slot DGS resonance; a cavity can be formed by taking a section of a waveguide and enclosing its front and back faces with conducting plates. Coupling into and out of the cavities is done through coupling probes or holes. The coupling probes may be either electric or magnetic. Allowing for standing waves instead of traveling waves by imposing addition boundary conditions (metal surfaces in front and back), various field configurations can be allowed (TEz, TMz, TEx, TEy, TMx, TMy) [62].

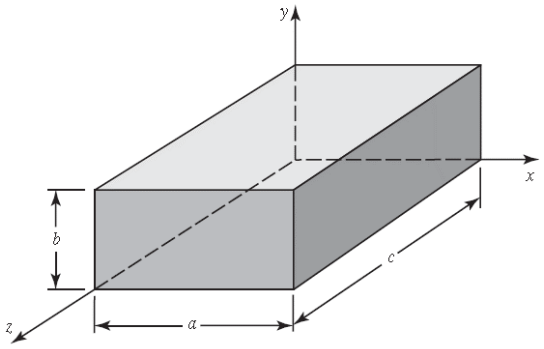

Figure 6.11: Rectangular cavity resonator [62]

Solving for the Helmholtz equation in a source free rectangular cavity medium, bounded by perfect electric walls, the resonance frequency for a TEz field configuration can be found by (1):

$$f_r^{TE}{}_{mnp} = \frac{1}{2\pi\sqrt{\mu\varepsilon}}\sqrt{\left(\frac{m\pi}{\alpha}\right)^2 + \left(\frac{n\pi}{b}\right)^2 + \left(\frac{p\pi}{c}\right)^2} \quad (2)$$

where:

m=0,1,2…

n=0,1,2…
p=1,2,3….
m and n not zero simultaneously

For this project, instead of probes we consider the coupling source to be the magnetic slot antenna (DGS). Thus, it is aimed to guide the unwanted MC radiation into the cavity and store it. Examining equation (2), the resonance is defined by the three characteristic dimensions (a, b, c), the mode order and the cavity material properties. Combining the parameters with the limitations in the array grid a suitable design can be defined.

To demonstrate the feasibility of this approach, the minimized dumbbell design was backed by a cavity and tuned to the desired resonance of two E-coupled RDRAs (Figure 6.12).

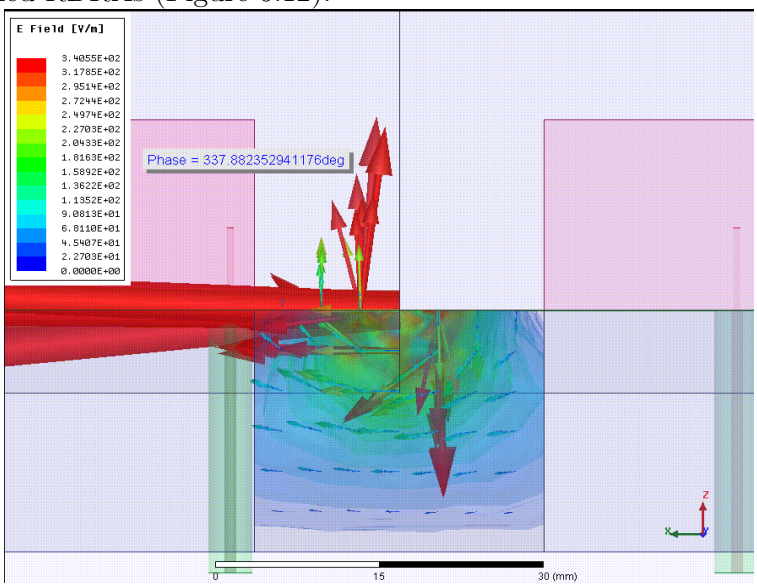

Figure 6.12: E-coupled RDRAs backed by a cavity at the RDRA resonance

When the DGS and the cavity was optimized to a desired frequency, the field configuration $TE^{y}_{111}$was accepted by the cavity. This can be identified by the E-field vector which has one antinode in x, no components in y and in z. The half antinode in z is shown because of the ground plane, which mirrors the mode.

Moreover, the necessary resonance revealed some added features of this combination. The DGS with the cavity creates one common RF structure, which behaves as one resonator. The air-filled cavity under the ground plane

has three tuning parameters which gives more design flexibility. To illustrate the aforementioned, the DGS stop band response between two E-coupled RDRAs was studied by linearly varying the height of the cavity (Figure 6.13).

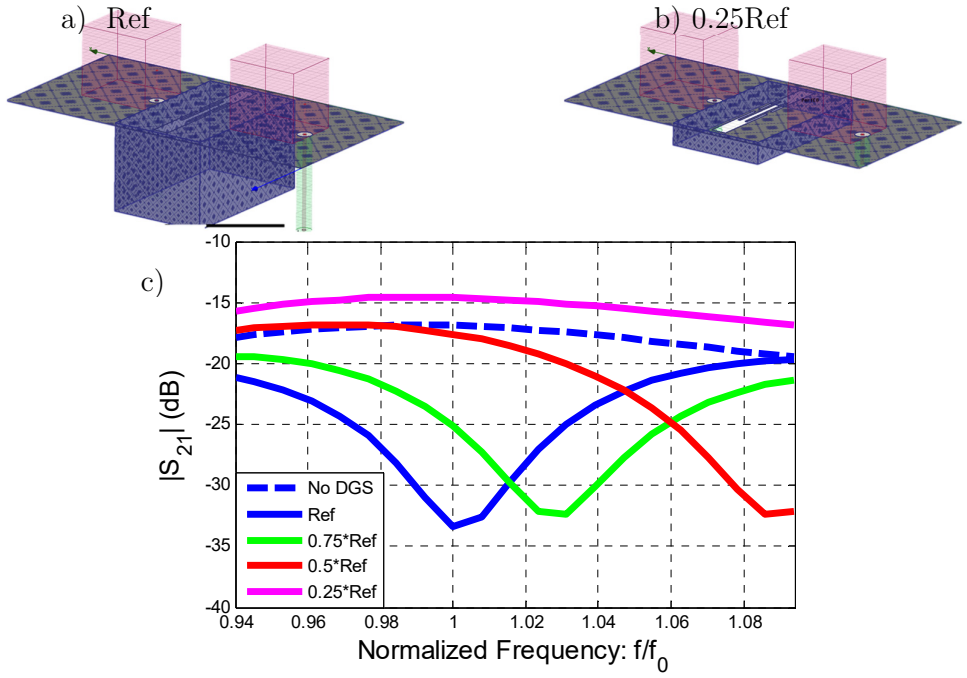

Figure 6.13: Stop band dependence by modifying the cavity height: a) Reference height b) 0.25*Reference height c) S21 of two E-coupled RDRAs, constant DGS coupling for 4 different air cavity depths: 0.25Ref: 0.25Ref: Ref

It is observed that for equidistant variations of the cavity height the non-equidistant frequency shift occurs which agrees with equation (2). Moreover, once the cavity was modified to a quarter of the reference height, MC got increased compared to the non-DGS case. In this case, the cavity is not able to support a resonance. However, the DGS still resonates. Therefore, currents on the DGS periphery are modified in such way that the radiation poynting vector is changing orientation. Thus, a higher portion of radiation is directed above the ground plane, which couples stronger the nearby antenna elements.

6.6 Application of DGS to different DRA antennas

It is important to verify if the tuned DGS can keep its MC reduction properties in case when DR antennas are modified. By DR antenna modifications one can understand here the usage of different value of

dielectric permittivity which results in variations of antenna dimensions and in consequence influences the coupling level between antenna elements. The variations in antenna geometry (different antenna shape) will be considered here as other type of DR antenna modification.

That kind of property is very desirable as it can simplify the process of array design. The designer can focus on tuning the matching of antenna element knowing that the presence of DGS assures the reduction of MC at the comparable level obtained based on previous analysis and it will not require the significant redesign of DGS. This would make the design process much easier and very different comparing to case of ring DGS where any modification of patch antenna (§11.1) influences the performance of ring DGS and any modification of ring DGS influences the matching of patch antenna (§5.2.1).

Three representative DRA examples follow in order to test the aforementioned property. The DRA element height ($\hat{z}$) as well as distance between antenna elements for all the cases is maintained the same.

6.6.1 RDRA (er=10) and reference CBDGS

Here the E-coupled configuration based on the DRA element will be used as a reference for comparison with other antenna configurations using different e_r or different geometry. As illustrated in Figure 6.14 the reduction in MC is significant in the required frequency band.

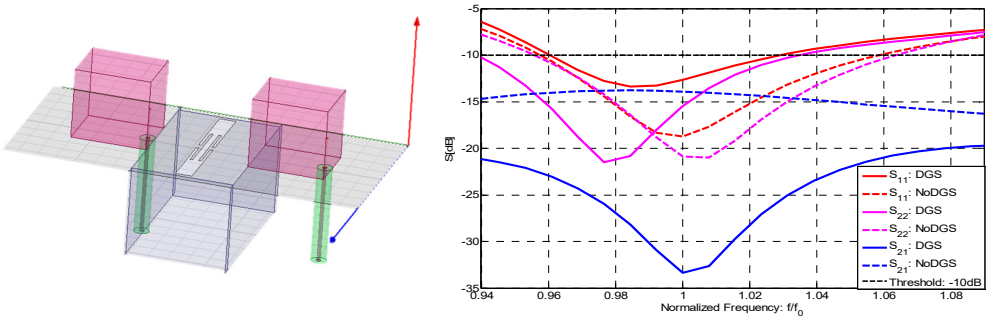

Figure 6.14: E-coupled rectangular dielectric (er: 10) resonator antennas with and without a DGS

The example above also shows how the MC is affecting the antenna impedance match and the resonance frequency of the element antennas. When the antennas are strong mutually coupled, the element antennas resonate close by 1fo. Once the MC is reduced then both antennas resonate

to lower frequency. This is attributed to capacitive effects for antennas with a DGS.

6.6.2 Lower dielectric permittivity RDRA (er= 5.75)

In order to verify the performance of DGS (showed in section 6.6.1) in case of stronger MC, the DRA antenna was designed using lower e_r. By using lower e_r the size of the radiator increased which resulted in closer distance between radiating elements and as consequence stronger MC.

Furthermore, different capacitive effects happened when the CBDGS was used which affected the impedance match for the RDRAs. This happened because the pin position for each resonator antenna maintains significant different distance from the CBDGS (compared to §6.6.1). Therefore, different capacitance between the probes of individual antennas and the CBDGS occurred which resulted in significant resonant frequency shifts. Without the CBDGS the E-coupled antennas have identical resonance frequencies whereas with the CBDGS an offset of 0.05fo is shown.

Although the coupling between elements increased from -14 dB (§6.6.1) to -11 dB (by making antennas larger) the current DGS structure still works. Slight difference in resonance frequency of DGS is caused by different locations of antenna probes, which requires additional fine tuning but does not detune the whole DRA-DGS configuration as it was observed in case of a patch antenna and ring DGS (§5.2.1).

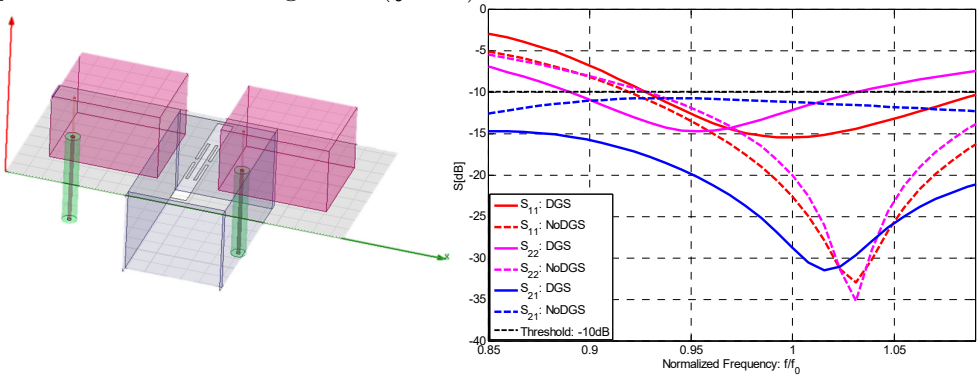

Figure 6.15: E-coupled rectangular dielectric resonator antennas with and without a DGS for a lower (er=5.75) dielectric permittivity

6.6.3 Cylindrical dielectric resonator shape (er=10)

In this example DR antenna with cylindrical shape was used to verify the performance of DGS from §6.6.1. The dielectric material is the same as it was used in the reference rectangular resonator in §6.6.1. In Figure 6.16 it is observed that for configuration without DGS the coupling between cylindrical antenna elements is at comparable level of -14dB as for configuration of rectangular DRA given in §6.6.1. In case when DGS structure is applied between cylindrical antenna elements very good reduction of MC is observed (up to 20dB). It can be noticed that overall DGS performance is very similar to the case from §6.6.1.

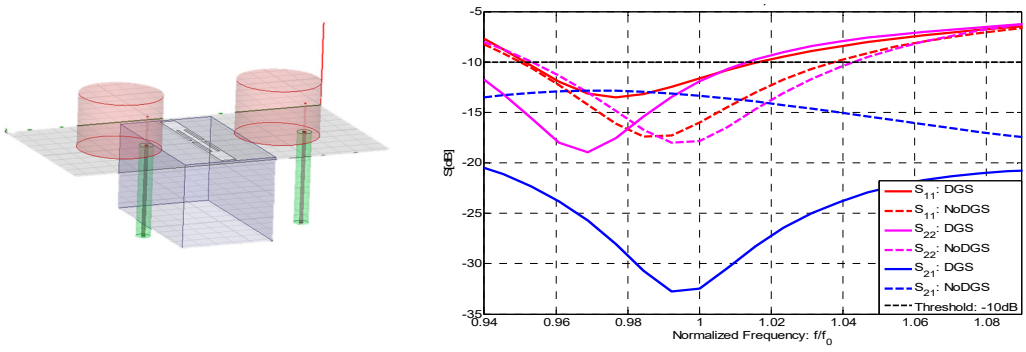

Figure 6.16: E-coupled cylindrical dielectric (er: 10) resonator antennas with and without a CBDGS

Based on the observations from the demonstrated example, it can be concluded that if antenna elements working at the same resonance mode and are made with material of similar RF properties the applying of pre-designed DGS from one antenna configuration to the other antenna configuration will result in comparable RF performance.

6.7 Discussion

Summing up, synthesis of an array element DGS RF structure arises challenges concerning either the array grid limitations, the bandwidth constrains and the electromagnetic phenomena. These challenges were studied and solutions were provided to create a frequency stable MC reduction RF structure. The flow chart of the approach that it was used to achieve the design (that meets the criteria which defined in this chapter) is shown in Figure 6.17.

To demonstrate the effectiveness of the proposed design, different coupling scenarios followed. Therefore (§6.6), different antennas were compared with different dielectric properties and shapes. The demonstrated studies indicated that the DGS was still able to reduce the coupling between antenna elements for antenna configurations. Small variations observed on the matching and coupling levels are attributed to non-identical capacitive effects for the examined scenarios. However, it is important to mention that in all the cases the MC reduction was maximum around the same frequency (fo). It also shows that the final DGS structure, once it is tuned, behaves as a separate RF component.

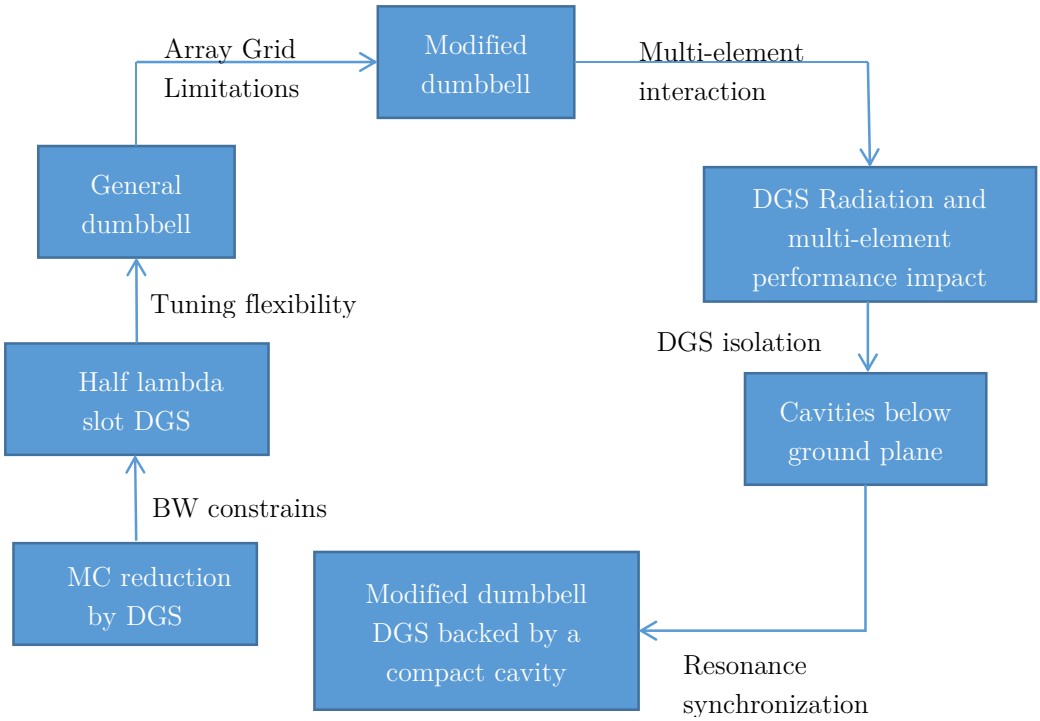

Figure 6.17: DGS array element synthesis: Overview on array challenges, EM studies and solutions

Based on the procedure from Figure 6.17, a tuned cavity with a minimized dumbbell DGS combined with RDRAs is shown in Figure 6.18. This forms the antenna-DGS element combination which will be used for further studies in planar arrays. The selection of rectangular DRA was based on ease of fabrication (compared to the CDRA) as the proposed decoupling method, for DRAs, is effective for both antenna geometries. The return loss and the coupling between two E-coupled RDRAs are plotted in Figure 6.18. Comparing the case without and with DGS, it is observed that MC is

significantly reduced. At resonance frequency, the MC has been reduced by 24 dB while at the lowest and highest frequencies of the operational band (defined where S11<-10dB) reduction of 9 dB and 5dB respectively has been achieved.

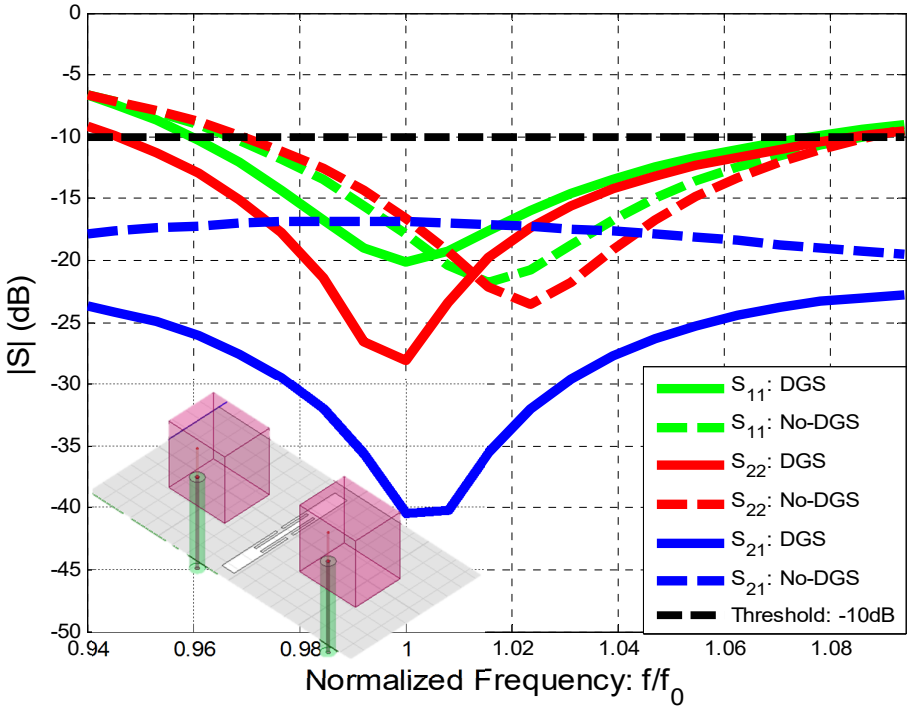

Figure 6.18: Minimized dumbbell between two E-coupled RDRAs: Transmission coefficient and elements return loss. Dotted lines represent the element without the DGS and solid lines with DGS

7 Scan performance in Infinite Arrays

The excitation principle and the physical phenomena of a parasitically excited defected ground structure were discussed in chapter 6. Finding a decoupling RF method compatible for array applications defined the first project milestone. The demonstrated MC reduction ability and the compactness of the final DGS design verified the milestone. Having the DGS design that meets the requirements it is possible now to apply it between antenna elements in array configuration.

This chapter evaluates the infinite array performance based on the element characteristics. The arrays under study are based on the final antenna-DGS element combination (from chapter 6). A single unit cell element makes the assumption of such identical infinite excited antenna-DGS elements. Moreover, the evaluation of the array is based on how well the embedded element can be excited for various scan angles with and without the DGS. In this way, it is able to obtain the characteristics of an element antenna where it has been affected by active neighboring identical elements for different scan angles.

Finally, the presented array scan results defined a favorable lattice configuration for further application on a finite array which is analyzed in chapter 8.

7.1 The micro-strip patch antenna arrays scan

Although in chapter 5 the examples on micro-strip patch antennas did not fulfill the requirements for the desired array RF structure, the examples examined for their scan abilities. Specifically, the single ring resonator and the dumbbell with lengthened arms DGS were evaluated. From the results (see Appendix 11.3), it was observed that slight BW enhancement achieved for the patch-ring case while the dumbbell improved the return loss levels. However, improvement in the scan performance was insignificant which makes them not important to be discussed further.

7.2 The dielectric resonator antenna arrays scan

The cavity backed dumbbell DGS between the E-coupled RDRAs provided significant isolation for the antennas. In addition it was able to satisfy the bandwidth and sensitivity constrains that were established in section 4.3.

As well, it complies with the array limitations studied in chapter 6. Therefore, the scan studies which follow are based on this structure.

7.2.1 DGS resonance frequency

As it was referred, the final DGS element is a parasitic resonator, which is able to maintain stable frequency resonance once it is tuned properly. Thus, in order to evaluate the performance of a DGS in different coupling schemes, an identical DGS structure was used for two lattice configurations. This aimed to observe how the DGS was going to affect different arrays, as different coupling effects experienced in each one.

The chosen lattices are described by rectangular and triangular antenna element placement. To tune the DGS, for both configurations, E-coupled RDRAs were used as shown in Figure 7.1.

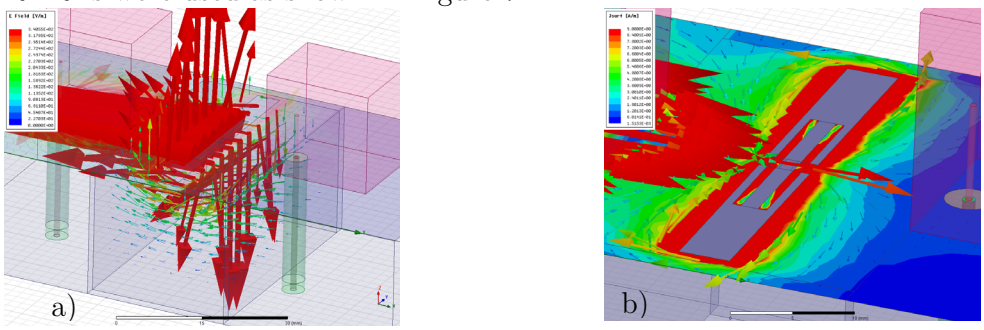

Figure 7.1: Modified dumbbell centered between two rectangular dielectric resonator antennas: a) Resonating slot and excited underground cavity mode: E-field magnitude b) ground plane currents: surface vector and complex magnitude

In terms of resonance frequency, the DGS tuned differently than the E-coupled antennas (see |S21|: plotted in Figure 7.2). The reason for this decision is connected with the assumption of the project. This study tries to identify if by reducing MC it can be possible to improve the matching stability for various scan angles. Therefore, by discriminating the DGS resonance from the antennas it can be easy to identify the impact of a DGS in the scan performance.

As illustrated in Figure 7.2, despite the non-overlapping resonance between the antennas, the DGS is able to reduce MC significantly in the whole band, up to 20dB (see f=0.96fo). Slight BW enhancement in observed for the RDRAs while the return loss levels are well maintained for both antennas below -20dB (at their resonance).

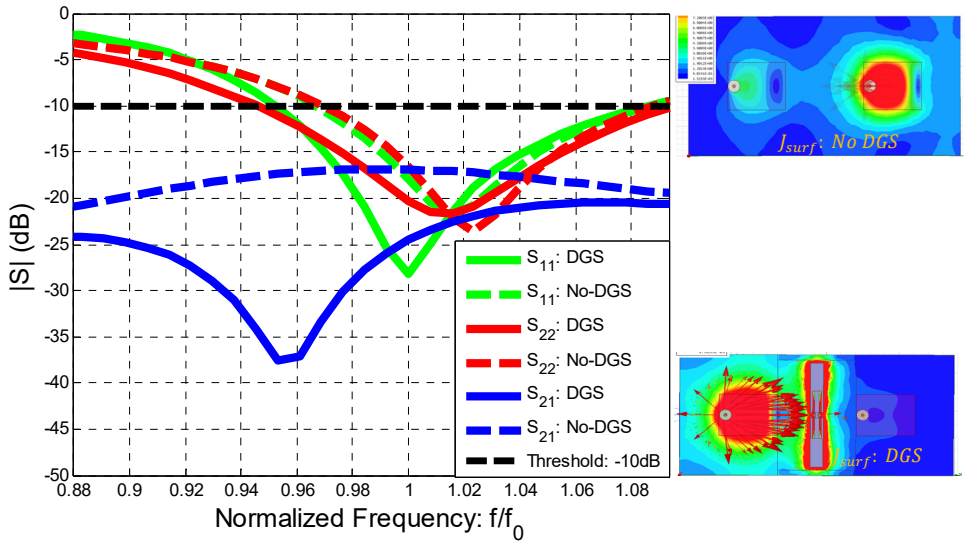

Figure 7.2: E-coupled rectangular dielectric resonator antennas and modified dumbbell: DGS vs. No-DGS

	DGS	No-DGS	BW-DGS/ No-DGS
S11	BW: 0.48 GHz	BW: 0.38 GHz	1.263 26.3% increased BW
S22	BW: 0.43 GHz	BW: 0.379 GHz	1.134 13.4% increased BW
MC			**Reduction**
S21 (at 0.96f0)	-37.0856	-17.1795	19.90 dB

Table 5: Modified dumbbell between E-coupled micro strip patch antennas: Reflection coefficients, antenna BW and MC with and without the DGS

7.2.2 Scan in a rectangular grid (RG)

7.2.2.1 RG configuration

The tuned antenna-DGS element is repeated periodically in a rectangular lattice and examined for its scan performance (see Figure 7.3). This configuration is characterized by equidistant element spacing for E as well as for H plane elements. The spacing is defined from the centralized position of the elements at 0.5λ regarding a favorable frequency in S-band, which is included in the operational bandwidth of the antenna elements. A 0.5λ inter-

element spacing is chosen in order to maintain a free grating lobe scan region and reasonable coupling between the elements.

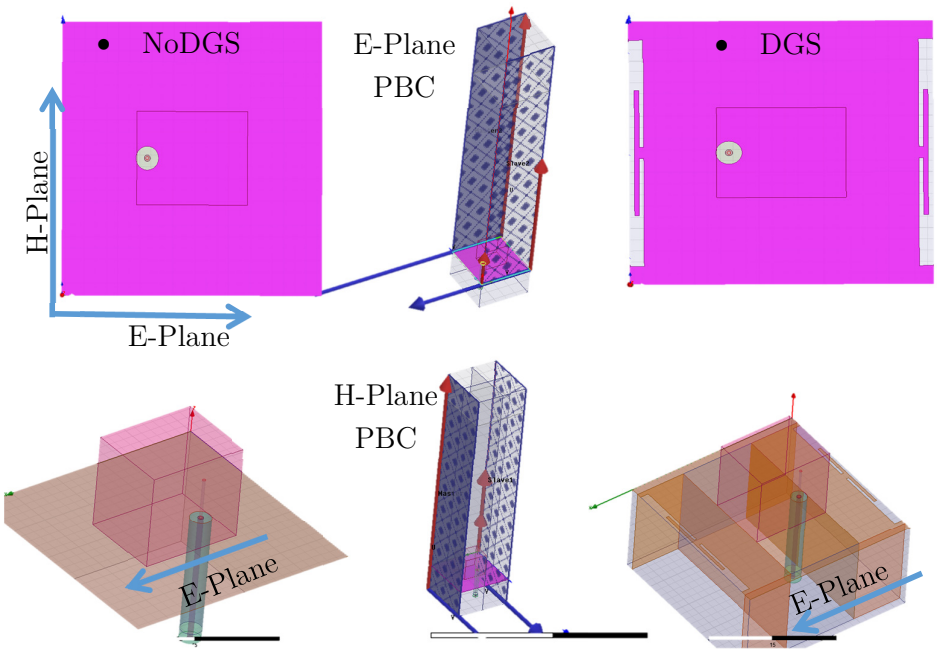

Figure 7.3: Rectangular Infinite Array UC with and without a DGS. In the middle the periodic boundary conditions that were used for this lattice configuration are illustrated

7.2.2.2 Scan analysis

Figure 7.4, illustrates the return loss levels that are frequency normalized with respect to the DGS resonance frequency. The scan angles are in elevation and simulated regarding the principal planes with and without the tuned DGS.

The important remarks from the scan results in Figure 7.4 are summarized as follows:

Without a DGS:

- In E plane, without a DGS the array is unable to exceed the radiating threshold
- H-plane without a DGS is more stabilized than E-plane

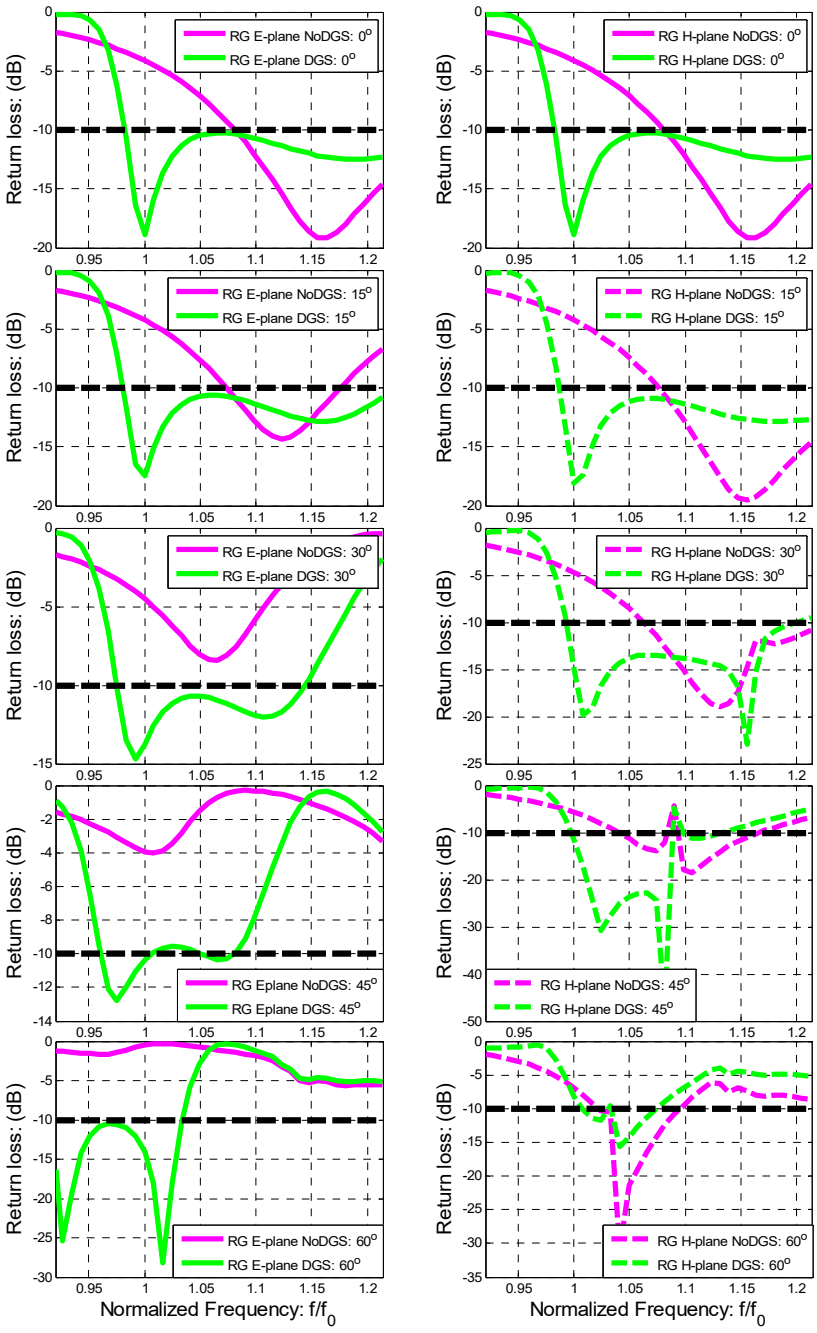

Figure 7.4: Rectangular grid scan performance with (green lines) and without DGS (purple): Scan performance from Broadside-60 degrees: normalized at the DGS resonance: Solid lines represent E-plane while discrete H-plane

With a DGS:

- The DGS caused BW ability for 30, 45 and 60 degrees

- BW enhancement for broadside and 15 degrees in E-plane
- BW enhancement for broadside, 15, 30 and 45 degrees
    - H-plane got benefit for all the angles, with an exception on 60 degrees which was not expected as the DGS is applied on E-plane
        - still 60 degrees exceed the radiation threshold.
- Focused on the DGS resonance (f=1fo), it is observed for both planes improved impedance match for all the scan angles.

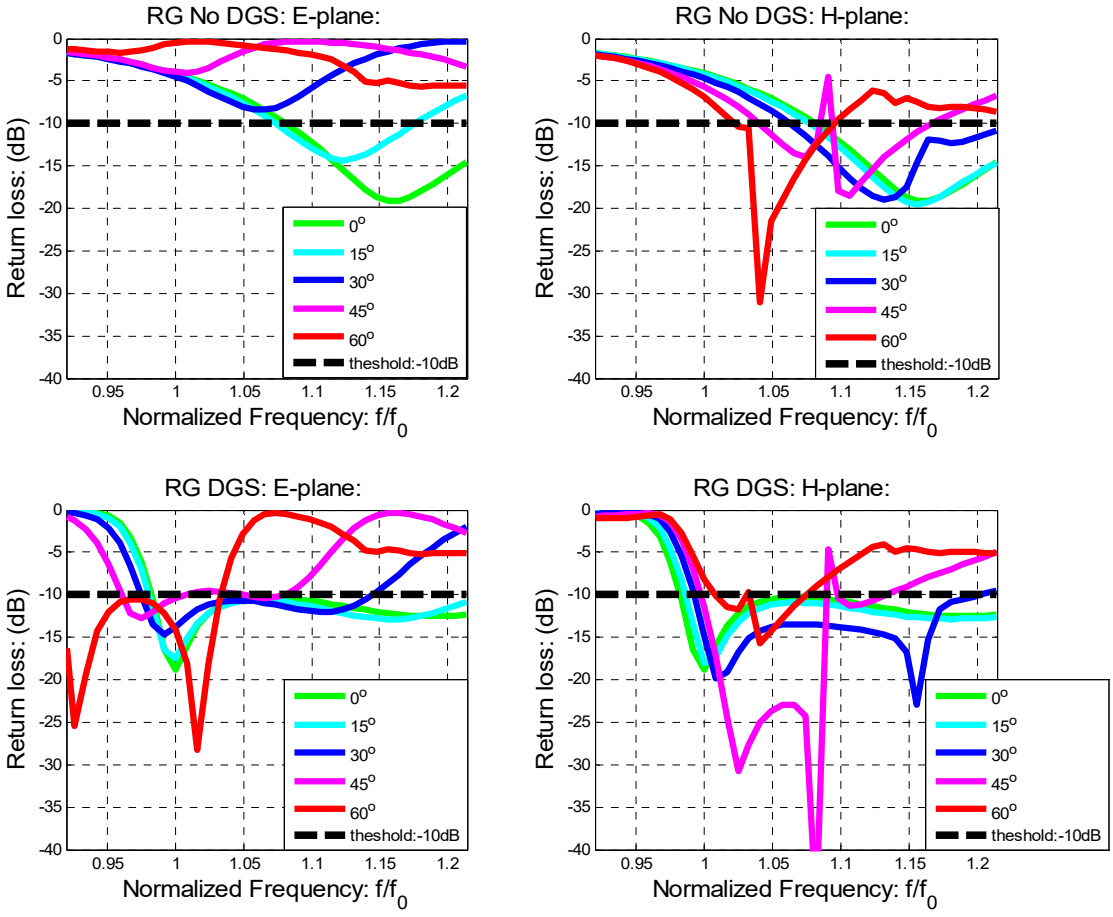

Figure 7.5: Rectangular grid comparison for E and H plane with and without a DGS: Scan angles from broadside to 60 degrees-normalization with respect to the DGS resonance frequency

Figure 7.5 demonstrates the global scan analysis by observing all the scan angles. Enhanced BW performance is achieved by including the DGS in the array. Once again, near the stop band of the DGS for both planes a sub-band resulted which can be considered as scan-able for all the angles. Therefore, it is indicated possible impedance match stabilization because of the DGS.

Finally, Table 6 summarizes the array bandwidth improvement by comparing the array with and without a DGS for each angle. Considerable enhancement is achieved for all the angles in both planes, except the 60 degrees in H-plane.

S11	**DGS (BW GHz)**	**No-DGS (BW GHz)**	**BW DGS/ No-DGS**
SCAN: 0^0	E-plane: 0.74 H-plane:0.74	E-plane: 0.45 H-plane:0.45	E-plane: 64% ↑ H-plane: 64% ↑
SCAN: 15^0	E-plane: 0.72 H-plane:0.6922	E-plane: 0.3107 H-plane:0.4834	E-plane: 32% ↑ H-plane: 43% ↑
SCAN: 30^0	E-plane: 0.514 H-plane:0.6724	E-plane: N/A H-plane:0.4596	E-plane: BW with DGS H-plane: 46% ↑
SCAN: 45^0	E-plane: 0.37 H-plane:0.2806	E-plane: N/A H-plane: a) 0.1321 b) 0.2234	E-plane: BW with DGS H-plane: a)112% ↑ b) 26% ↑
SCAN: 60^0	E-plane:0.35 H-plane: 0.2035	E-plane: N/A H-plane: 0.2230	E-plane: BW with DGS H-plane:0.09% ↓
			Scan able band in both Planes for all angles:
Scan able band for all angles:	BW: 0.152	BW: 0.2	**BW: 0.08**

Table 6: Embedded element bandwidth with and without DGS-RDRA-element in a rectangular grid: Measurement from Figure 7.4

7.2.3 Scan performance in a triangular grid (TG)

7.2.3.1 TG motivation

In this chapter the study on application of DGS for arrays in triangular grid configuration will be presented. Using the triangular grid in array antennas is attractive for radar applications because of diagonal position of grating lobes and increased element spacing in one of the plane of the array. For a rectangular grid, when beam is scanned, grating lobes appear first in the principal planes while for triangular grid grating lobes enter the visible spectrum diagonally [63]. This is an advantage for the systems that have requirements on large beam scan coverage along azimuth (e.g. radars for naval systems) as for large scan angles side-lobe levels in the azimuth plane are lower compared to the rectangular grid (Figure 7.6).

In addition, the principal planes in a triangular grid are able to tolerate larger spacing between elements without grating lobes in the visible spectrum. Using triangular grid allows to obtain larger spacing in one of the principal planes for the antenna elements. This means, for a particular plane, that the MC can be reduced just by choosing the configuration which has larger distance between elements in the plane of interest or in the plane where the MC is stronger (in most cases this is E-plane). In this case, the extra distance between the elements gives more space and flexibility for additional RF structures that can be placed between antenna elements and these structures can be used for reduction of MC.

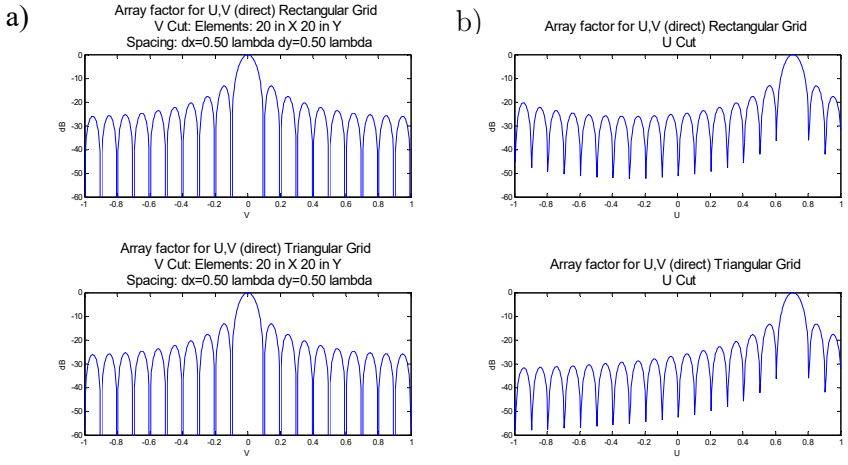

Figure 7.6: RG vs TG array factor: Side-lobe levels a) broadside and b) wide scan angle

7.2.3.2 TG E-plane shift configuration

Named as E-plane shift configuration (Figure 7.7), the RDRA elements are rearranged such that every other element is displaced. Therefore, the tuned defected ground structure is in centralized location (Figure 7.9). Specifically, the DGS is placed in a cross (coupling) location between E-coupled and H-coupled elements.
As follows from this position, it is studied how the DGS performs when it is excited from both polarizations, thus synthesizing one element that it can be used to potentially benefit both planes. Compared to the rectangular grid, in this configuration the H-coupled elements are influenced from the new lattice configuration (λ spacing) as well as from the DGS presence. On the other hand, E-plane elements maintain the same inter-element spacing while the diagonal element distance decreases.

Here the E-coupled MC is not provided as the DGS design is identical to the one used in the rectangular grid (Figure 7.2).

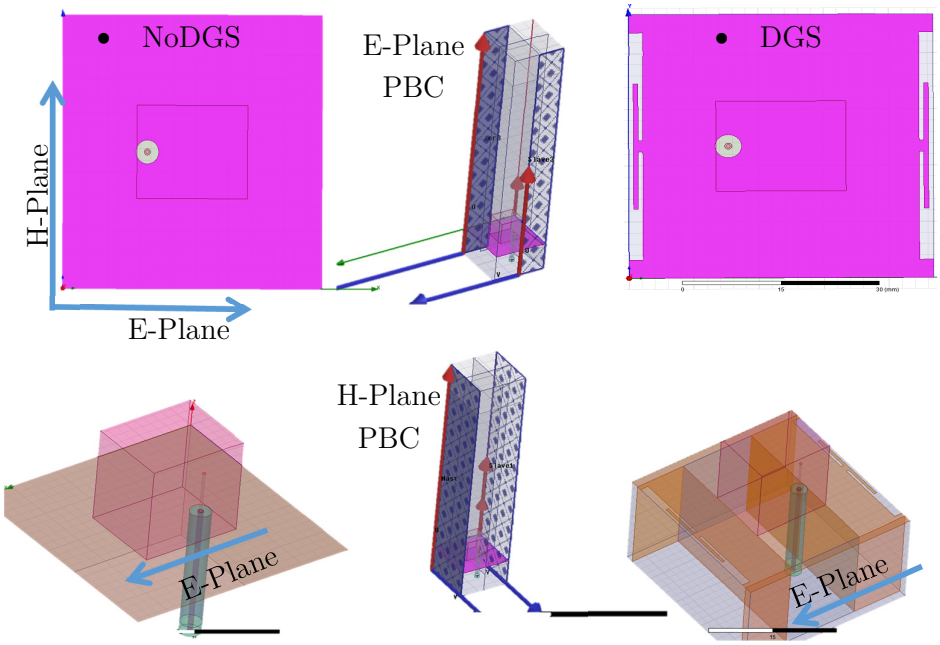

Figure 7.7: Triangular Infinite Array UC with and without a DGS. In the middle the periodic boundary conditions that were used for this lattice configuration are illustrated

a) 2D Top view

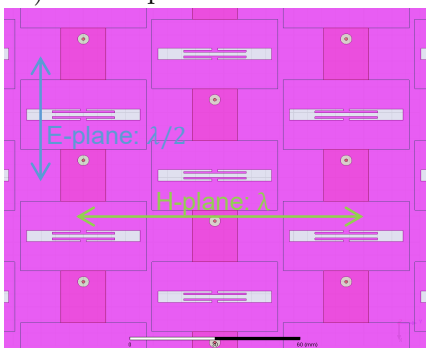

b) 3D Side view

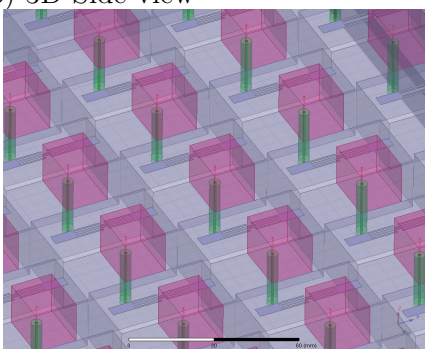

Figure 7.8: E-plane lattice representation (adopted from the finite array in chapter 8)

7.2.3.3 Scan analysis

Figure 7.9, illustrates the return loss levels that are frequency normalized with respect to the DGS resonance. The scan angles are in elevation (from broadside to 60^{o}) and simulated for the principal planes with and without the tuned DGS. As in the rectangular configuration, the important remarks from the scan results are summarized as follows:

Without a DGS:

- In E plane, without a DGS the array is unable to exceed the radiating threshold for 30, 45 and 60 degrees
- H-plane without a DGS is more stabilized than E-plane

With a DGS:

- Focused on the DGS resonance (f=1fo), it is observed for both planes improved impedance match for all the scan angles.
- The DGS caused operational bandwidth for 30, 45 and 60 degrees
- Significant BW enhancement for broadside and 15 degrees in E-plane (see Table 7)
- BW enhancement for broadside, 15, 30 and 45 degrees in H-plane
    - H-plane got benefit for all the angles
- The array with the DGS has the ability to radiate for all the scan angles in a specific sub-band, in both planes, which was unable without a DGS

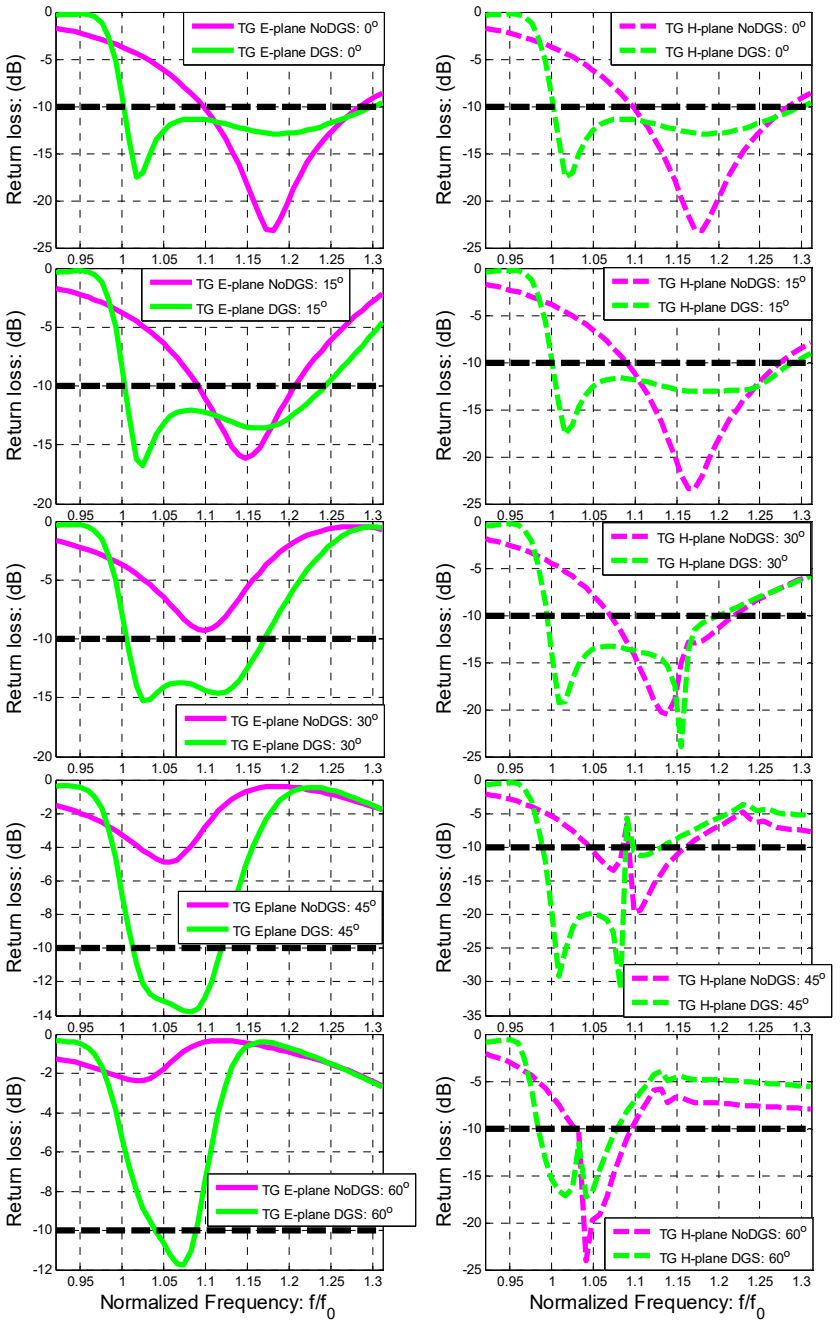

Figure 7.9: Triangular grid scan performance with (green lines) and without DGS (purple): Scan performance from Broadside-60 degrees: normalized at the DGS resonance: Solid lines represent E-plane while discrete H-plane

Figure 7.10, illustrates the global scan analysis by comparing all the scan angles. Enhanced BW performance is achieved by including the DGS in the array. Moreover, near the stop band of the DGS for both planes a sub-band

resulted which is considered scan-able for all the examined angles. Therefore, because of the DGS it is indicated possible impedance match stabilization and in parallel BW enhancement.

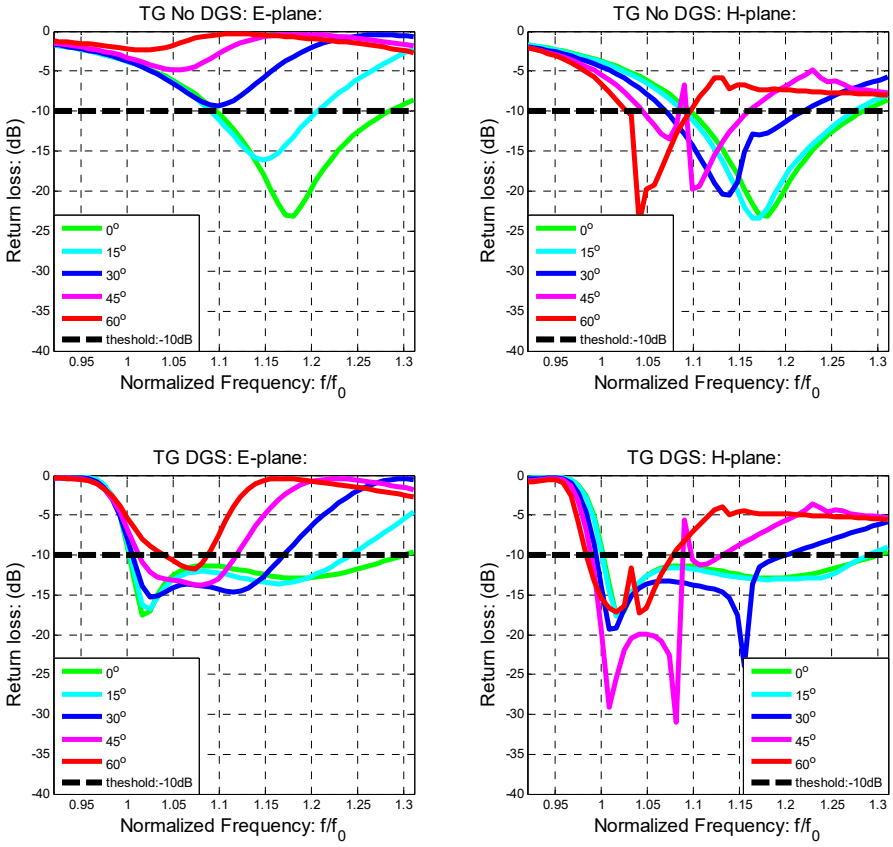

Figure 7.10: Triangular grid global comparison for E and H plane with and without a DGS: Scan angles from broadside to 60 degrees

Finally, Table 7 summarizes the array bandwidth improvement by comparing the array with and without a DGS for each angle.

Conclusion:

- One RF structure benefits both planes in terms of bandwidth and impedance match

S11	DGS (BW GHz)	No-DGS (BW GHz)	BW-DGS/ No-DGS
SCAN: 0^0	E-plane: 0.9125 H-plane: 0.9125	E-plane: 0.5755 H-plane:0.5762	E-plane: 59%↑ H-plane:59% ↑
SCAN: 15^0	E-plane: 0.7337 H-plane:0.8813	E-plane: 0.3549 H-plane:0.5646	E-plane: 206%↑ H-plane: 56%↑
SCAN: 30^0	E-plane: 0.5028 H-plane:0.6324	E-plane: N/A H-plane:0.455	E-plane: BW with DGS H-plane: 38%↑
SCAN: 45^0	E-plane: 0.3238 H-plane:0.3055	E-plane: N/A H-plane:0.1218, 0.2084	E-plane: BW with DGS H-plane: a) 251%↑ b) 47%↑
SCAN: 60^0	E-plane:0.174 H-plane: 0.2884	E-plane: N/A H-plane: 0.2066	E-plane: BW with DGS H-plane: 40%↑
			Scan-able band in both Planes for all angles:
Scan-able band for all angles:	BW: 0.1474	BW: 0.2324	**BW: 0.1181**

Table 7: Embedded element bandwidth with and without DGS-RDRA - element in a triangular grid: Measurements from Figure 7.9

7.3 DGS impact in the scan performance

Focused on the DRA elements, without a defected ground structure, because of the large dielectric permittivity (RDRA er=10 vs Patch er=4.4) the intense near fields detuned the scan abilities of this resonator significantly. In E-plane only broadside and 15 degrees were scan-able, where in contrast H-plane had significantly better operational BW for the various scan angles. However, the shift in resonance for both planes, from angle to angle, defined the arrays as inefficient for scan purposes for both planes.

When the tuned DGS was used in the infinite arrays, bandwidth enhancement for the scan angles achieved. This phenomenon observed for E as well as H-plane for the rectangular and the triangular lattice. A characteristic example is shown in Figure 7.11 for the rectangular grid,

focused on the plane where the DGS is applied (E-plane). While scan at 60 degrees is impossible without a DGS, by using the DGS operational BW occurred with significant roll-off. In parallel, it cannot be neglected the BW enhancement in broadside and the overlap in operational bandwidth with the DGS. Without a DGS this was not possible at all.

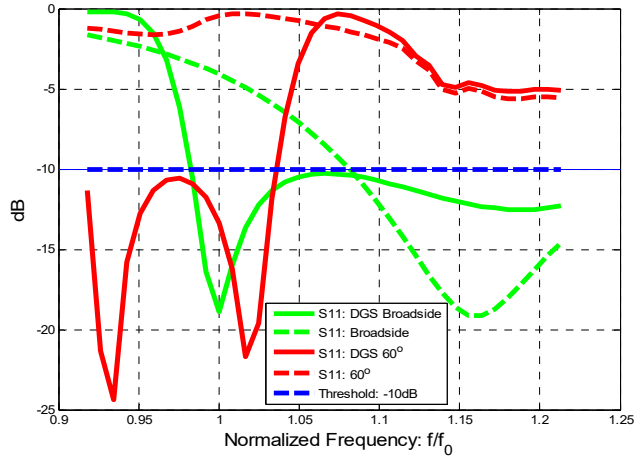

Figure 7.11: Embedded element return loss in infinite RDRA array (RG): DGS vs no-DGS broadside vs 60 degrees scan in E-plane: Band normalized to the DGS resonance frequency as shown from the transmission coefficient in Figure 7.2

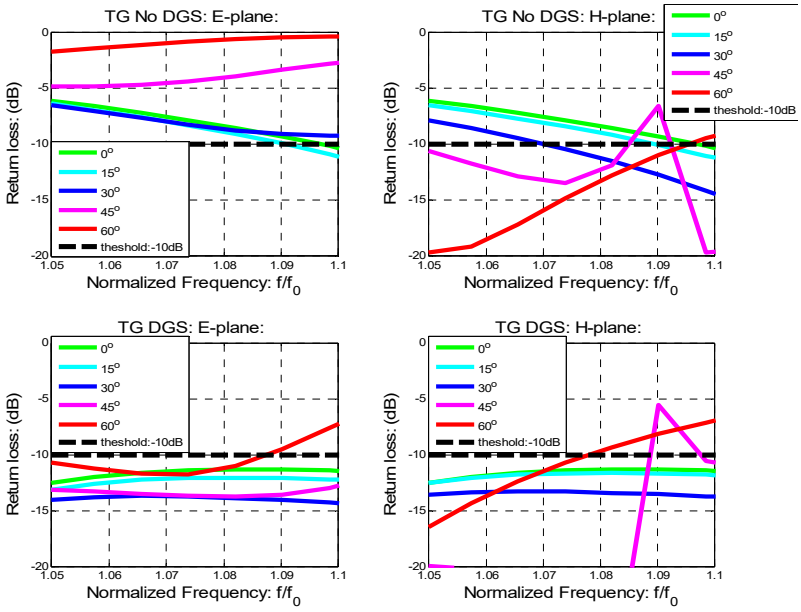

Figure 7.12: Sub-band frequency region in the triangular grid where all the scan angles exceed the radiation threshold. Both E and H planes plotted, with and without a DGS

Focused on the adjacent frequencies near the DGS resonance, it has resulted a region where scan operation is efficient for all the angles, in both planes for the examined lattice configurations (RG see fig: and TG). To demonstrate this, in Figure 7.12 the referred sub-band is plotted for both planes regarding the TG, with and without a DGS. In other words, impedance match stability achieved for the various scan angles, in the band near the DGS resonance for the principal planes. The demonstrated result verifies the assumption of the project.

7.4 Discussion

Examining the scan performance by reducing MC accomplished the first research goal. For this purpose, significant scan performances analyzed to demonstrate the use of a defected ground structure between active antenna elements and different lattice configurations (Figure 7.13).

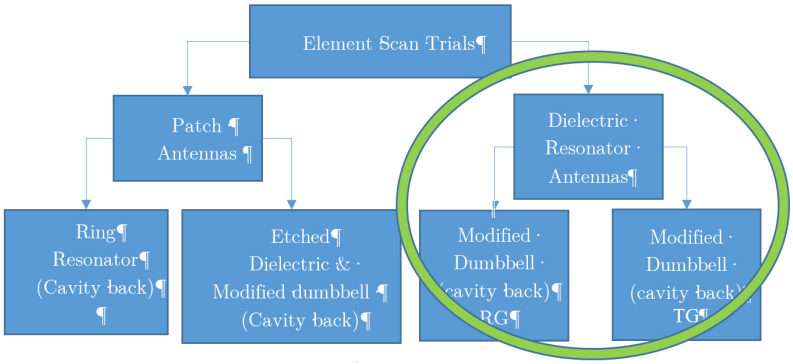

Figure 7.13: Antenna-DGS configurations constituting infinite arrays which examined for the scan performance from the feed point of view (the patch trials can be found in the appendix)

The RDRA combined with the cavity backed modified dumbbell DGS indicates possible BW enhancement in parallel to impedance match stability for various scan angles. For this antenna-DGS combination, by comparing the scan performance between two different lattice configurations, similar effects have been identified. Therefore, taking into account the desired features of a triangular configuration, the designed DGS collects undoubtedly features that require to be examined in a more demanding design (finite array analysis follows in the next chapter).

8 The 11x11 RDRA-DGS triangular array

MC reduction has been achieved by RF structures, which are designed by exploiting the ground plane. Therefore it was able to examine the scan performance by reducing MC in infinite arrays. This accomplished the research milestone of the project. The chosen antenna-DGS designs that are presented in chapter 7, showed novel phenomena in the scan examples. The RDRA combined with the modified dumbbell cavity backed DGS indicates BW enhancement in parallel to scan stabilization for two array configurations. These phenomena, which were observed in infinite arrays, make the antenna-DGS designs meaningful to investigate further in finite arrays.

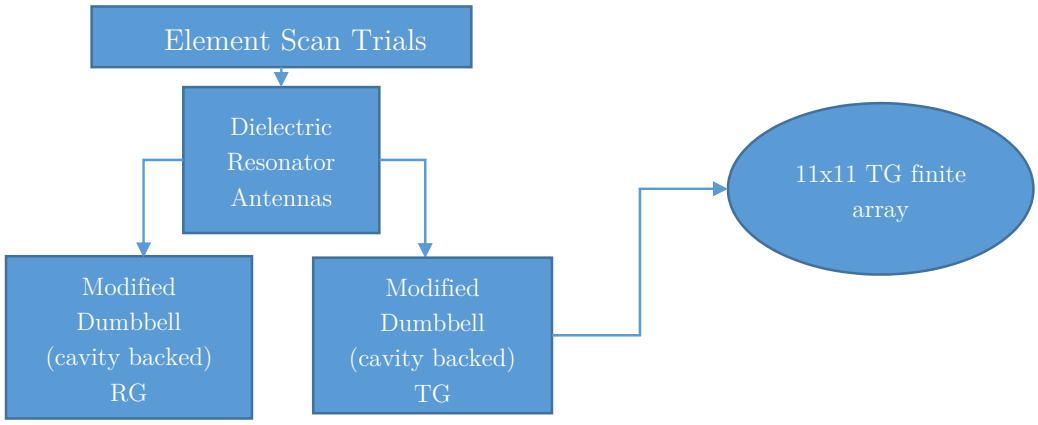

Figure 8.1: Element scan trials and selection antenna-DGS array element

In this chapter, finite array analysis follows constituted by 121 antenna elements. The selected lattice arrangements designed and compared with and without the periodic placement of defected ground structures. This analysis is more resource demanding than the infinite array but gives the opportunity to examine more realistic coupling and radiation phenomena.

Passive analysis is made first by exciting one element in the array and match load the rest. The analysis is focused to examine the impact of a DGS in the MC reduction of a finite array. Therefore, return loss, BW and the embedded patterns are compared with and without a DGS.

Active performance follows (important for phased arrays), in which all the antenna elements are excited. The center element active reflection coefficient is compared to the UC embedded element reflection coefficient. It is expected that the infinite array represents similar effects which happen at the central element of large finite array. Moreover gain and realized gain

are compared to the maximum available defined by the aperture of the array.

8.1 Array design layout with and without DGS

In previous chapters it has been addressed the benefit of using a defected ground structure between two E-coupled RDRA elements. There MC has been reduced significantly. Moreover, the scan performance in a triangular grid declared improved scan abilities by including the DGS in the array. Here the cavity backed modified dumbbell DGS replicated multiple times periodically creating thus a finite array of 11x11 unit elements.

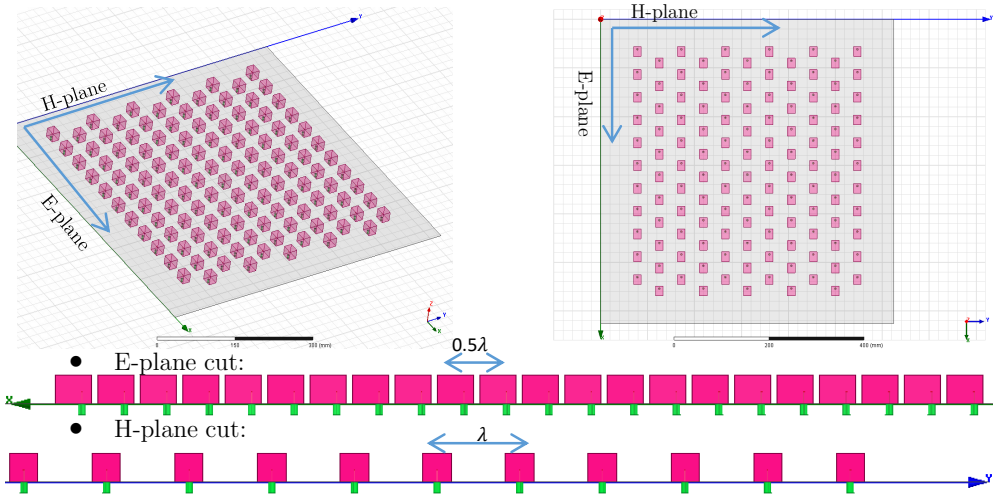

Figure 8.2: 11x11 finite array RDRA- No DGS triangular grid:

Figure 8.2 illustrates the array configuration without a DGS. The distance between H-coupled elements is one wavelength (frequency in S-band), thus MC levels can be reduced compared to 0.5λ antenna element spacing. On the other hand, E-coupled elements they are separated by a 0.5λ distance (instead of λ) and is expected to have strong coupling, similar to E-coupled elements placed in a rectangular grid. More benefits from this configuration are discussed in § 7.2.3.

Figure 8.3 illustrates the DGS placement advantage in this grid. The tuned backed cavity modified dumbbell is in a cross position between the E-coupled and H-coupled elements. Maintaining the same lattice arrangement for the antenna elements as in Figure 8.2, both planes (orthogonally) face the DGS compared to a rectangular grid. In a rectangular grid only E-coupled elements can benefit by the synthesized

DGS (see Figure 8.4a). Therefore, it is interesting to study how the DGS will respond by both excitations, in this cross coupling antenna-DGS element position.

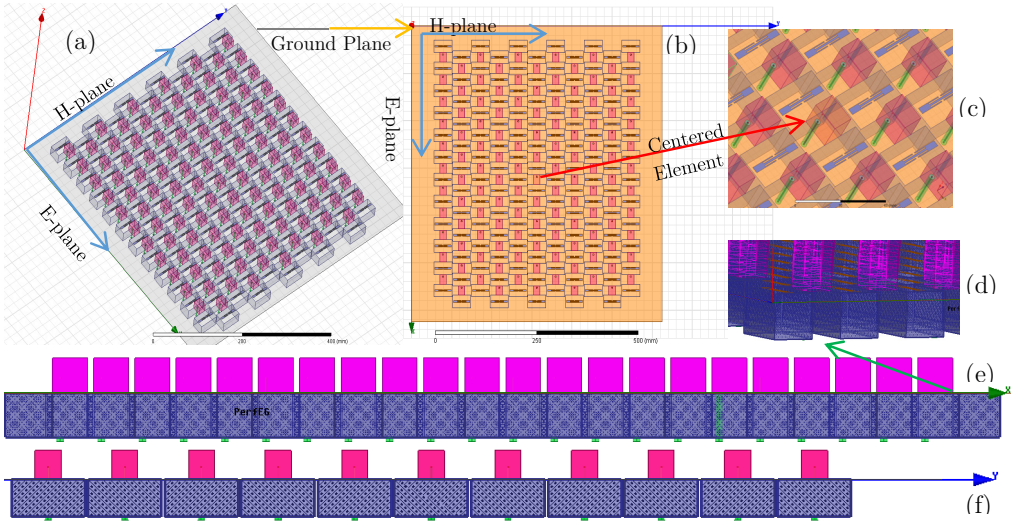

Figure 8.3: 11x11 finite array RDRA-DGS triangular grid: (a) side view (b) top view (c) centered element, dgs and nearby antenna elements (d) underground cavities E-plane discontinuity gaps (e) E-plane cut (f) H-plane cut

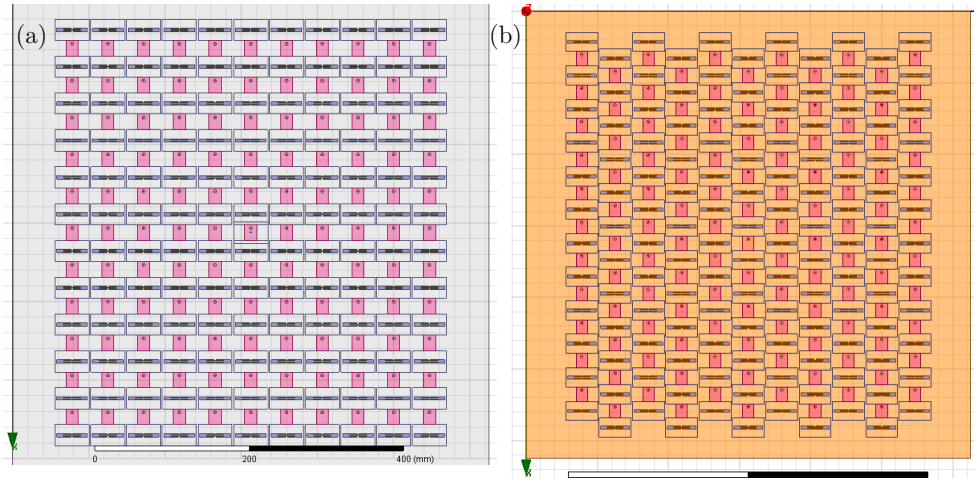

Figure 8.4: Synthesized DGS placement ability in different lattice: (a) Rectangular compared to (b) triangular grid

8.2 Embedded element approach

Embedded element analysis estimates the phased array properties of an array. Exciting one element in a dense array, feed as well as radiation

properties are affected. In this way, it is evaluated the efficiency of an element antenna influenced by the nearby parasitically excited elements.

Specifically, the excited element will not account reflection losses only by its individual impedance mismatch but the receive power from the parasitically excited elements will contribute to it. In the same manner, the element radiation pattern (embedded) will not only have the radiation characteristics of the single element. The embedded pattern is an interference pattern of the excited element and the parasitic patterns; the constructive and destructive field summations modulate the ideal stand-alone pattern resulting to dips or nulls.

Evaluating the resulting patterns is an important array analysis as the embedded patterns of the elements combined with the array configuration (array factor) can give a first estimate for the element efficiency in the array scan performance. For example, dips or nulls can cause in-efficient array beam radiation in a particular direction. Moreover, as stated by [64], the gain and directivity variations of the fully broadside uniform excited array can be explained by the gain of the embedded elements. The array gain can be found by summing up the realized gain of the embedded elements.

8.2.1 Return loss

Figure 5 depicts the embedded reflection coefficient for the arrays presented in Figure 8.2 (without DGS) and Figure 8.3 (with DGS). The reflection coefficient for each element in both arrays is well below the radiation threshold for the desired frequency.

Significant bandwidth enhancement is shown with a DGS in the array. Bandwidth roll-off achieved by a secondary frequency resonance. This resonance is combined with the resonance without a DGS. It is interesting this phenomenon as it is valid for all the elements in the array. Regarding the center element in the array, with a DGS its bandwidth enlarged by 37.5% (similar effect for the rest elements).

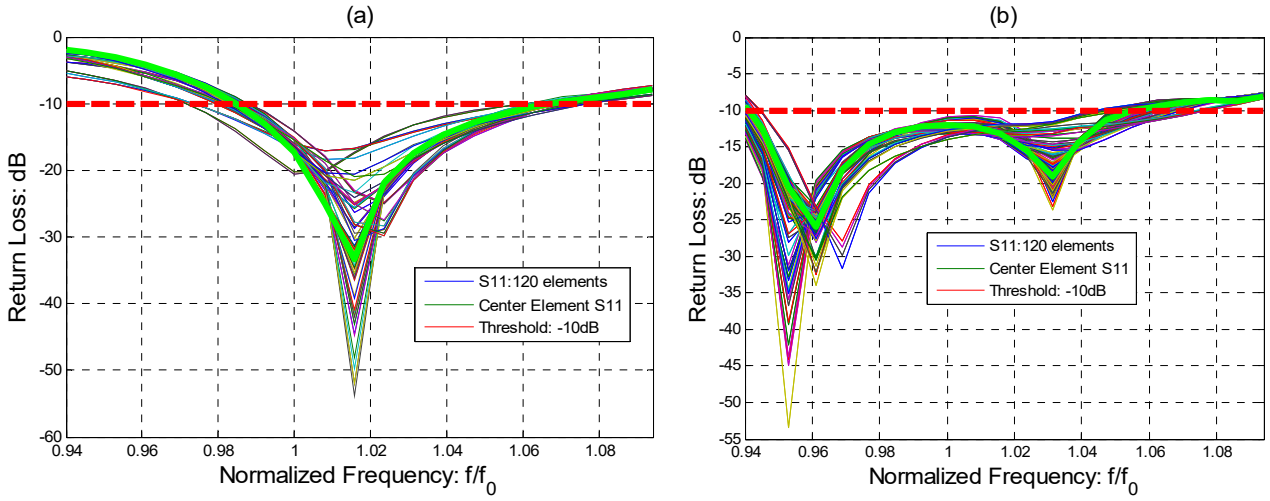

Figure 8.5: Embedded reflection coefficient normalized at the isolated RDRA resonance frequency: All the elements without (a) and with (b) a DGS

8.2.1.1 DGS resonance pole and BW enhancement

The main concern of this study is to address how this extra BW is able to be supported. In order to provide a physical explanation about this phenomenon 4 different return loss examples compared. Figure 8.6 depicts the reflection coefficient for the stand alone element antenna RDRA (red), the tuned DGS resonance between two E-coupled RDRAs (blue curve with (solid) and without (dashed) a DGS) and the embedded reflection coefficients of the center element in the finite TG array (FATG-CE 11x11) with (solid green) and without (dashed green) a DGS. In all cases the RDRA element maintains the same physical size and dielectric properties.

Regarding the finite array without the DGS, BW significantly shrinks and shifts towards higher frequencies compared to the reference stand alone case. Thus, it is concluded that reflections towards the excited element from the parasitically excited elements induced considerable impedance mismatch for the interested lower-band. Importing the DGS at resonance frequency lower that the desired (fo), causes significant reduction in mutual couply adjacent to that resonance. Thus, a secondary resonace for the embedded RDRA-DGS is accepted and merged with the previous one.

Overall, the enhanced bandwidth is a combination between the improved isolation in lower frequencies (the destructive interference elliminated there) and the bandwidth allowed by the TG lattice. The above comparison

reaveals that the enhanced bandwidth in the finite array, when the DGS was added, is a result of the reduced MC.

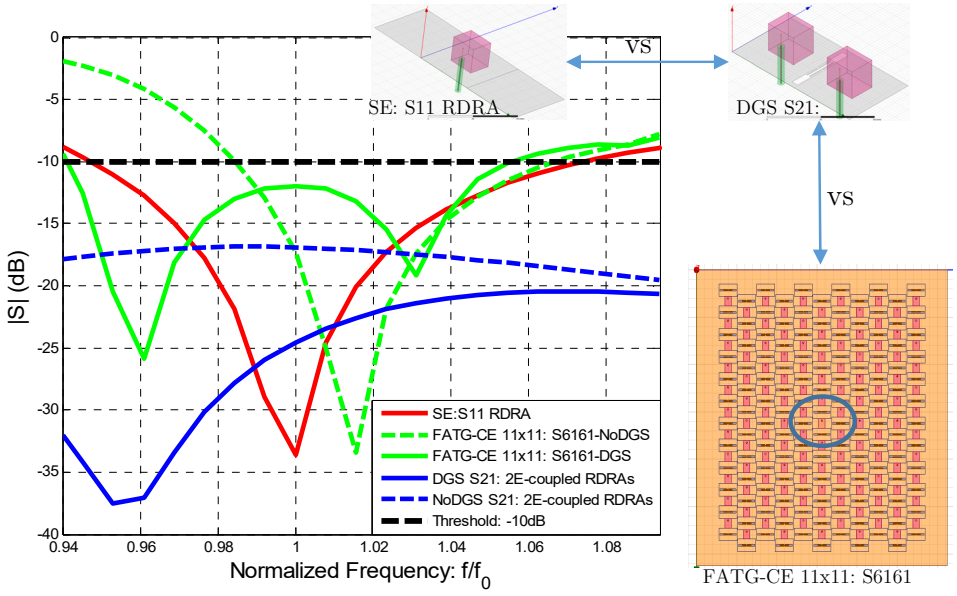

Figure 8.6: Return loss comparison between the stand-alone element antenna (red), the center embedded reflection coefficient with (green solid) and without (green dashed) a DGS and the tuned DGS resonance (blue-solid and dashed) between two E-coupled RDRAs

8.2.2 Array DGS excitation and antenna element couplings

As examined in chapter 6, the synthesized DGS acts as a meander magnetic dipole. Tuned and placed orthogonally between E-coupled antenna elements, the DGS can be excited by surface currents caused by the propagated MC electric near fields. The E-plane excitation, made it to radiate dominantly below the ground plane. In a triangular configuration, it is interesting to examine how the synthesized DGS resonates by exciting it from multiple planes. Therefore, this analysis helps to identify which reduction from the nearby elements allowed the enhanced bandwidth.

In this triangular antenna array configuration the DGS position was assigned between E-coupled elements as it was validated and tuned in §7.2.1. The H-coupled antennas (which are aligned in parallel to the DGS resonance length) and the 4 adjacent diagonal elements regarding the excited central element doubt the validated DGS efficiency in this new array configuration. This placement raised the concern that it can affect in a

negative way the DGS decoupling mechanism. For instance, it could have changed the radiation direction, towards the antennas-above the ground plane, thus increasing instead of decreasing the MC.

8.2.2.1 E and diagonal coupled elements

To study the different DGS coupling excitations and analyze the phenomena, focus made on the center element in the array (Figure 8.7). There, by the six adjacent neighboring antennas, the E and diagonal plane couplings extracted. In addition, the return loss added to compare the radiation ability of the excited antenna in the band of interested. Moreover, inter-element couplings and return loss without a DGS depicted for reference.

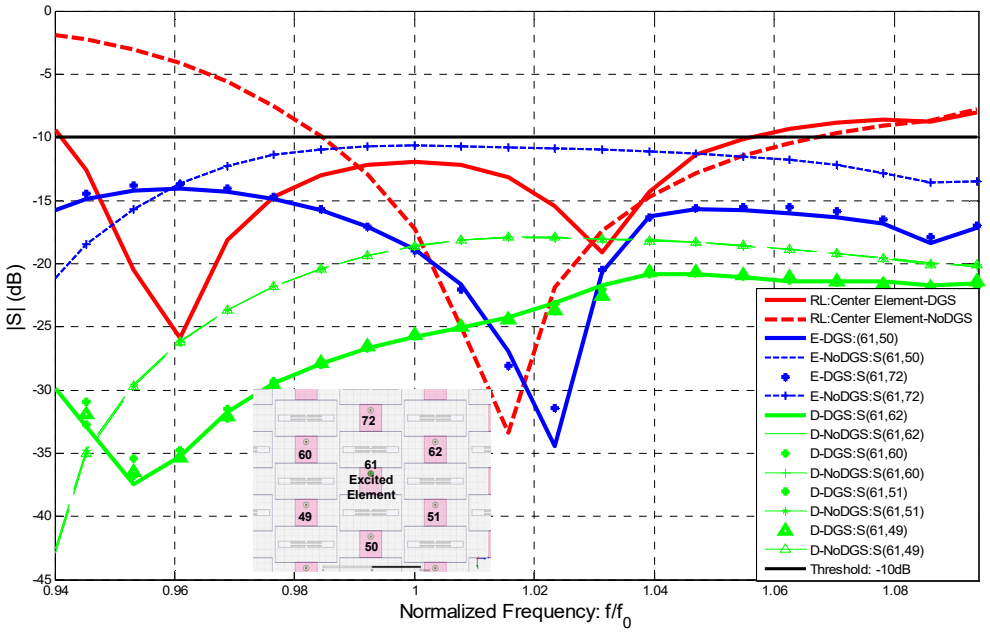

Figure 8.7: DGS compared to no DGS array: Center element return loss (RL-red color), E-plane (blue) and diagonally (green) coupled elements. Dashed non-bold lines correspond to the configuration without a DGS

E-coupled elements get reduction by 3dB in the radiation band with the DGS (blue curves stand for elements 72, 50). One can say that the coupling is increased for lower frequencies. However, it is important to take into account the new operational bandwidth. The DGS allowed a new band of effective radiation which makes the coupling effects to alter. Still, this increased coupling is lower than the coupling in an operational frequency

band region without a DGS. Moreover, close to the desired operational frequency, at 1.022fo, a resonant pole occurs with MC reduction of 24dB.

Regarding the 4 adjacent diagonal elements (green curves), MC drops down by 5 dB (0.95fo-1.02fo) in most of the radiation band and by 7 dB at the desired operational frequency (fo). Notably, the mirrored elements (62-49, 60-51, 72-50) present the same coupling (symmetrical elements with respect to the center element). Nevertheless, a resonance pole can be identified 0.96fo in a 10dB reduction.

Furthermore, it gives insights how the DGS element behaves for different excitation angles (in the plane of the array). The E-coupled elements (72, 50) can make the DGS to resonate significantly (having a pole and reduction of 24 dB) at a specific frequency, whereas the diagonal elements (45 degrees) excite it less but in broader band. This observation shows that in this configuration the DGS operation (tuned between E-coupled RDRAs) is angle depended. This can be explained by capacitive effects that are triggered by nearby excited defections. The DGS periodicity in this dense triangular placement made possible inter DGS-interaction (above the ground plane between the resonating defections) which shifts its operation compared to the referenced tuned behavior between E-coupled RDRAs (Figure 7.2).

Regarding the E-coupled elements the resonance pole has shifted slightly on higher frequency operation. This is because near the primary DGS two adjacent DGS elements are excited simultaneously by H-plane near fields. The three DGS elements interacted above the ground plane which creates a small group effect. On the other hand, the diagonal elements maintain similar operation to the reference tuned DGS (same resonance pole). This can be explained by the two orthogonally excited DGS elements located between the diagonal RDRAs and the center-excited element. Their coupling is lower than what is occurred for the DGS element in E-plane.

8.2.2.2 H coupled elements

Orthogonal to the excited element, H-coupled elements in the proposed triangular grid are located in a larger spacing than a rectangular grid (λ compared to 0.5λ). Thus, the levels compared to the rectangular array should exhibit lower coupling because of the spacious configuration in H-plane. Figure 8.8 demonstrates the statement by analyzing the referred arrays without a DGS (dashed green vs. dashed red). Although the

impedance match at 1.02fo is exactly the same, MC in the triangular grid is significantly lower. Moreover, the noticeable shift in resonance frequency indicates how the lower interaction affects the element impedance match. The triangular arrangement, because of lower capacitance between the antenna elements, tries to shift the resonance towards the primary design frequency (fo evaluated for a stand-alone RDRA).

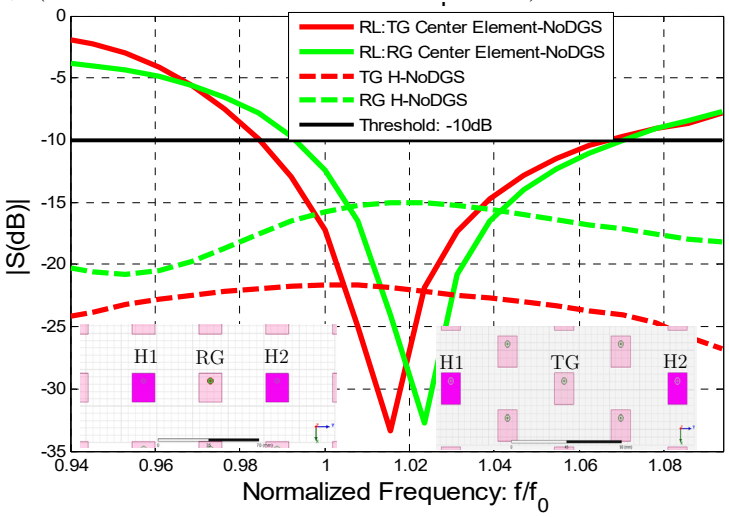

Figure 8.8: Rectangular (green: RG) compared to triangular grid (red: TG) H coupled elements (H1, H2) cross talk with the center element. Solid lines represent the central element return loss while dashed the adjacent element transmitted power

Knowing that H-plane coupling in the proposed triangular grid gets reduced, the effects further investigated in the presence of a DGS. Figure 8.9 demonstrates that the parallel DGS excitation by the H-plane near-fields, makes possible MC reduction. Moreover, it is interesting that occurs in the same resonance that the E-coupled elements were exciting the DGS (Figure 8.7). In both cases a transmitting deep between the H-coupled and E-coupled antenna elements occurs around 1.3fo, which makes the particular synthesized RF element effective for both planes (although tuned for E-plane). Furthermore, the shift in resonance is similar because three nearby DGS elements interact above the ground plane.

However, on the lower frequencies increased coupling from 0.94fo-0.98fo resulted (Figure 8.9). The improved impedance bandwidth (which before was not available) can explain this phenomenon. Specifically, without a DGS for the higher frequencies (1.04fo-1.09fo) the impedance match levels are comparable with the ones obtained with a DGS, thus there the transmitting levels towards H-coupled elements are similar. In the center

sub-band (0.98fo-1.04fo), DGS resonates thus lower coupling occurs. In contrary, the difference in impedance match for the lower band (0.94fo-0.98fo) is significant. The antennas without a DGS are mismatched and reflect most of the input power whereas with a DGS at least 90% of the power transferred to the far field. Therefore, in those frequencies significant radiation is now possible which couples stronger the elements.

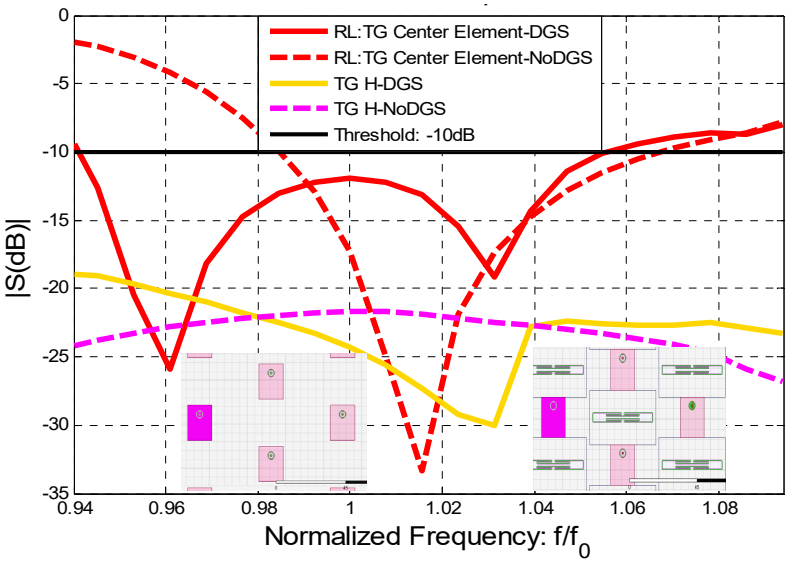

Figure 8.9: Triangular grid (TG) 11x11 RDRA-DGS array: H-coupled elements comparison with and without DGS. Red color represents the matching of the center element (RL) $|S_{6161}|$ and pink color the coupling between the center element and the H-coupled elements. Solid lines represent the DGS impact on matching and coupling.

Overall, E-coupled, D-coupled (diagonal) and H-coupled elements are able to benefit from the DGS triangular placement by the reduction in their coupling. Each reduction is characterized by shifts in resonance frequency caused by capacitive effects of the excited DGS elements.

It is concluded that the diagonal MC reduction is the main cause of the observed BW enhancement, as the improved resonance in the center element return loss overlaps with DGS resonance excitation by the diagonal coupling.

8.2.3 Array DGS coupling near-field analysis

The Array-DGS feed point of view revealed that the synthesized RF DGS component, in its centralized location between E and H coupled elements, benefits the elements located in the principal planes as well on the diagonal

planes. The mentioned study focused on adjacent nearby antenna elements by analyzing and comparing the amount of coupled power.

In order to give more insights about the occurred physical phenomena, here the electric near field study is analyzed in the array by exciting the central element. In this way, a global point of view is illustrated as the effects are studied for the whole array. The interactions between the antenna elements are translated by the intensity of the magnitude in the underground cavities. Therefore, a coupling profile can be identified as well as which are the critically affected coupled elements. This analysis can be considered as an alternative way to evaluate the de-coupling DGS abilities (Figure 8.10).

High intensity in the cavity (red color) means significant MC reduction between the nearby elements. In other words, the more intense the DGS element is the more critical coupling without a DGS occurs between the antenna elements, as the DGS excitation is stronger.

Three different zones addressed based on the criteria and the excited centered element. From electromagnetic point of view, these zones indicate the coupling dissipation in the array by exciting one element. Zone 1, which is excited from E-coupled elements, is illustrated as the most active coupling sector (for this particular frequency). On the orthogonal plane, excited by H-coupled elements, low intensity cavities resulted forming the second zone. In between them, a third zone occurs with intermediate coupling excitation compared to the previous zones. Moreover, they are characterized by an exponential decaying intensity away from the excited element, with the highest resulting attenuation in Zone-2 and the lowest in Zone-1.

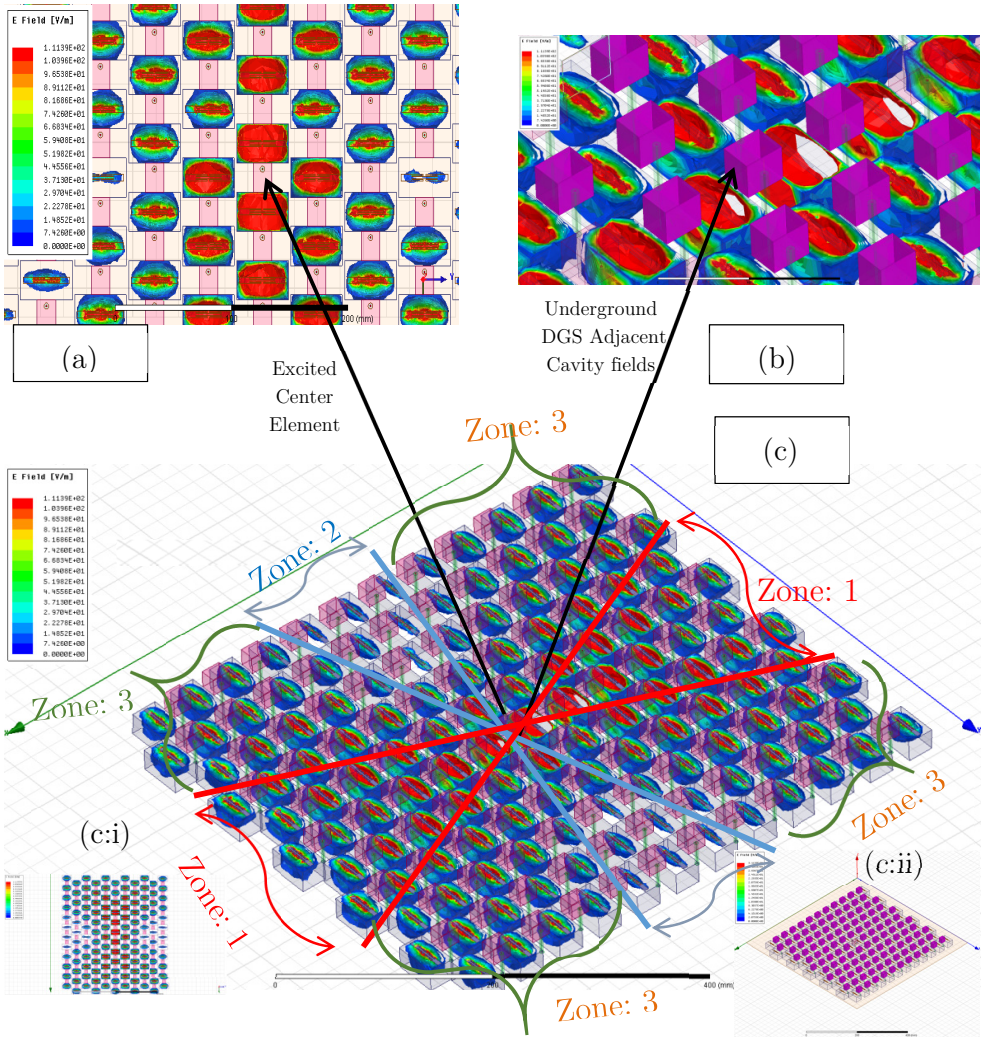

Figure 8.10: Embedded center element near-field analysis (a) Top view 36 adjacent nearby elements b) underground cavity fields for the adjacent DGS elements (c) 3D array side view underground fields: (i) top-view (ii) side-view array antenna elements

The 3D view (c) declares electric field intensity in all the cavities. Although the array is large, coupling induced even for the edge elements. Furthermore, the lattice element placement enables symmetrical coupling effects, observed by similar intensity cavity fields in symmetric locations (e.g. edge elements). Finally, focused on the array top view and the observations that were mentioned, the coupling dissipation follows a profile described by a mirrored triangle exponential decaying distribution.

8.2.4 Embedded patterns with and without DGS

8.2.4.1 Electric field patterns of the center excited element

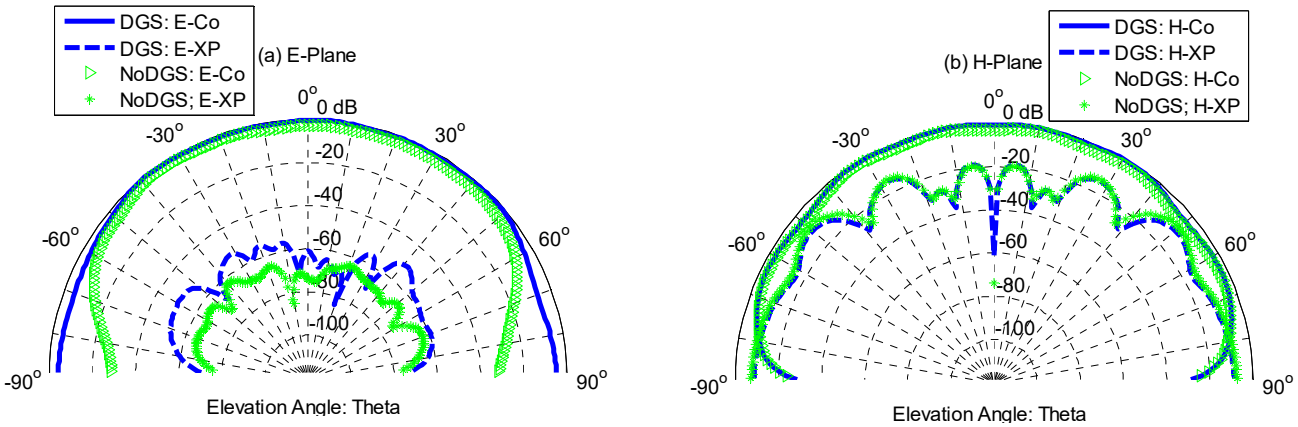

Figure 8.11: Electric field embedded patterns of the center element in the finite TG array

The electric field patterns of the center excited element shows that the cross polarization components for H plane remain unaffected with the DGS. On the other hand, the E-plane cross-components are slightly increased. Moreover, cross polarization pattern distribution in H-plane exhibits symmetry while in E-plane is asymmetric, with and without a DGS. This can be concluded as a trade-off between improvement in the pattern for E-plane with a slight cost in cross polarization. Overall, the cross polarization levels are maintained less than -18dB, over the entire angular range at the selected frequency for both planes.

8.2.4.2 Patterns in principle planes

The embedded patterns for the elements in the array, of the TG-11x11 array, are illustrated in Figure 8.12 and Figure 8.13, for E and H plane correspondingly. This analysis for each element is important. The superposition of the element pattern provides the phased array antenna gain at the position of the scanned beam [65]. It observed that variability from element to element is shown in the patterns. Even if the array is consider large enough, for the chosen dielectric resonator antenna elements, MC is not identical from element to element. Therefore the angular distribution varies dramatically.

- Element pattern improvement is observed in case of using DGS

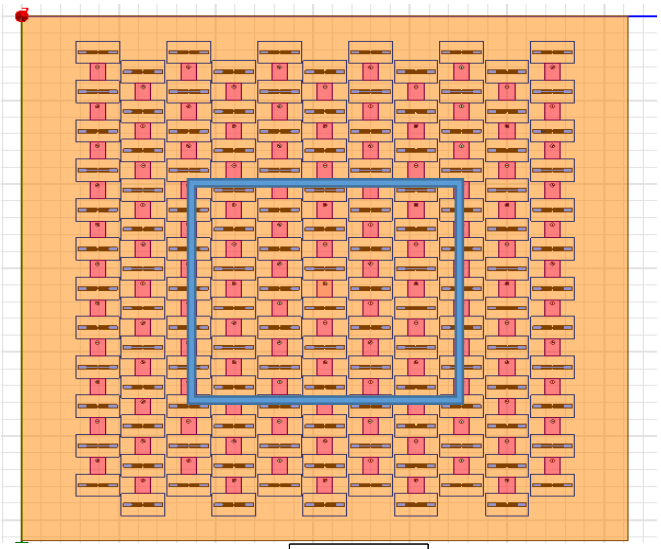

- E -plane patterns

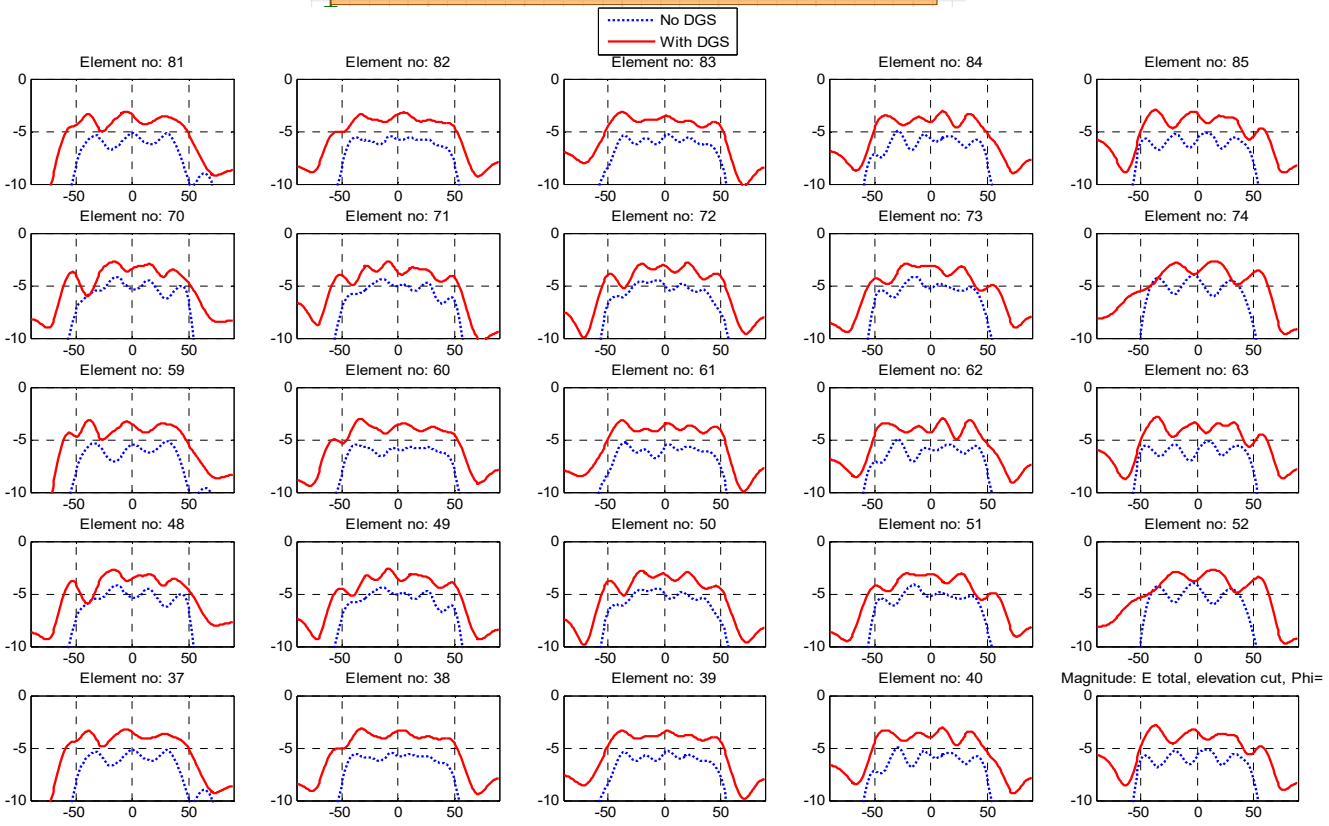

Figure 8.12: E-plane embedded patterns

- Element pattern improvement is observed in case of using DGS

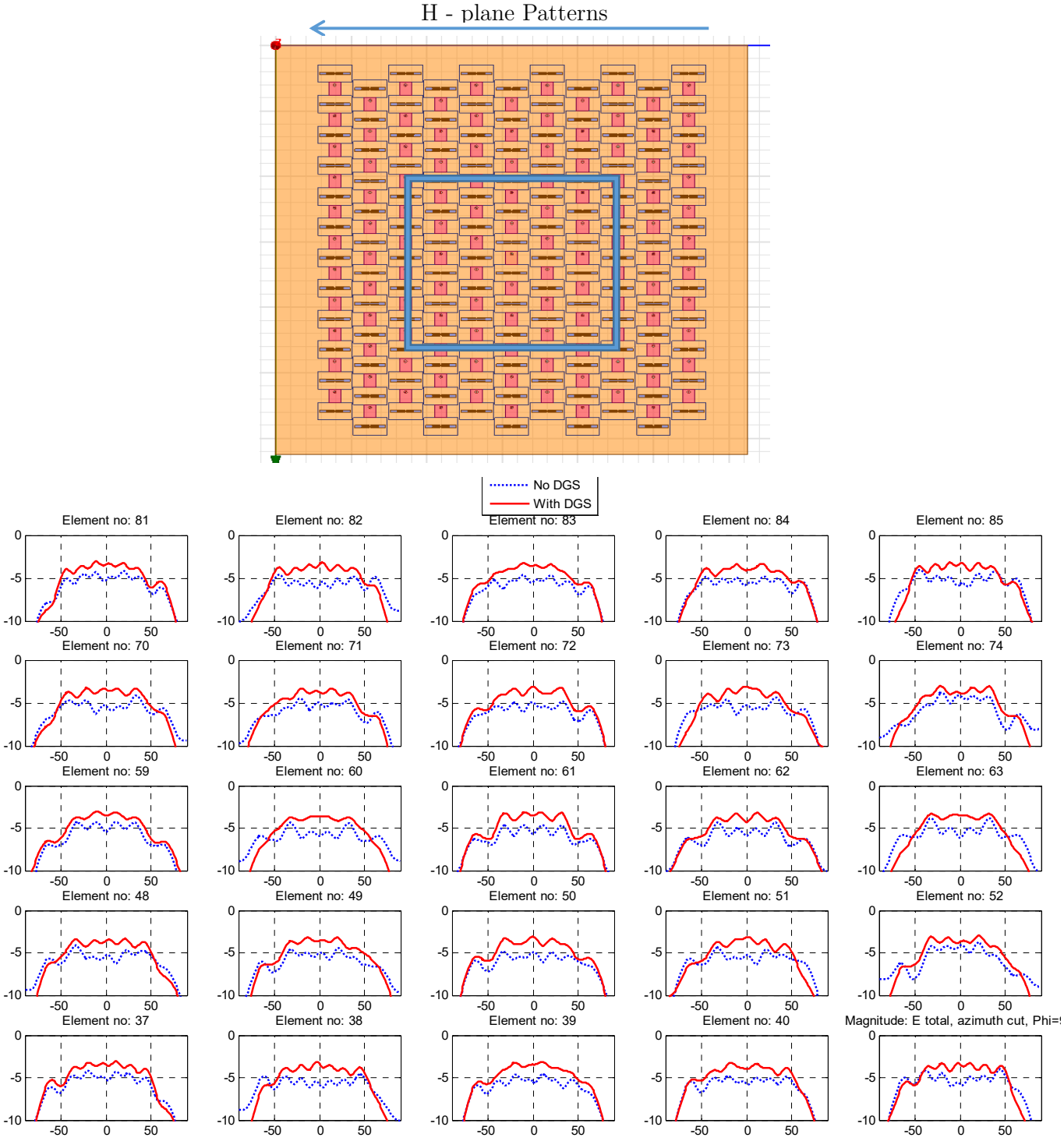

Figure 8.13: H-plane embedded patterns

For all the patterns reduction in element ripples are shown as well as more equalized amplitude levels from element to element with the DGS. Therefore, the effect of a DGS in this array can be translated into gain for each element at the scan angles where the patterns are improved.

For the array configuration in rectangular grid (RG) element pattern results for 5x5 and 11x11 finite RDRA arrays are shown in the appendix (§11.4.1, §11.4.2 correspondingly). For these RG arrays, in case where DGS was applied the patterns in E-plane were significantly improved compared to H-plane (see Figure 8.14).

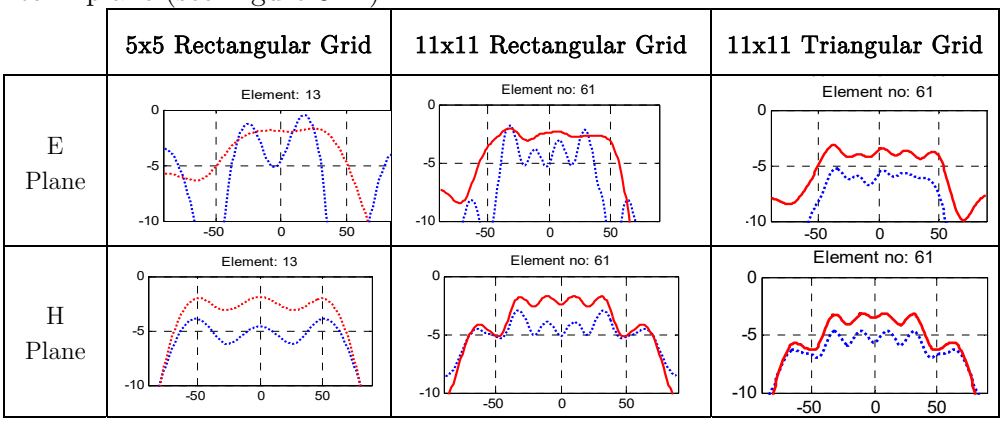

Figure 8.14: Centered embedded patterns for different antenna-DGS finite arrays

This is because the DGS was dominantly excited by E-coupled DRAs while in the triangular configuration the DGS is in a centralized position between E, H and D coupled elements. That leaves space for further optimization of DGS shape to make it working more efficient in both planes in triangular grid configuration. On the other side, from the configuration of strongly coupled 5x5 DRA elements it can be observed that applying DGS to small arrays results in significant quality improvement for the element patterns. This solution could be used in applications where small arrays are used but the quality of element patterns is important.

8.3 Active element approach

An active finite array analysis defines an integral part of this work in order to verify a possible phased array application. Here all the elements in the array are uniformly excited and the active reflection coefficient is measured in each of the array ports. In this layout, the inter element interaction effects are much more severe than what it was faced for the embedded analysis. The received power which is accepted by nearby excited

(active) elements on an already excited port influences the impedance match for each element in the array.

8.3.1 Active reflection coefficient

Figure 8.15, compares the active array without a DGS and with it. Without DGS (Figure 8.15a) the array is not able to radiate efficient in the band of interest. The majority of the elements can exceed the radiation threshold on higher frequencies which is out of the examined band. This because there MC reduces because of the electrically larger lattice inter-element spacing compared to those wavelengths. Moreover, the active operation created for certain ports (e.g. at 0.98fo) reflection coefficient higher than 0dB; this translates to amplification of the input signal while it is reflected back. Physically, those particular element antennas are almost completely mismatched and received energy from adjacent excited elements superimposes to it. Overall, only 5 elements out of 121 are able to radiate efficient for the designed frequency (fo). On the other hand, when the DGS is in between the elements in the array significant impedance match improvement in the whole band occurs. It is important to mention that at the resonance frequency of the tuned DGS (0.96fo) almost all the elements have a return loss below the radiation threshold (except 6).

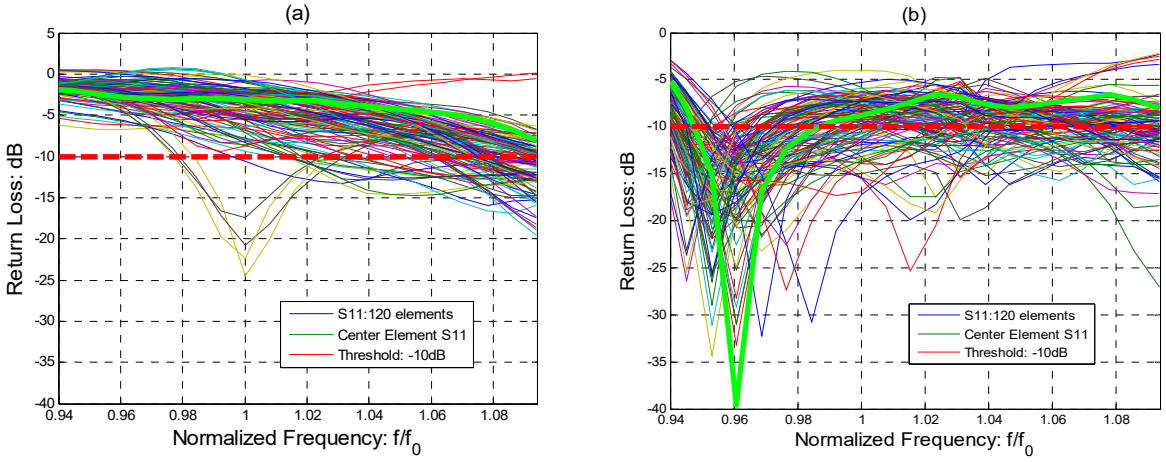

Figure 8.15: Active reflection coefficient without (a) and with DGS (b): Both figures include the return loss for all the elements in the uniform active array. The red-line shows the radiation threshold (-10dB) while the green bold line the reflection coefficient of the center element

To gain physical insights for the DGS impact in the active operation the active center element return loss compared to the embedded and infinite

array case (see Figure 8.16). It is demonstrated that at the frequency where the DGS was tuned (between 2E-coupled RDRAs: blue curve at 0.96fo) the embedded (green solid), the active (red solid) and the infinite array (pink solid) reflection coefficient are well matched. On the contrary, without a DGS (corresponding colors: dashed at 0.96fo) all of them are mismatched.

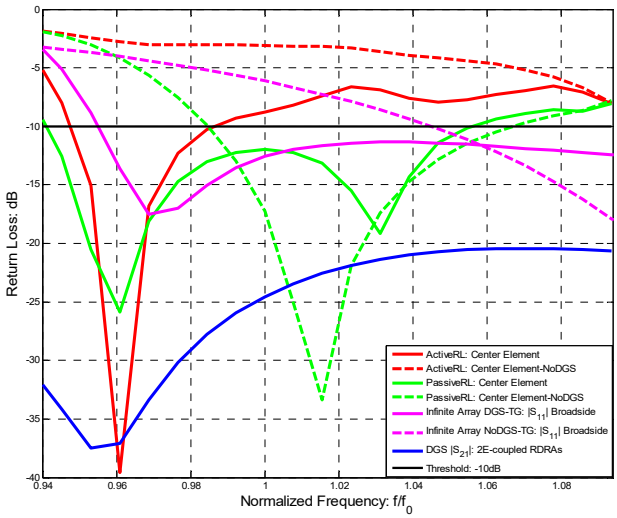

Figure 8.16: Center element active reflection coefficient (red) compared to the embedded reflection (Passive: green) with (solid) and without DGS (dashed)

The difference between the embedded reflection coefficient with and without DGS was attributed to MC reduction between the diagonal elements (§8.2.2). As it is shown from the observations in Figure 8.16, this is also valid for the active return loss in the 11x11 finite and infinite arrays (which both represent fully excited arrays). The resonance in both arrays is similar and improved with a DGS compared to the corresponding arrays without a DGS. However, the frequency resonance levels and the operational BW characteristics differ. The infinite array presents enhanced operational BW whereas in the finite array this operational bandwidth enhancement is limited close to the DGS stop-band. This is because the arrays are not experiencing the same interactions. The infinite array assumed identical excited elements, thus the same coupling was occurring for each element in the array. In the finite array this is not true as it is a truncated version of the infinite array. Edge effects alter the coupling conditions and as consequence, the impedance of each element is affected. As a result, the impedance match for both arrays differs [3].

To demonstrate the aforementioned edge effect in the impedance match, several elements in the finite array characterized by enhanced bandwidth are illustrated in Figure 8.17. The active return loss from the selected elements shows quite enlarged operational bandwidth. These elements are located at edges of the array. For those elements the influence by neighboring elements is reduced therefore they can tolerate a larger bandwidth.

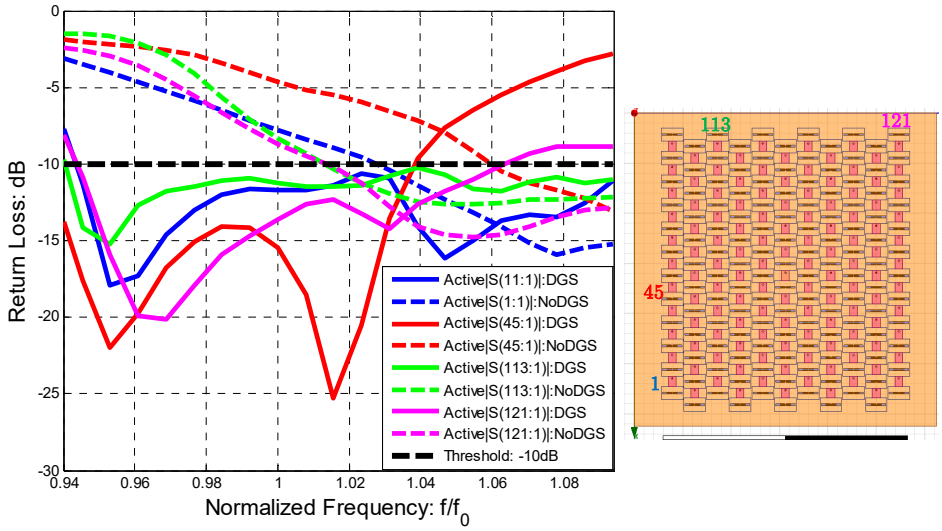

Figure 8.17: Active reflection coefficient with and without DGS for selected array elements: enhanced operational bandwidth with the DGS is observed

Another reason, which can be combined with the edge effects, is the intense near field excitation from the dielectric element antenna, that it has been used. A larger finite array may be required in order to represent identical effects as in the infinite array for the central element antenna.

Overall, in the active finite array, the DGS makes possible to obtain a stabilized frequency resonance for the majority of the elements near the DGS stop band and improved impedance match for the remaining band (although is not exceeding the radiating threshold).

8.3.2 DGS total array effect

The fully excited array produces an interference pattern in the far field which is the superposition of all the patterns of the element antennas [66]. Here uniform amplitude excitation is used for the elements with no additional phase shift from element to element. Therefore a beam is directed at the broadside direction (see Figure 8.18).

The broadside beam pattern is compared with and without a DGS. By comparing the directivity with the gain it is shown that the beam peak difference is negligible. This is because low losses have been dissipated in the dielectric material that it was used for the resonator antennas. Therefore, dielectric losses have minor impact on the realized gain. Thus we can directly compare the directivity with the realized gain with and without a DGS.

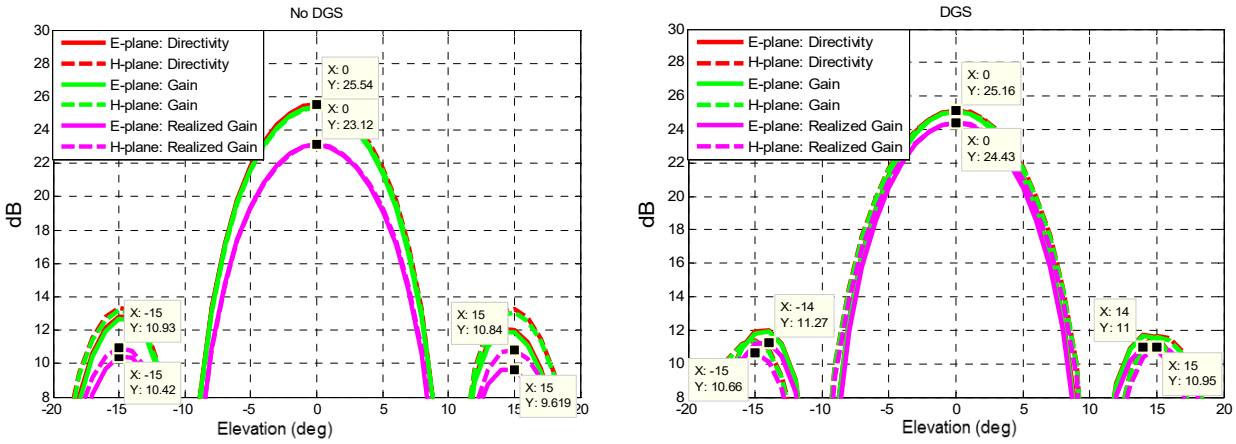

Figure 8.18: Directivity, Gain vs Realized Gain for the 11x11 fully excited RDRA-DGS broadside triangular array: LHS No DGS, RHS DGS

It is observed that the maximum realized gain with the DGS is improved by 1.3dB. This gain for the broadside beam can be explained by the improved active reflection coefficient in the array. In order to validate the efficiency of the array the maximum expected directivity is compared to the simulated realized gain.

The maximum directivity assumes ideal element radiators for the array with maximum directivity of 6dBi. Considering the embedded element maximum available total radiation efficiency, as mentioned by [64], in combination with the triangular lattice, the frequency of operation and the amount of elements the maximum available directivity of the array is found to be 25.8dBi. Therefore, the simulated array realized gain at 24.43dBi, with the DGS, is considered reasonable. The difference can be explained by the non-idealized patterns in the finite array, the small dielectric losses and the active impedance variability of the element antennas in the selected frequency. Table 8 summarizes the simulated directivity, gain and realized gain with and without a DGS for the triangular array configuration as well as for rectangular array.

Figure 8.19, depicts the realized gain for the principal planes with and without a DGS. The total array pattern that is obtained by the excited resonator element antennas is considered reasonable. The first side-lobe levels maintained below -13.16dB. Increased side-lobes are observed with the DGS for E plane on the secondary side-lobes. Finally, asymmetries occurred for higher order side lobes regarding the patterns with and without the DGS impact.

	RG		TG: E-plane shift	
[dBi]	No DGS (dBi)	With DGS (dBi)	No DGS (dBi)	With DGS (dBi)
Directivity	25.26	25.28	25.52	25.17
Gain	25.11	25.19	25.37	25.08
Realized gain	23.02	24.38	23.13	24.43
Maximum available directivity	25.8 (dBi)			

Table 8: Directivity, gain, realized gain and maximum available directivity for the 11x11 rectangular and the triangular arrays: Data presented with and without a DGS. With the DGS 1.3 dB improvement of realized gain for both arrays is observed

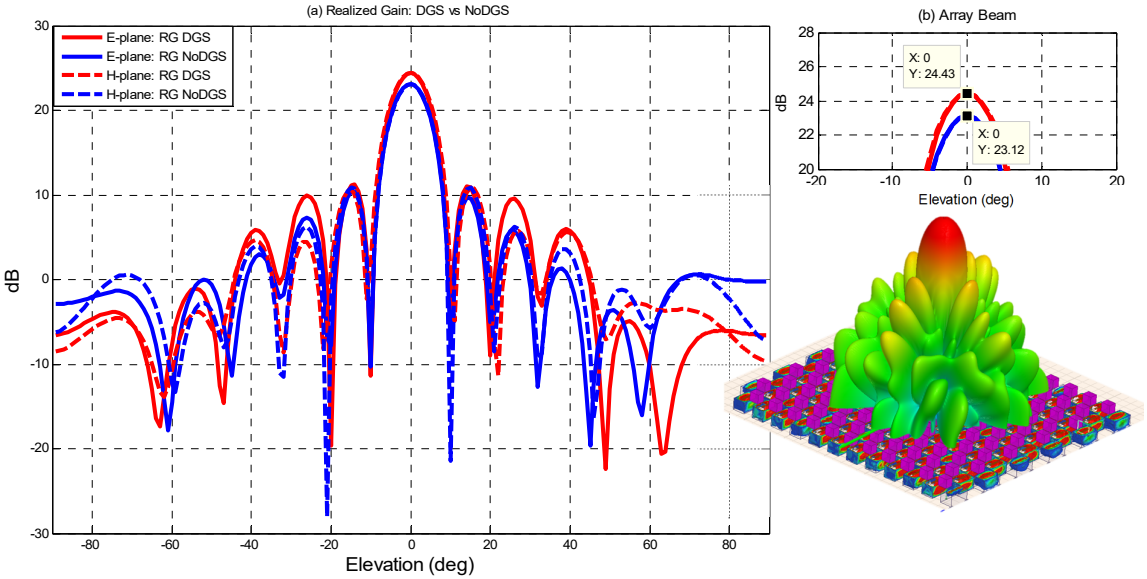

Figure 8.19: Realized gain of the fully excited 11x11 TG RDRA array with (red curves) and without (blue curves) a DGS: (a) Total array pattern (b) Array beam peak at broadside

8.4 Discussion

This chapter has approached the DGS functionality in a more complex design layout than the infinite array (see chapter 7). This was done in order to apply the proposed method as well as to examine the array radiation effects.

Based on the infinite scan performance the array antenna in triangular grid configuration was selected for further analysis. The criteria for this selection were based on the azimuth naval radar scan preferences and the centralized location of the DGS in a cross position between E-coupled, H-coupled and Diagonal-coupled elements.

The embedded analysis (from the feed point of view) verified BW enhancement for all the elements, compared to the array without DGS. Furthermore, this passive analysis made possible to investigate the coupling effects, which indicated the reason of the BW enhancement. Specifically, by investigating the nearby-coupled elements, it was concluded that MC reduction from diagonal elements, mainly, caused the extra BW enhancement. This conclusion is based on the correlation between the DGS stop band characteristics and the element coupling effects by including the DGS in the finite array. Moreover, the proposed triangular DGS-lattice arrangement was able to decouple significantly E as well as the H coupled elements. From the radiating point of view, the embedded patterns present improved quality (compared to the array without a DGS). Less ripples and deeps as well as more equalized amplitude levels were observed. These angular quality pattern effects are therefore translated in array bean scan gain enhancement.

The active analysis, which followed, provided insights for the DGS application on a fully excited array. For that reason, regarding the antenna element impedance match, the infinite and the finite arrays were compared. In both cases, the compared active reflection coefficient had similar resonance frequency, regarding the center element in the finite array. However, the return loss levels varied which resulted in different operational bandwidth. The differences can be explained by the uneven MC from element to element. This is observed by the variability of the embedded element patterns. Edge effects in combination with the intense coupled dielectric resonator antenna element, which was used in the array, can be

considered as the sources of this variability. Therefore, it can be concluded that the limited size of the array (11x11), which was used in the presented examples, is not large enough to become fully comparable with the effects observed for infinite array. On the other side in practical applications the antenna arrays always have finite dimensions and edge effects of finite arrays have to be taken into account. Despite that, similar bandwidth trends were obtained. Finally, the realized gain of the fully excited 11x11 element array has increased by incorporating the DGS in the phased array (by 1.3dB).

9 Conclusions

9.1 Discussion and conclusions

In the presented work, the reduction of MC (MC) between antenna elements was investigated. During the investigations, operational bandwidth, surface current distribution, near fields and radiation patterns were examined for coupled antenna elements. These investigations were considered as the performance parameters for evaluation of various decoupling methods.

The need for a compact structure that reduces MC applicable in antenna arrays with d=0.5λ led to investigate the possibility of exploiting the available ground plane by local modifications (also called in literature as "defects"). Ease of fabrication (2D) and low cost of implementation (GP etching technique) made the method more applicable compared to various decoupling methods provided in literature. Those methods required increased complexity for the feeding network, bulky structures in the substrate or redesign of the antenna architecture (see §3.2). Therefore, in order to verify the DGS coupling reduction ability selected designs from literature were reproduced. Furthermore, they were modified in order to obtain physical insights for their operation considering in parallel desirable BW requirements. That was realized by creating resonating ground plane defects between E-coupled antenna elements. Examples on substrate antennas resulted in narrowband MC reduction. In order to meet larger bandwidth requirements it was decided to extend the tests towards the antennas on metal plate. In this class of antennas, dielectric resonator antennas (DRAs) were chosen for further studies. This broadband antenna combined with simple slot-DGS showed potential for broad mutual coupling reduction. In the next step, supporting the DGS slot with a cavity located below a ground plane resulted in enhanced isolation bandwidth between the E-coupled antennas. As a final step, the combined DGS-cavity structure was examined for its resonance dependence on the antenna element geometry and material variations. Results showed good and stable RF performance of the designed RF structure. It is worth to mention that in case of combination patch antenna and DGS ring resonator as an element for reduction of MC any modification applied to patch antenna influenced the performance of ring DGS and any modification of ring DGS influenced

the matching of patch antenna. Similar effects as for ring DGS were also observed for combination of patch and PIR (see §4.4.1, §5.2.1 and §11.1).

However, it was a challenge to investigate the expansion of the proposed method in a more complicated scenario, such as a planar array. Therefore, extra constrains regarding the limited area between the antenna elements (0.5λx0.5λ) needed to be considered. To satisfy that, a structure named in literature as dumbbell DGS was chosen. The new structure design, compared to the slot, provided more parameters of resonance tuning which in parallel maintained similar isolation bandwidth. In this way it was possible to create smaller element with RF performance similar to DGS slot resonator. This dumbbell element was not yet sufficient to provide the broader BW performance in a layout that fits in the limited array grid area. Therefore, additional modifications in geometry of dumbbell element were applied which resulted in five tuning parameters.

For that type of DGS element physical insights regarding its operation were studied (not frequently described in literature for phased arrays yet). The perspective of facing a DGS as a parasitically excited antenna was studied. Specifically, near field analysis of interactions between antenna elements and DGS demonstrated that the excited resonant defection produced radiation below the ground plane, which raised concerns about its functionality in a dense array. To illustrate the possible inter-DGS cross talk, the DGS shielding effect was examined. Results showed that MC below the ground plane caused an inter-DGS group response which resulted in less effective reduction of MC compared to multiple closely shielded DGS. Based on that, the multi element DGS application in an array was considered as not suitable. Therefore, to tackle the underground radiation as well as the need for a stable RF decoupling structure, a cavity was created below the ground plane under the DGS. Tuned on the DGS resonance, the cavity can accept and store the underground DGS radiation and isolate each DGS below the ground plane from nearby radiations. The combination of DGS with cavity allows to obtain effective and frequency stable decoupling structure which fulfills the requirements (regarding size and RF performance) to be placed between antenna elements in array configuration. In this way the first project milestone has been achieved.

Compared to the experiments with micro-strip patch antennas, the RDRA-DGS scan performance provided enlarged operational BW for the examined

scan angles (broadside-60°) and scan stability for two lattice configurations (rectangular and triangular). It was further demonstrated that frequency stable impedance match of antenna element overlapped with the frequency region where the DGS showed the strongest decoupling between antenna elements. The observed phenomenon confirms the assumption that by reducing/controlling MC it can be possible to obtain a better matching stability for various scan angles.

In the next step the array antenna in triangular grid configuration was selected for further analysis. This aimed to verify the applicability of the proposed method as well as to examine the array radiation effects. The analysis (from the feed point of view) verified BW enhancement for all the elements. Specifically, by investigating the nearby-coupled elements, it was concluded that MC reduction from diagonal elements caused the extra BW enhancement. Moreover, the proposed triangular DGS-lattice arrangement was able to decouple significantly E as well as the H coupled elements. As a consequence, from the radiating point of view the embedded patterns had improved quality (compared to the array without a DGS). Less ripples and deeps as well as more equalized amplitude levels were observed.

The performed analysis showed that by applying the DGS structure between DRA antenna elements for array in triangular lattice the scan performance and the quality of the elements patterns is improved. In the next step the further studies were done to provide insights for the DGS application on a fully excited array. For that reason, regarding the antenna element impedance match, the infinite and the finite arrays were compared. In both cases, the compared active reflection coefficient had similar resonance frequency. However, differences resulted in terms of operational bandwidth. It can be concluded that the limited size of the array 11x11 which was used in the presented examples is not large enough to become fully comparable with the effects observed for infinite array. On the other side in practical applications the antenna arrays always have finite dimensions and edge effects of finite arrays have to be taken into account. Despite that, similar bandwidth trends were observed. Finally, the realized gain of the fully excited 11x11 element array has increased by incorporating the DGS in the phased array (by 1.3 dB). This improvement was observed as well as for an 11x11 RDRA array (Table 9).

	RG		TG	
[dBi]	No DGS (dBi)	With DGS (dBi)	No DGS (dBi)	With DGS (dBi)
Realized gain	23.02	24.38	23.13	24.43

Table 9: Realized gain with and without a DGS for 11x11 rectangular and triangular RDRA array configurations

It is important to remind that the main goal of this thesis was to observe the impact of mutual coupling reduction on antenna array performance and not find a general solution for mutual coupling reduction regarding various type of radiators. That means that proposed techniques and structures may not be applicable to all types of antennas but only to the restricted class of radiators. The class of antennas that were successfully examined in this thesis was DRAs on metal plate. On the other side, based on additional experiments performed on antennas on substrate it was observed that by locating the DGS with backed cavity between patch antennas resulted in reduction of mutual coupling in significantly broader band compared to the results presented in the literature (§5.2.2). Limited improvement on scan performance for the patch antennas (§7.1) leaded to the conclusion that more extensive studies are required on patch array performance with DGS that exceeded the framework of this thesis.

Overall, it has been shown that applying the DGS in planar arrays constituting of DRAs, results in bandwidth improvement, improved matching for higher scan angles, reduction of element pattern ripples and more equalized amplitude levels between elements. It is concluded that proposed reduction of MC by using DGS with cavity for arrays consisting of DRAs can be used as a method to stabilize impedance matching for various scan angles. It should be added here that the proposed reference DRA array (without DGS elements) was not fully optimized regarding the scan performance. Based on that it is possible that for better scan optimized array the scan improvement observed by applying DGS elements can be less pronounced. On the other side, it is expected that the improvement of element patterns quality in case of reduced mutual coupling should be observable.

9.2 Recommendations for future work

The DRA arrays combined with the concept of DGS and cavity is a research project with many more potentials which provides plenty exploration possibilities for the future. In terms of the possible DGS configurations only a part of them, in this thesis, were simulated and analyzed.

For more compact designs, where the thickness of the array plays important role, the possibilities of reduction of the cavity depth would be an asset. Compact shapes can be obtained by the use of dielectric filled cavities such that they will reduce the necessary height below the ground plane. For example, lossy dielectric materials may be used in order to dissipate the power accepted in the cavities. In this way, the cavity size will maintain a compact shape as the resonant frequency will be tuned according to the relative permittivity of the chosen material. However, the impact on the DGS operational bandwidth should be considered by the selected dielectric cavity properties.

Based on the presented results it is observed that the presence of DGS between antenna elements in E-plane significantly reduces the MC. It can be noticed that for the array elements configured in rectangular grid direct coupling between neighbor elements occurs in H-plane where no DGS were located (Figure 8.4a). This arises question how the addition of a DGS structure placed in H-plane would influence the array performance. What type of structure could be used in order to reduce the MC in H-plane? Finding answers on these questions and assuming that reduction of MC in H-plane gives measurable improvements one could go a step further towards triangular grid. For the triangular grid configuration of the array DGS element is placed between antenna elements both in E- and H-plane. The further studies could be focused on the extended properties of DGS by creating "hybrid DGS" which would allow to obtain comparable MC reduction in both planes.

The next question that is interesting to be answered is how the presence of DGS would influence the side lobe levels in larger array antennas. In order to properly perform this test, array antenna (with and without DGS) consisting more than 24 element in one direction and few elements in other

should be simulated. In this way the proper amplitude taper could be applied which would result in low side lobes. Based on the observed improvement of element patters it is expected to obtain lower side lobes level in case of array with DGS. This comparison could be performed for various scan angles.

In addition, the DGS-cavity concept should be further studied in patch antennas designs that suffer from severe surface waves. A DGS centralized position between antennas in combination with state of the art reduction methods, can provide further reduction in MC. For example, a possible candidate method to be combined with is the multilayer dielectric architecture [42].

Finally, although the modified dumbbell DGS with a cavity provided good performance in the tested arrays antennas, it cannot be used to generalize the performance limitations of defected ground structures as elements for MC reduction. More DGS shapes should be simulated to extend the cavity backed DGS options and to broaden the selection space of the available DGS shapes for DRAs. An option for generating novel shapes can be through the supershape formula. This formula uses just few parameters and can create naturalistic shapes with gentle curves. So, having an overview on different DGS layouts and the corresponding properties, depending on the antenna array configuration one can have the right starting point for further optimization. For example, in dense arrays with element spacing smaller than half lambda an alternative cavity backed DGS can be proved more efficient in operational bandwidth and stop band response than the modified dumbbell.

10 References

[1] Mohammadian, Alireza H., Noel M. Martin, and Donald W. Griffin. "A theoretical and experimental study of mutual coupling in microstrip antenna arrays." *IEEE transactions on antennas and propagation* 37.10 (1989): 1217-1223.

[2] Yang, Fan, and Yahya Rahmat-Samii. "Microstrip antennas integrated with electromagnetic band-gap (EBG) structures: A low mutual coupling design for array applications." *IEEE Transactions on Antennas and Propagation* 51.10 (2003): 2936-2946.

[3] Mailloux, Robert J. *Phased array antenna handbook*. Vol. 2. Boston: Artech House, 2005.

[4] Pozar, David M. "The active element pattern." *IEEE Transactions on Antennas and Propagation* 42.8 (1994): 1176-1178.

[5] Henault, Simon, and Yahia Antar. "Unifying the Theory of Mutual Coupling Compensation in Antenna Arrays." *IEEE Antennas and Propagation Magazine*57.2 (2015): 104-122.

[6] Bhattacharyya, Arun K. *Phased array antennas: Floquet analysis, synthesis, BFNs and active array systems*. Vol. 179. John Wiley & Sons, 2006.

[7] Niow, C. H., Y. T. Yu, and H. T. Hui. "Compensate for the coupled radiation patterns of compact transmitting antenna arrays." IET microwaves, antennas & propagation 5.6 (2011): 699-704.

[8] Zam, Mariusz, and S. Piotr. "Comment on'Compensate for the coupled radiation patterns of compact transmitting antenna arrays'." *IET Microwaves, Antennas & Propagation* 8.10 (2014): 719-723.

[9] Bobor-Oyibo, F., S. J. Foti, and D. Smith. "Techniques to Improve the Wide Angle Scanning Performance of Multiple Beam Smart Antennas." (2013).

[10] Nascimento, Daniel Chagas, and Jose Carlos Silva Lacava. "Analysis and Design of Probe-Fed Linearly-Polarized Microstrip Antennas on FR4 Substrates." *IEEE Latin America Transactions* 6.12 (2014): 965-970.

[11] Nascimento, D. C., and JC da S. Lacava. "Cavity-backed hybrid microstrip antenna on FR4 substrate." *2013 IEEE Antennas and Propagation Society International Symposium (APSURSI)*. 2013.

[12] Munk, B. A., T. W. Kornbau, and R. J. Mailloux. "Comments on" On the use of metallized cavities in printed slot arrays with dielectric substrates"[with reply]."*IEEE transactions on antennas and propagation* 36.7 (1988): 1036-1041.

[13] Awida, M. H., and A. E. Fathy. "Design guidelines of substrate-integrated cavity backed patch antennas." *IET microwaves, antennas & propagation* 6.2 (2012): 151-157.

[14] Diallo, Aliou, et al. "Study and reduction of the mutual coupling between two mobile phone PIFAs operating in the DCS1800 and UMTS bands." *IEEE Transactions on Antennas and Propagation* 54.11 (2006): 3063-3074.

[15] Ranvier, S., et al. "Capacity enhancement by increasing both mutual coupling and efficiency: A novel approach." *2007 IEEE Antennas and Propagation Society International Symposium*. IEEE, 2007.

[16] Chebihi, Anissa, et al. "A novel isolation technique for closely spaced PIFAs for UMTS mobile phones." *IEEE Antennas and Wireless Propagation Letters* 7 (2008): 665-668.

[17] Rahmat-Samii, Yahya, and H. Mosallaei. "Electromagnetic band-gap structures: classification, characterization, and applications." *Antennas and Propagation, 2001. Eleventh International Conference on (IEE Conf. Publ. No. 480)*. Vol. 2. IET, 2001.

[18] Gonzalo, Ramon, Peter De Maagt, and Mario Sorolla. "Enhanced patch-antenna performance by suppressing surface waves using photonic-bandgap substrates." *IEEE Transactions on Microwave Theory and Techniques* 47.11 (1999): 2131-2138.

[19] Naser-Moghadasi, Mohammad, et al. "Compact EBG structures for reduction of mutual coupling in patch antenna MIMO arrays." *Progress In Electromagnetics Research C* 53 (2014): 145-154.

[20] Zhai, Guohua, Zhi Ning Chen, and Xianming Qing. "Mutual coupling reduction of compact four-element MIMO slot antennas using metamaterial mushroom structures." *Antenna Technology (iWAT), 2015 International Workshop on*. IEEE, 2015.

[21] Lin, B-Q., et al. "Uniplanar EBG structure with improved compact and wideband characteristics." *Electronics Letters* 44.23 (2008): 1362-1363.

[22] Li, Zhengyi, et al. "Reducing mutual coupling of MIMO antennas with parasitic elements for mobile terminals." *IEEE Transactions on Antennas and Propagation* 60.2 (2012): 473-481.

[23] Zhang, Qi-Chun, Jindong Zhang, and Wen Wu. "Reduction of Mutual Coupling Between Cavity-Backed Slot Antenna Elements." *Progress In Electromagnetics Research C* 53 (2014): 27-34.

[24] Ghosh, Jeet, et al. "Mutual Coupling Reduction Between Closely Placed Microstrip Patch Antenna Using Meander Line Resonator." *Progress In Electromagnetics Research Letters* 59 (2016): 115-122.

[25] Breed, Gary. "An introduction to defected ground structures in microstrip circuits." *High Frequency Electronics* 7 (2008): 50-54.

[26] Park, Jong-Im, et al. "Modeling of a photonic bandgap and its application for the low-pass filter design." *Microwave Conference, 1999 Asia Pacific*. Vol. 2. IEEE, 1999.

[27] Guha, Debatosh, Sujoy Biswas, and Chandrakanta Kumar. "Printed antenna designs using defected ground structures: a review of fundamentals and state-of-the-art developments." *Forum for Electromagnetic Research Methods and Application Technologies (FERMAT)*. 2011.

[28] Arya, Ashwini K., M. V. Kartikeyan, and A. Patnaik. "Defected ground structure in the perspective of microstrip antennas: a review." *Frequenz* 64.5-6 (2010): 79-84.

[29] Yu, Yantao, et al. "Dual-frequency two-element antenna array with suppressed mutual coupling." *International Journal of Antennas and Propagation* 2015 (2015).

[30] Xiao, S., et al. "Mutual coupling suppression in microstrip array using defected ground structure." *IET microwaves, antennas & propagation* 5.12 (2011): 1488-1494.

[31] Salehi, Mohsen, et al. "Mutual coupling reduction of microstrip antennas using defected ground structure." *2006 10th IEEE Singapore International Conference on Communication Systems*. 2006.

[32] Biswas, Sujoy, and Debatosh Guha. "Stop-band characterization of an isolated DGS for reducing mutual coupling between adjacent antenna elements and experimental verification for dielectric resonator antenna array." *AEU-International Journal of Electronics and Communications* 67.4 (2013): 319-322.

[33] Karmakar, Nemai C., et al. "Quasi-static analysis of defected ground structure." *TENCON 2005-2005 IEEE Region 10 Conference*. IEEE, 2005.

[34] Ghosh, Chandan Kumar, Bappaditya Mandal, and Susanta Kumar Parui. "Mutual coupling reduction of a dual-frequency microstrip antenna array by using u-shaped dgs and inverted u-shaped microstrip resonator." *Progress In Electromagnetics Research C* 48 (2014): 61-68.

[35] Salehi, Mohsen, and Ayaz Ghorbani. "Elimination of scan blindness in microstrip scanning array antennas using defected ground structure." *2007 European Microwave Conference*. 2007.

[36] Veisee, Soroush, Mahsa Keshavarz Hedayati, and Shahrooz Asadi. "A novel compact defected ground structure and its application in mutual

coupling reduction of a microstrip antenna." *Turkish Journal of Electrical Engineering & Computer Sciences* 24.5 (2016): 3664-3670.

[37] Ghosh, Chandan Kumar, Susmita Biswas, and Durbadal Mandal. "Study of Scan Blindness of Microstrip Array by Using Dumbbell-Shaped Split-Ring DGS." *Progress In Electromagnetics Research M* 39 (2014): 123-129.

[38] Hou, D-B., et al. "Elimination of scan blindness with compact defected ground structures in microstrip phased array." *IET microwaves, antennas & propagation* 3.2 (2009): 269-275.

[39] Guha, D., et al. "Defected ground structure to reduce mutual coupling between cylindrical dielectric resonator antennas." (2008).

[40] Zainud-Deen, S. H., Hend A. Malhat, and K. H. Awadalla. "Mutual coupling reduction in dielectric resonator antenna arrays embedded in a circular cylindrical ground plane." *Applied Computational Electromagnetics Society Journal* 25.12 (2010): 1129-1135.

[41] Kristensson, Gerhard, Peter Waller, and Anders Derneryd. "Radiation efficiency and surface waves for patch antennas on inhomogeneous substrates." *IEE Proceedings-Microwaves, Antennas and Propagation* 150.6 (2003): 477-483.

[42] Valavan, S. E., D. Tran, and A. G. Yarovoy. "A dielectric-contrast technique for effective mitigation of mutual coupling between dual-band array radiators." *The 8th European Conference on Antennas and Propagation (EuCAP 2014)*. 2014.

[43] Alexopoulos, N., and D. Jackson. "Fundamental superstrate (cover) effects on printed circuit antennas." *IEEE Transactions on antennas and propagation* 32.8 (1984): 807-816.

[44] Saidulu, V., et al. "Dielectric Superstrate Thickness Varying on the Characteristics of Square Patch Antenna."

[45] Llombart, Nuria, et al. "Impact of mutual coupling in leaky wave enhanced imaging arrays." *IEEE Transactions on Antennas and Propagation* 56.4 (2008): 1201-1206.

[46] Farahbakhsh, Ali, Gholamreza Moradi, and Shahram Mohanna. "Reduction of mutual coupling in microstrip array antenna using polygonal defected ground structure." *Applied Computational Electromagnetics Society Journal* 26.4 (2011): 334-339.

[47] Bait-Suwailam, Mohammed M., Omar F. Siddiqui, and Omar M. Ramahi. "Mutual coupling reduction between microstrip patch antennas using slotted-complementary split-ring resonators." *IEEE Antennas and Wireless Propagation Letters* 9 (2010): 876-878.

[48] Nikolic, Marija M., Antonije R. Djordjevic, and Arye Nehorai. "Microstrip antennas with suppressed radiation in horizontal directions and reduced coupling." *IEEE transactions on antennas and propagation* 53.11 (2005): 3469-3476.

[49] Ghosh, Chandan Kumar, and Susanta Kumar Parui. "Reduction of mutual coupling between E-shaped microstrip antennas by using a simple microstrip I-section." *Microwave and Optical Technology Letters* 55.11 (2013): 2544-2549.

[50] James, J. R., and A. Henderson. "High-frequency behaviour of microstrip open-circuit terminations." *IEE Journal on Microwaves, Optics and Acoustics* 3.5 (1979): 205-218.

[51] Caloz, Christophe, et al. "A simple and accurate model for microstrip structures with slotted ground plane." *IEEE microwave and wireless components letters* 14.3 (2004): 127-129.

[52] Biswas, Sujoy, et al. "New Defected Ground Plane Structure For Microstrip Circuits And Antenna Applications."

[53] Arya, Ashwini K., M. V. Kartikeyan, and A. Patnaik. "Efficiency enhancement of microstrip patch antenna with defected ground structure." *Recent Advances in Microwave Theory and Applications, 2008. Microwave 2008. International Conference on*. IEEE, 2008.

[54] Ghatak, Rowdra, Manimala Pal, and Biswajit Sarkar. "Realization of miniaturized quadrature hybrid coupler with reduced length branch arms using recursively loaded stubs." *Progress In Electromagnetics Research Letters* 43 (2013): 45-54.

[55] Liao, Shry-Sann, et al. "A novel compact-size Ka-band branch-line coupler."*2006 Asia-Pacific Microwave Conference*. IEEE, 2006.

[56] Elhiwairis, Mohamed Yasir Omer, et al. "Miniaturized size branch line coupler using open stubs with high-low impedances." *Progress In Electromagnetics Research Letters* 23 (2011): 65-74.

[57] You, Bin, and Junqing Zhang. "A novel defected ground structure with lengthened etched gap and microwave filter design." *2009 5th International Conference on Wireless Communications, Networking and Mobile Computing*. IEEE, 2009.

[58] Wyant, Andrea, and Jayanti Venkataraman. "Optimization of Reduced Size Microstrip Patch with slots using a Genetic Algorithm." *Department of Electrical Engineering, Rochester Institute of Technology* (2008).

[59] Pasakawee, Sarinya, and Zhirun Hu. "Electrical small meander line patch antenna." *2012 6th European Conference on Antennas and*

Propagation (EUCAP). IEEE, 2012.

[60] Salgare, Ms Dhanashri S., and Mrs Shamala R. Mahadik. "A Review of Defected Ground Structure for Microstrip Antennas." (2015).

[61] Gulbrandsen, Fredrik. "Design and Analysis of an X-band Phased Array Patch Antenna." (2013).

[62] Balanis, Constantine A. "Advanced engineering electromagnetics. 1989." *ed: John Wiley & Sons*.

[63] Chebolu, S. R., K-F. Lee, and R. Q. Lee. "Comparison of rectangular and triangular microstrip arrays." *Antennas and Propagation Society International Symposium, 1992. AP-S. 1992 Digest. Held in Conjuction with: URSI Radio Science Meeting and Nuclear EMP Meeting., IEEE*. IEEE, 1992.

[64] Kildal, Per-Simon, Abbas Vosoogh, and Stefano Maci. "Fundamental Directivity Limitations of Dense Array Antennas: A Numerical Study Using Hannan's Embedded Element Efficiency." *IEEE Antennas and Wireless Propagation Letters* 15 (2016): 766-769.

[65] Visser, Hubregt J. *Array and phased array antenna basics*. John Wiley & Sons, 2006.

[66] Constantine, A. Balanis. "Antenna theory analysis and design." *Microstrip Antennas third edition, John wiley & sons* (2005).

[67] Liu, Jingxian, Wen-Yan Yin, and Sailing He. "A new defected ground structure and its application for miniaturized switchable antenna." *Progress In Electromagnetics Research* 107 (2010): 115-128.

[68] Horii, Yasushi, and Makoto Tsutsumi. "Harmonic control by photonic bandgap on microstrip patch antenna." *IEEE Microwave and Guided Wave Letters* 9.1 (1999): 13-15.

[69] Kumar, Chandrakanta, and Debatosh Guha. "Defected ground structure (DGS)-integrated rectangular microstrip patch for improved polarisation purity with wide impedance bandwidth." *IET Microwaves, Antennas & Propagation* 8.8 (2014): 589-596.

11 Appendix

11.1 DGS Ring resonator vs. PRI sensitivity test

This section studies how sensitive is the Ring DGS and the PRI by the variations in geometry dimensions of the element radiators. In this concept the micro-strip Patch antennas (see §4.4.1 and §4.4.2) in H-plane, where decreased and increased in order to shift the resonant frequency of the radiating elements. This was aimed to observe how the DGS resonators would react to those frequency shifts. The criterion for this comparison is how stable the stop band response, in the referred cases, remains by the geometrical variations in the design (see Figure 11.1 Figure 11.2).

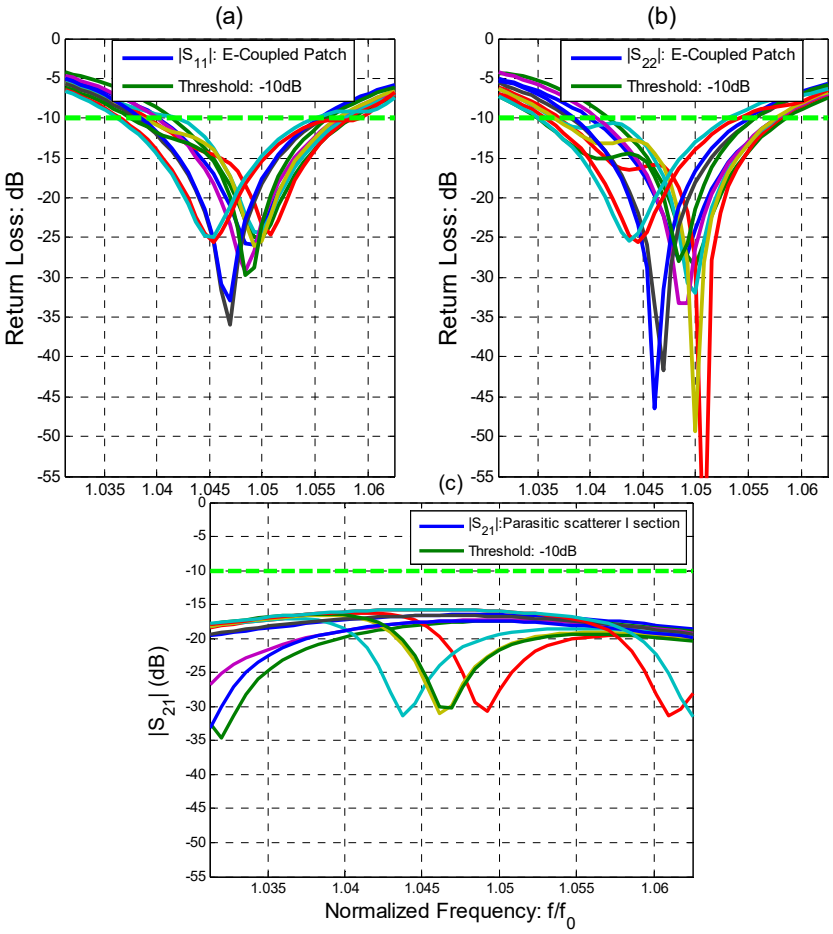

Figure 11.1: Resonance sensitivity for the parasitic scatterer I section between two microstrip patch antennas. a) Patch 1 impedance match b) Patch 2 impedance match c) transmission coefficient for the patch antennas

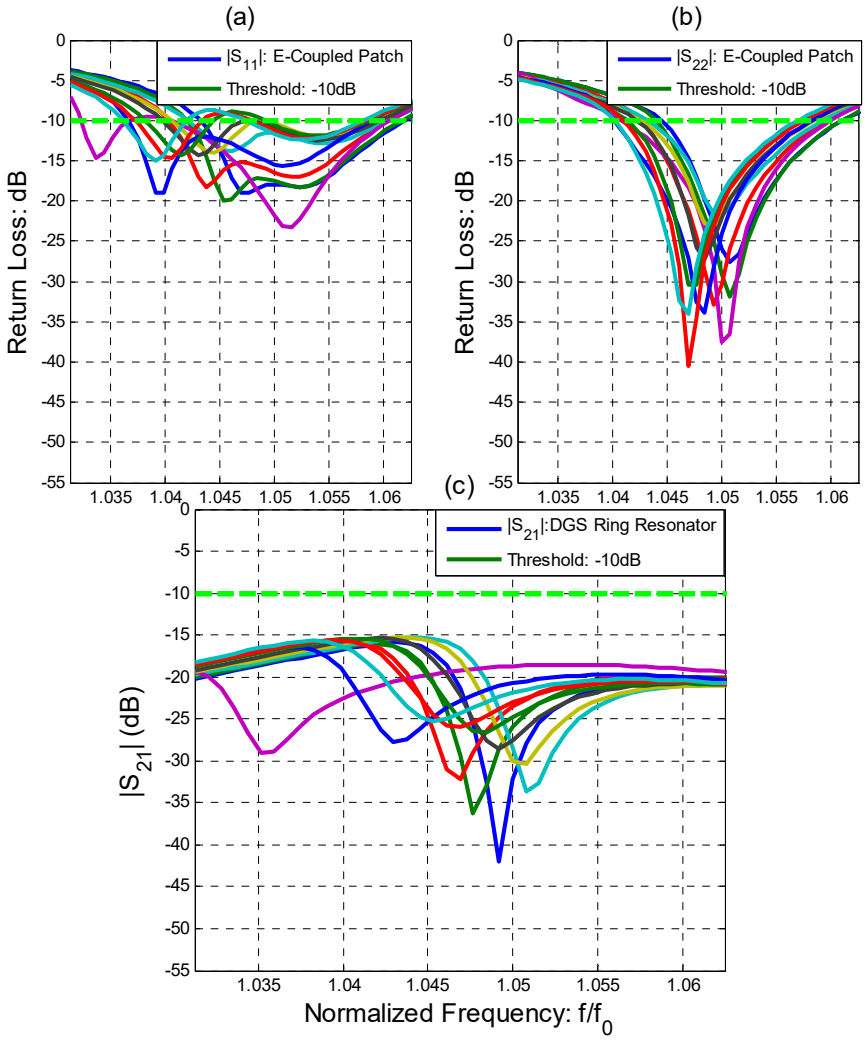

Figure 11.2: Resonance sensitivity for the DGS Ring resonator by geometrical variations on two microstrip patch antennas. a) Patch 1 impedance match b) Patch 2 impedance match c) transmission coefficient for the patch antennas.

As illustrated from the figures above both resonant structures are influenced by the variability in the design and the different impedance match of the antennas. Focused on the transmission coefficients, for both cases although the linear steps where identical, the Ring resonator is more stable than the PRI. This is observed by more resonances than the PRI which are concentrated nearby the tuned resonance (~1.5fo). It cannot be neglected that for certain values the Ring resonator causes bandwidth enhancement for the nearby patch antenna.

It should be noted here the superior performance of the cavity backed DGS (Figure 5.9), which is indicated by comparing the three sensitivity tests that they have been demonstrated in this thesis.

11.2 DGS Ring Resonators and E-coupled patch antennas radiation in a semi-period

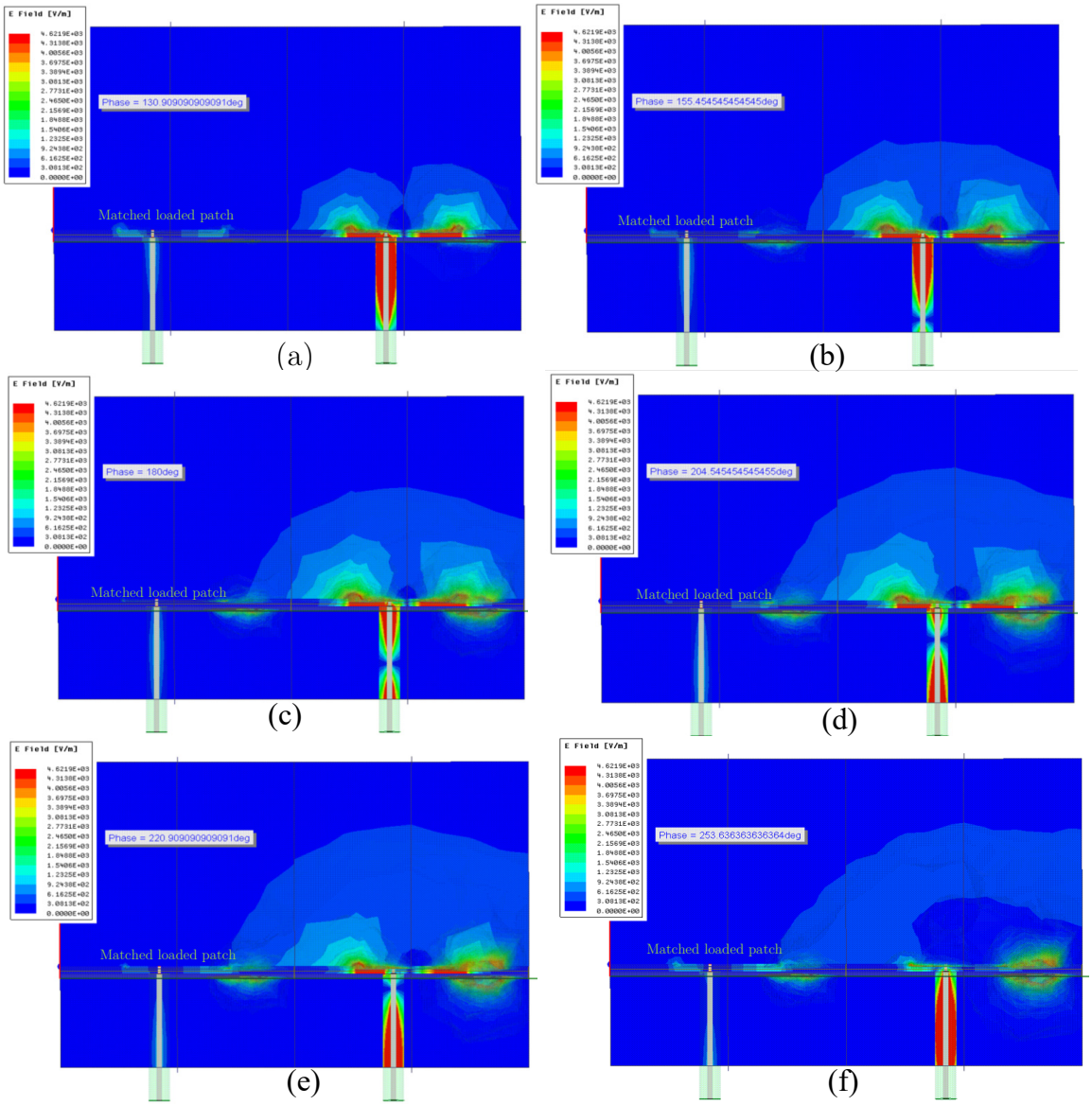

Figure 11.3: DGS radiating nature: E-coupled microstrip patch antennas one excited: E-plane side view for various phase instances. Description can be found in §6.4.2

11.3 Antennas on substrate DGS scan

The infinite arrays under investigation are based on examples that were able to provide MC reduction but not satisfying all the requirements which were established in §4.3. Specifically, the single slot resonator §4.4.1 and the modified dumbbell §5.2.2 are studied for their impact on the scan performance in micro-strip patch antenna arrays.

11.3.1 Ring Resonator

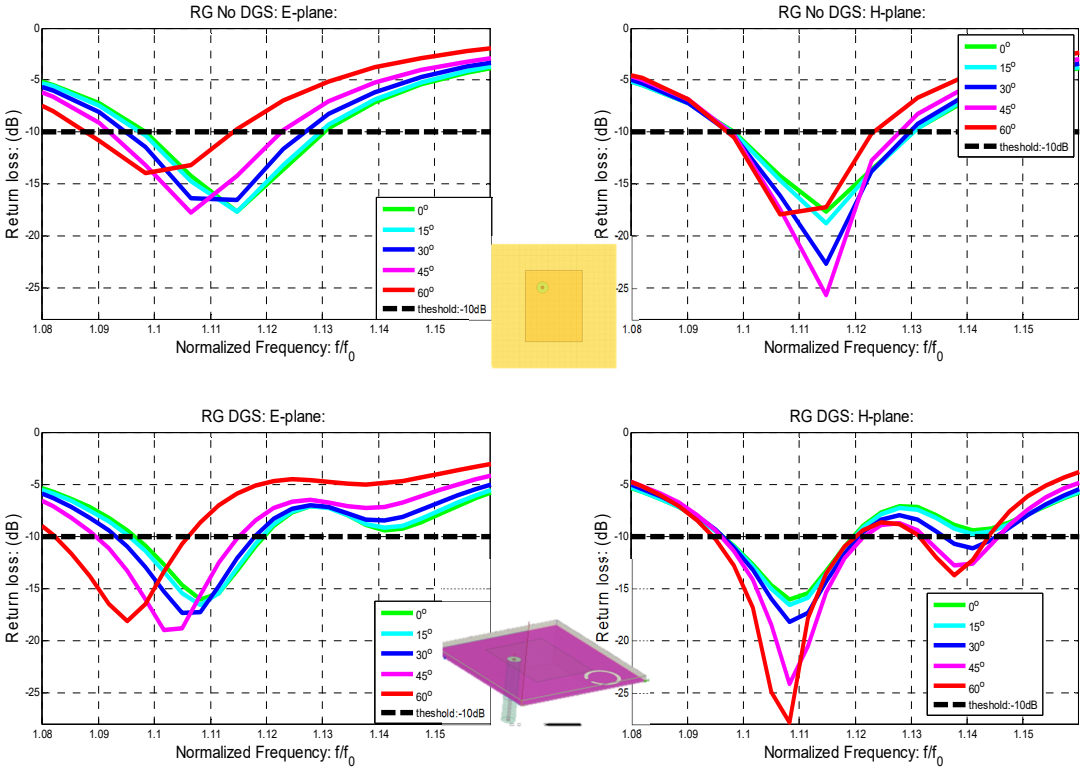

Figure 11.4: Micro-strip patch antenna and Ring resonator DGS: scan from broadside to 60^o

Observations regarding Figure 11.4 and Figure 11.5:

- H-plane is stable for all scan angles for both configurations.
  - DGS enhances the return loss levels for 60^o and 45^o, while equalizing broadside 15^o and 30^o.
- H-plane is more stabilized than E-plane for both configurations
- E-plane levels are more equalized and improved for 60 and 45 degrees for the DGS configuration

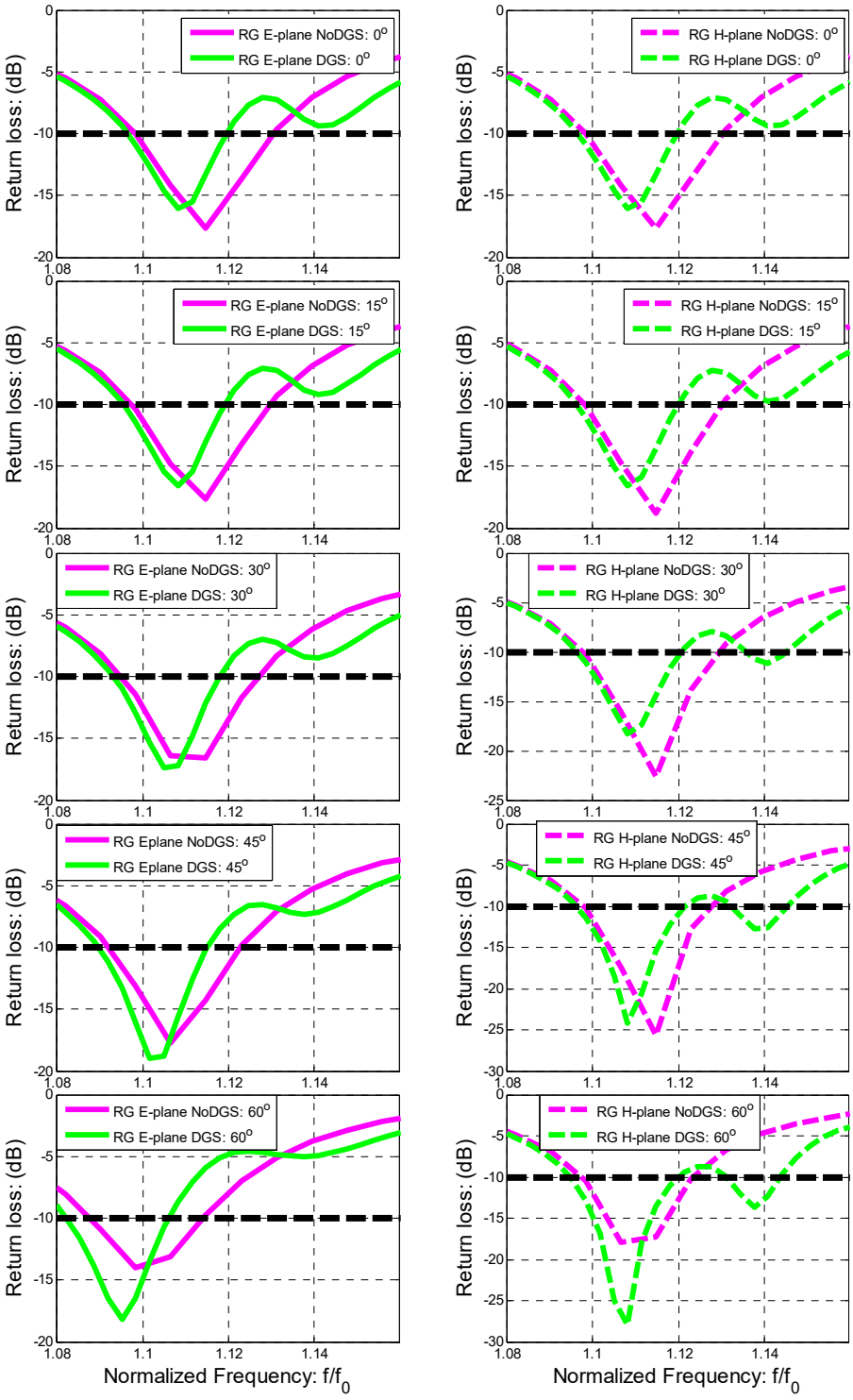

Figure 11.5: Angle by angle with (green) and without (pink) a DGS for the principal planes (E: solid lines, H: discrete lines))

Comments:

- Frequency bandwidth improvement in H-plane for all scan angles.
- For E-plane similar trend as for configuration without DGS is observed for higher scan angles 45 and 60 degrees.
- Current DGS placement benefits both planes but is more effective for H-plane (H-plane coupling was greater than E-plane coupling)
- Potential bandwidth enhancement in parallel to MC reduction by DGS

11.3.2 Modified dumbbell-etched dielectric

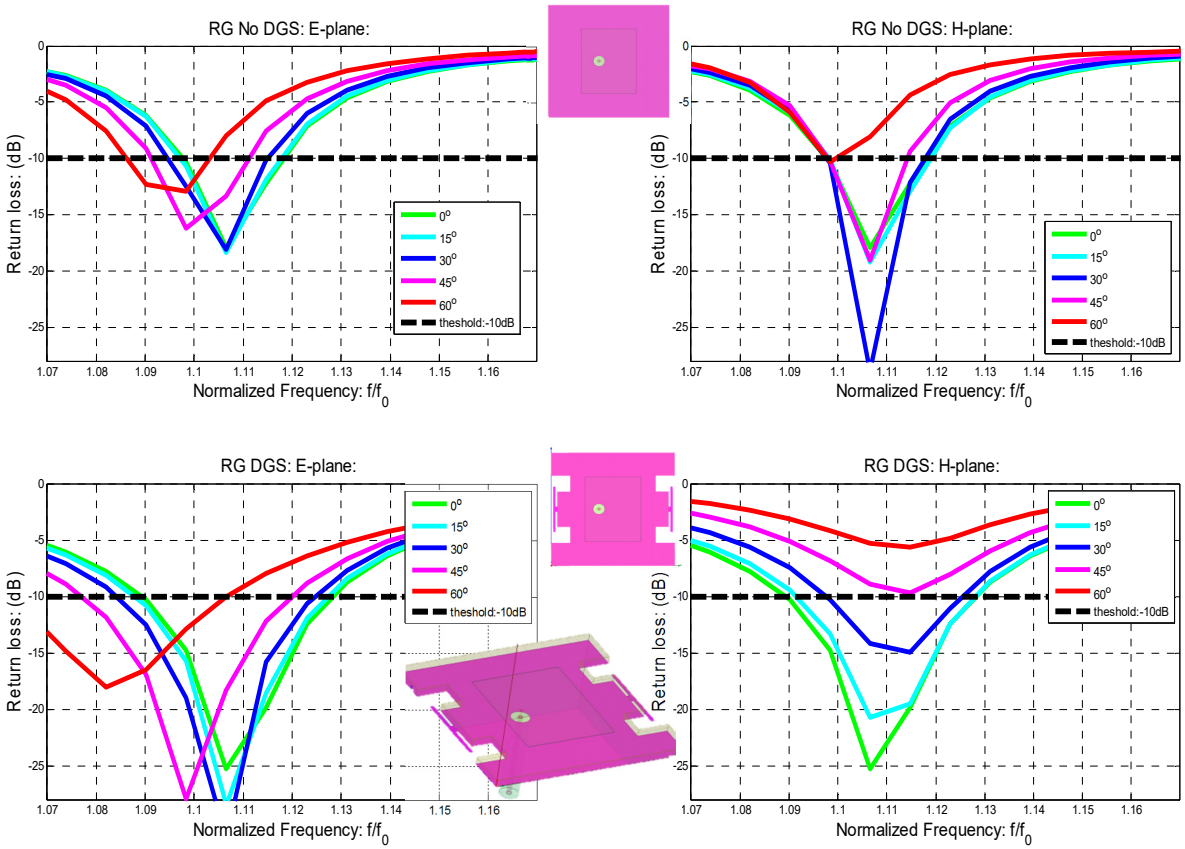

Figure 11.6: Micro-strip patch antenna, etched dielectric and modified dumbbell DGS: scan from broadside to 60^o

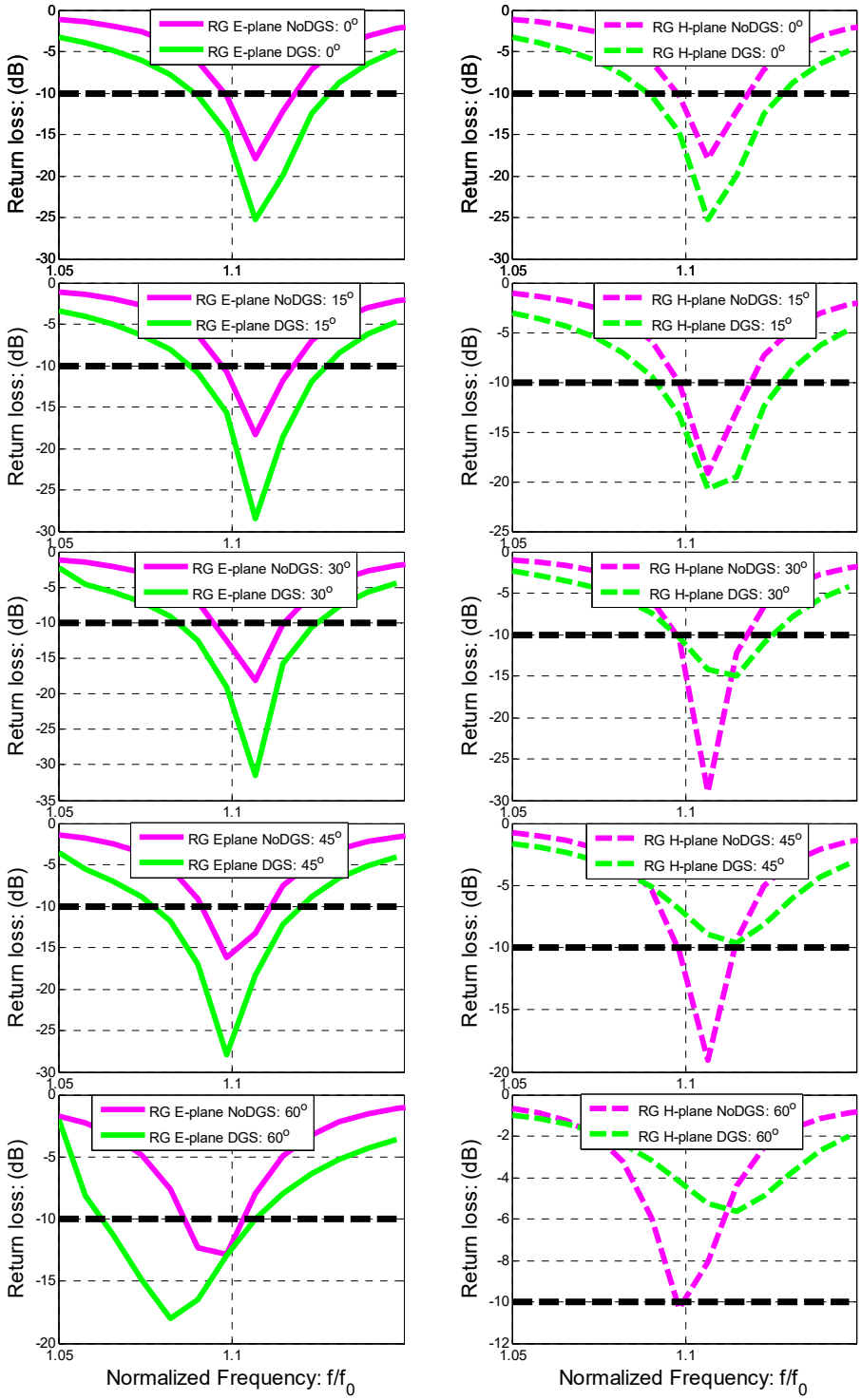

Figure 11.7: Angle by angle with (green) and without (pink) a DGS for the principal planes (E: solid lines, H: discrete lines))

From scan results in Figure 11.6 and :Figure 11.7:

- Observations:
    - E-plane return loss levels get benefit without significant shift
        - BW increased for each scan angle (no roll-off)
    - H-plane broadside reflection level gets the benefit while other scan angles have significant mismatch compared to not having a DGS. However, negligible shift in resonance
- Comments:
    - Reduces MC in E-plane but H plane impedance match for wide scan angles is mismatched.
        - Possible increased MC for H plane in wide angles
    - The centered DGS placement between the patch antennas eliminates any possible capacitive effects between the antennas and the slot defection (observed in the ring resonator example).

11.4 Embedded Patterns with and without a DGS

This section provides the embedded patterns for finite RDRA arrays in a rectangular grid. Moreover, all the element patterns for the analyzed triangular array (see chapter §8), 121 elements, are illustrated as well. This demonstration makes possible to show the impact of the final DGS cavity backed for small arrays, large arrays as well as for different lattice configurations. Further explanations are provided in §8.2.4.2.

11.4.1 The 5x5 RDRA RG planar array

- Element pattern improvement is observed in case of using DGS

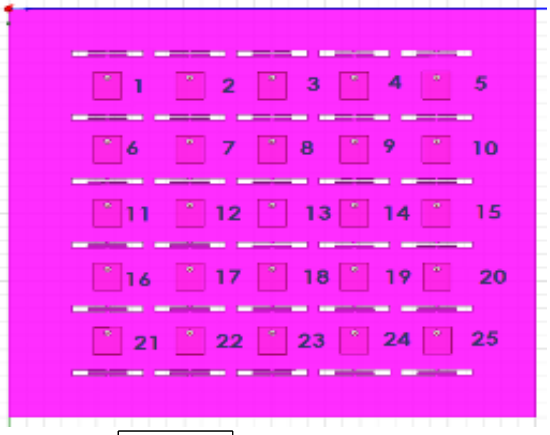

- E -plane patterns

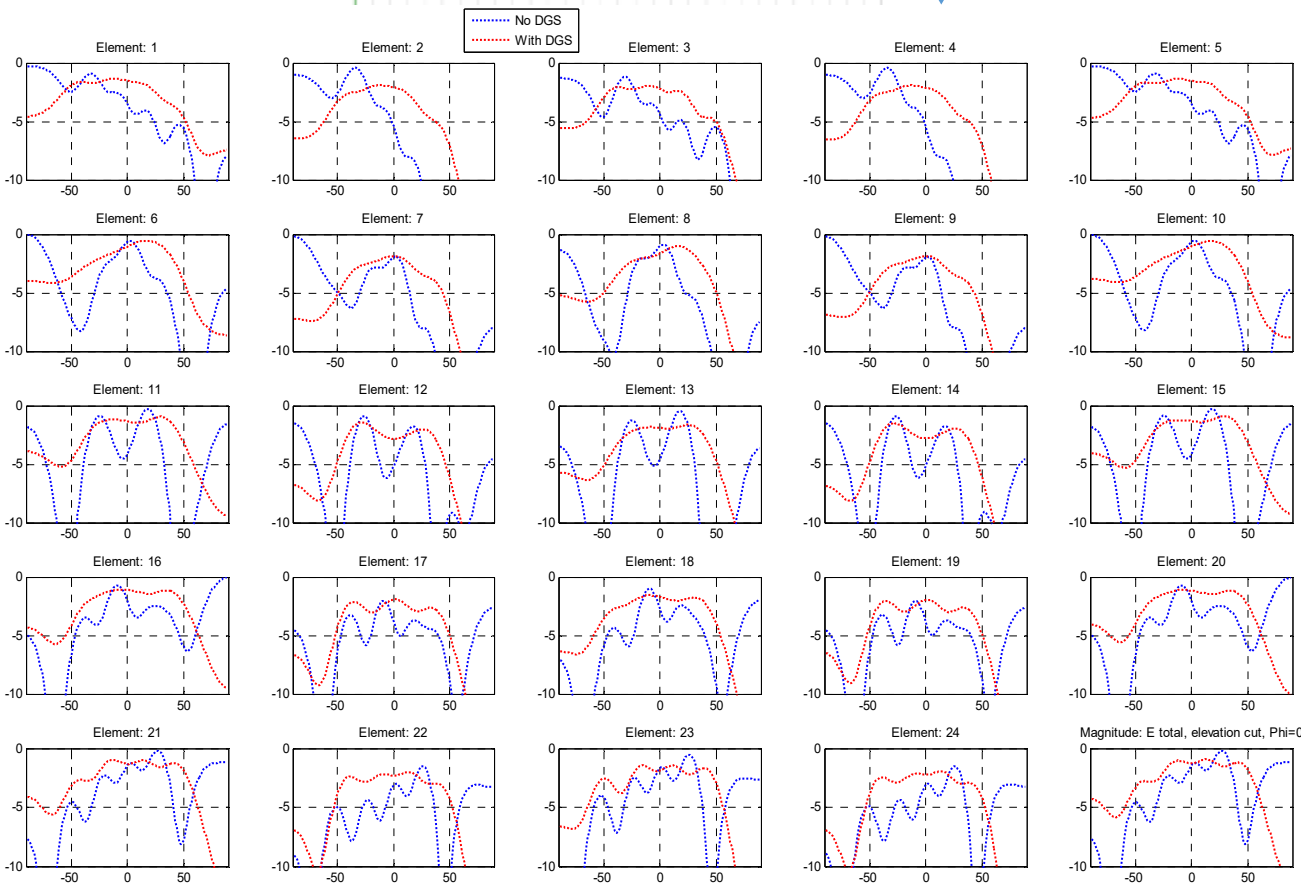

Figure 11.8: 5x5 RDRA array in rectangular grid: E-plane embedded patterns

- Element pattern improvement is observed in case of using DGS

- H - plane Patterns

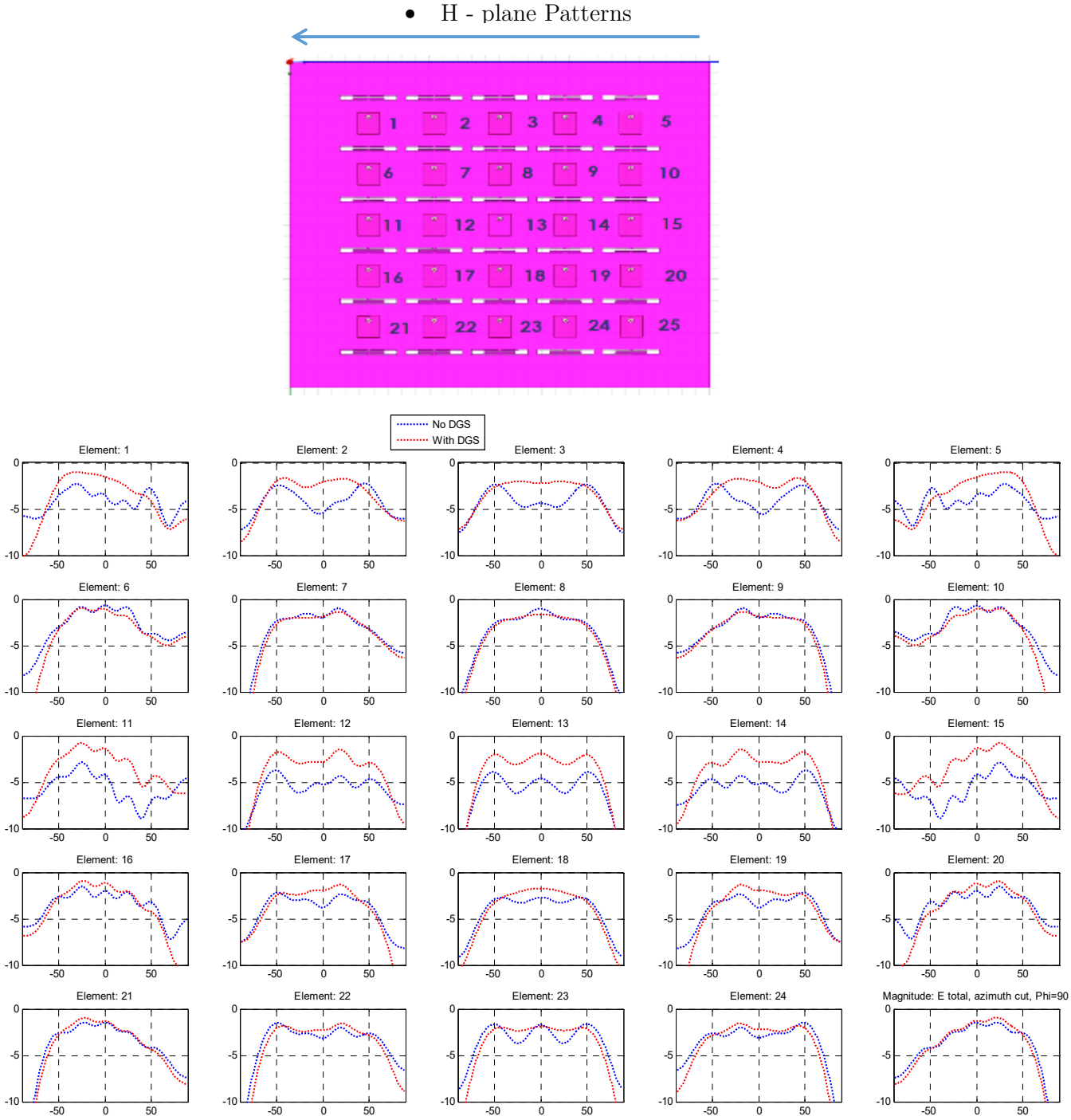

Figure 11.9: 5x5 RDRA array in rectangular grid: H-plane embedded patterns

11.4.2 The 11x11 RDRA RG planar array

- Element pattern improvement is observed in case of using DGS
  - 5x5 centered elements

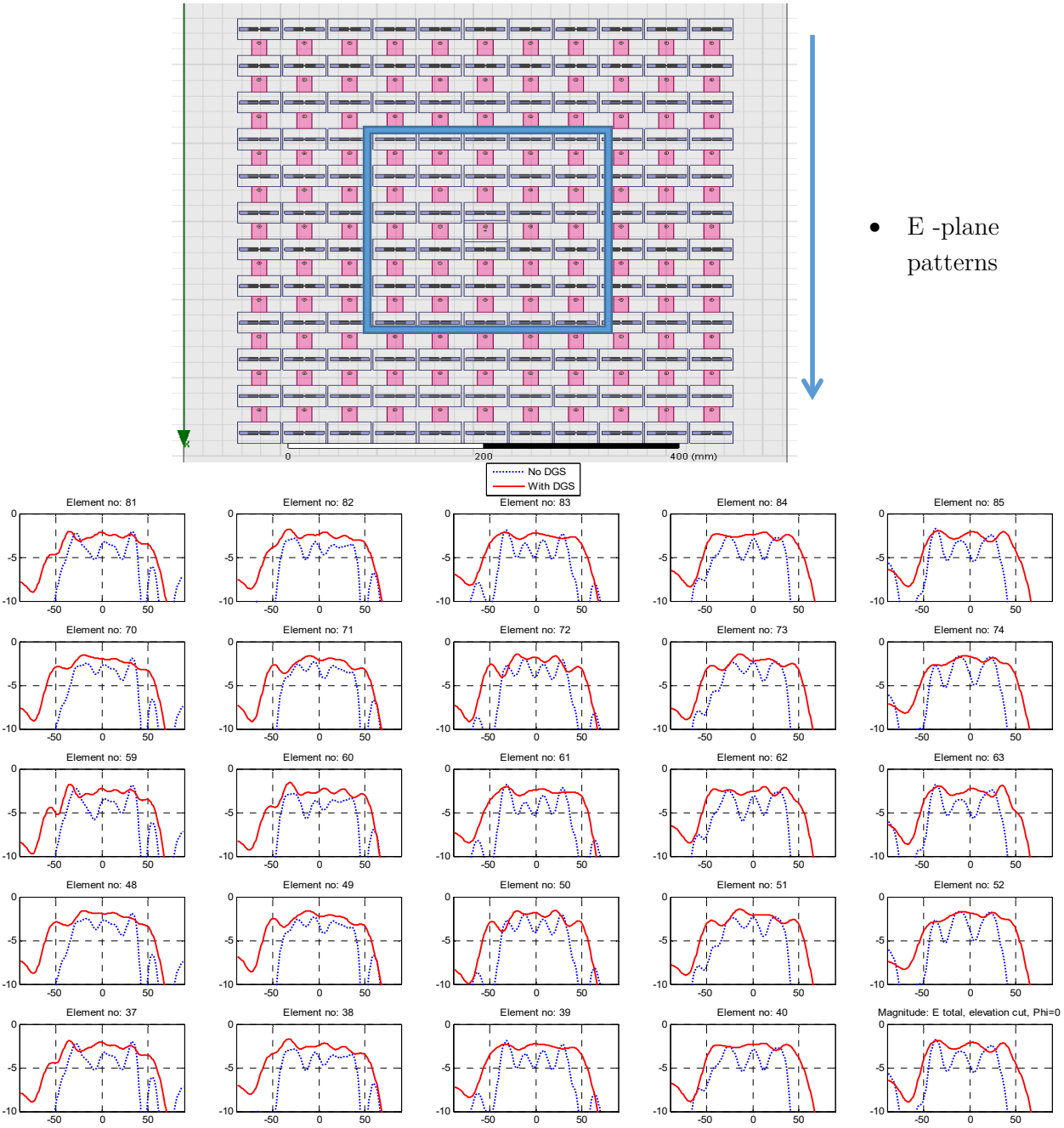

- E -plane patterns

Figure 11.10: 11x11 RDRA array in rectangular grid: E-plane embedded patterns of the 5x5 centralized elements

- Element pattern improvement is observed in case of using DGS
  - 5x5 centered elements
    - H - plane Patterns

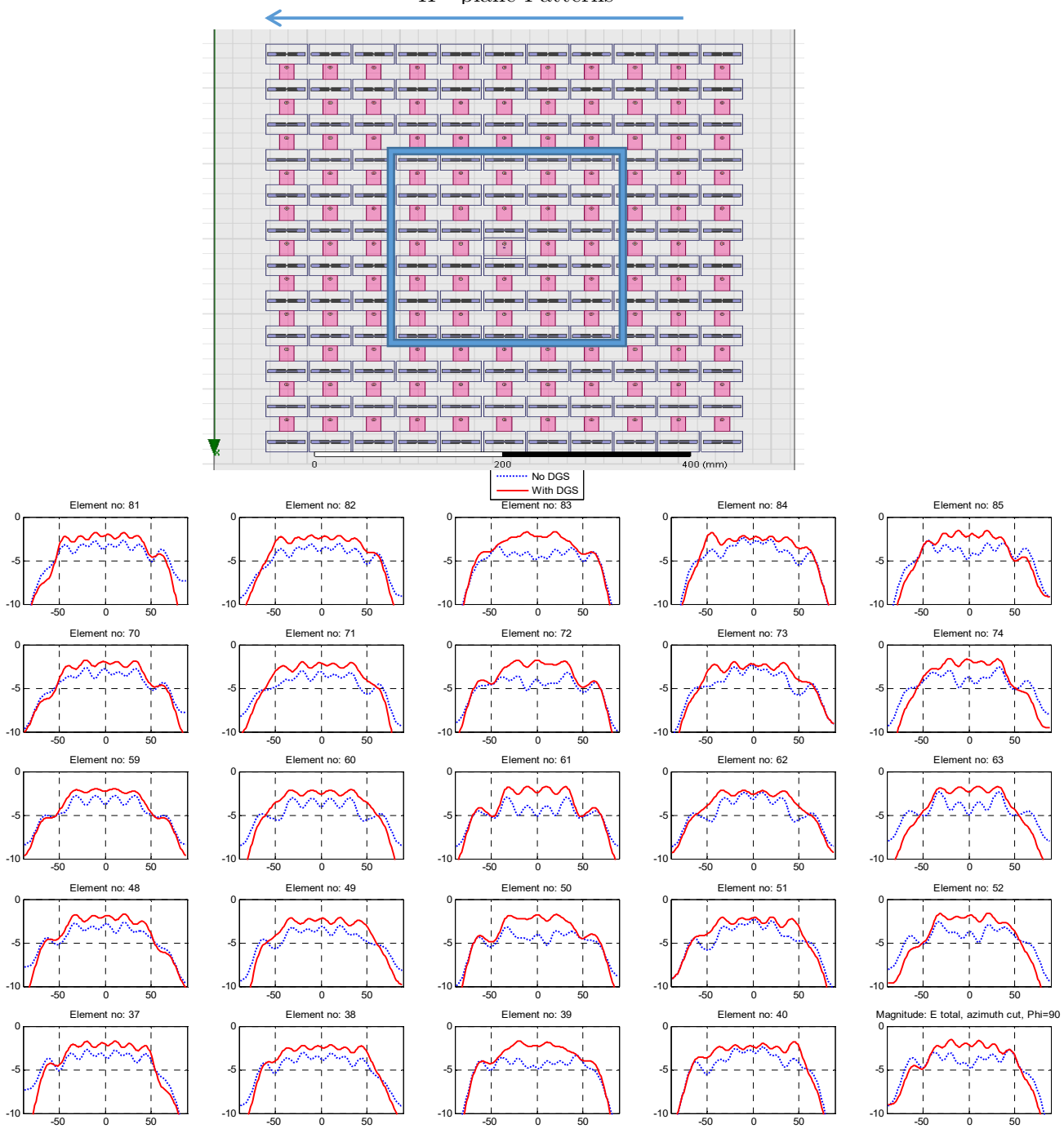

Figure 11.11: 11x11 RDRA array in rectangular grid: H-plane embedded patterns of the 5x5 centralized elements

11.4.3 The 11x11 RDRA TG planar array

- Element pattern improvement is observed in case of using DGS
  - The centered 5x5 patterns are illustrated in §8.2.4.2

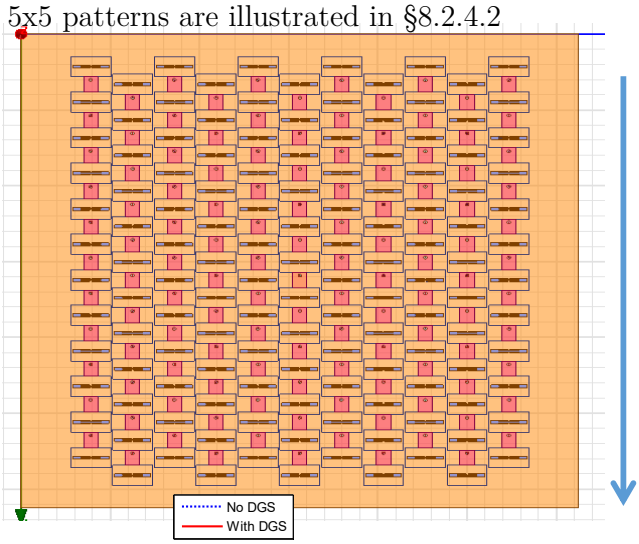

- E -plane patterns

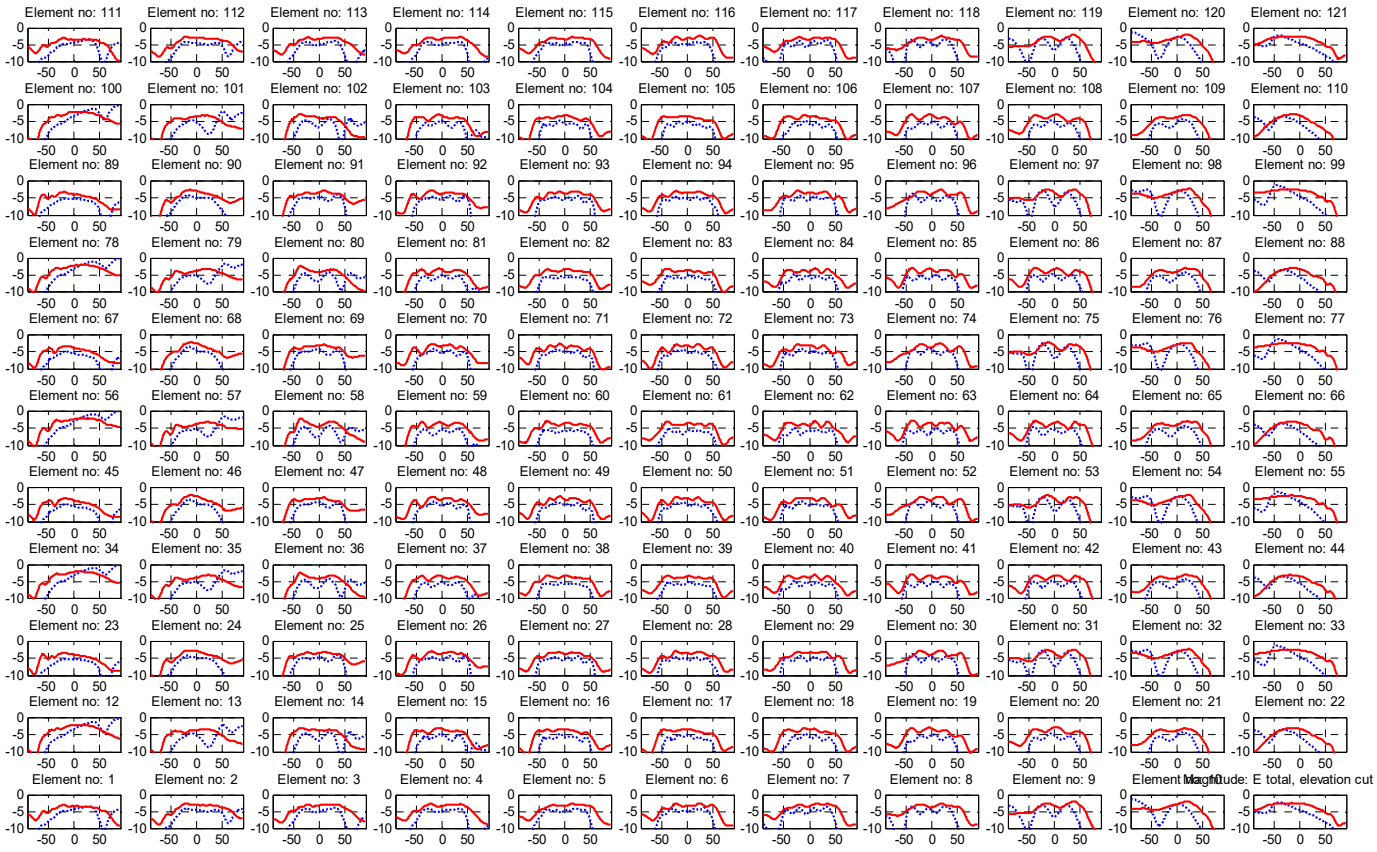

Figure 11.12: 11x11 RDRA array in a triangular grid: E-plane embedded patterns

- Element pattern improvement is observed in case of using DGS
  - The centered 5x5 patterns are illustrated in §8.2.4.2

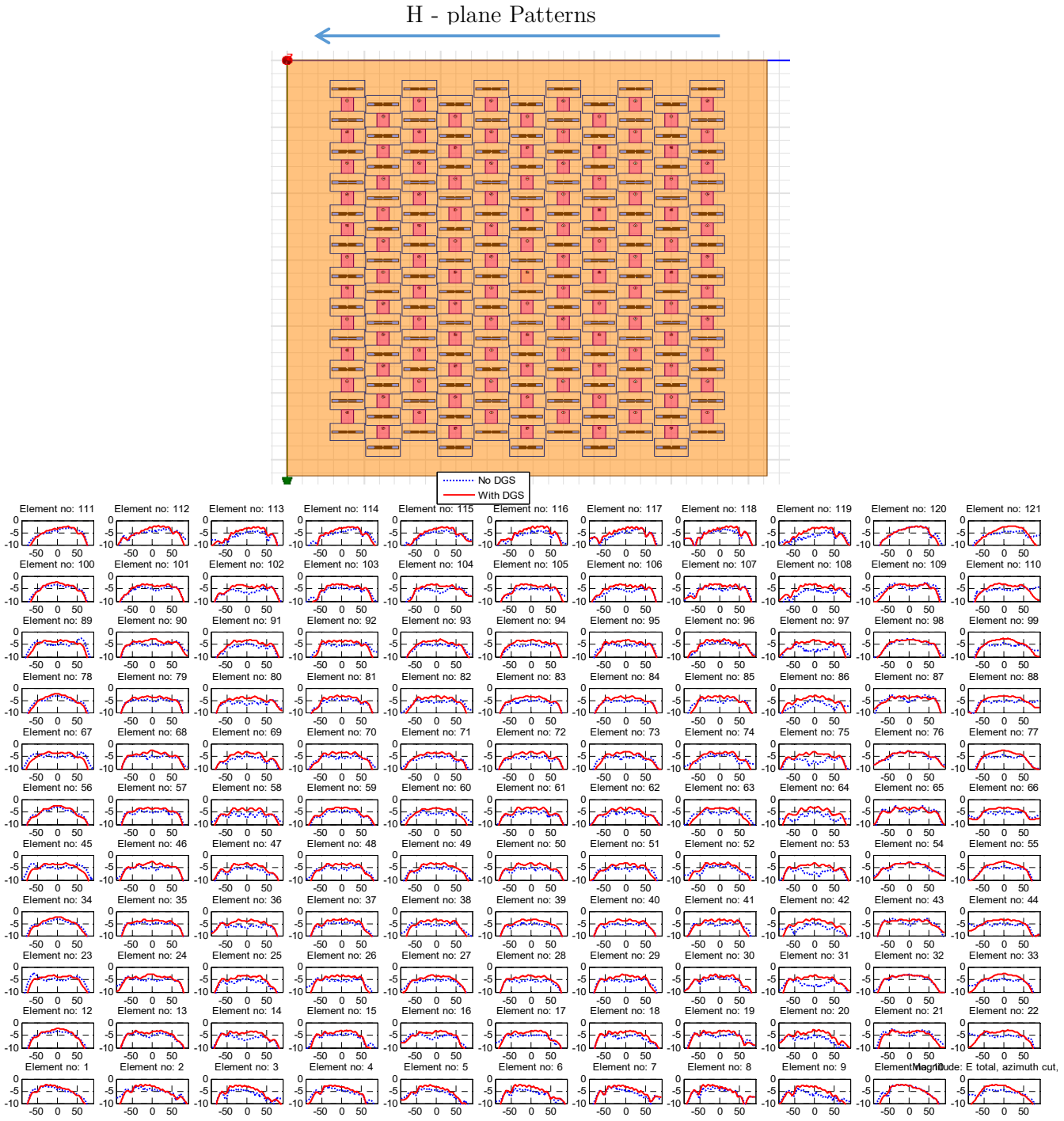

Figure 11.13: 11x11 RDRA array in a triangular grid: H-plane embedded patterns